BIOMIMETIC MICROSCALE PLATFORMS FOR THE VISUALIZATION OF BIOLOGICAL PROCESSES: FROM GUVS TOWARDS ARTIFICIAL CELLS

Inauguraldissertation

zur

Erlangung der Würde eines Doktors der Philosophie
vorgelegt der
Philosophisch-Naturwissenschaftlichen Fakultät
der Universität Basel

von

Martina Garni

aus Deutschland

Basel, 2020

Genehmigt von der Philosophisch-Naturwissenschaftlichen Fakultät

auf Antrag von

Prof. Dr. Wolfgang Meier

(Universität Basel)

Fakultätsverantwortlicher/Dissertationsleiter

Prof. Dr. Corinne Nardin

(Université de Pau)

Korreferent

Basel, den 27.02.2018

Prof. Dr. Martin Spiess

(Dekan)

“It's a long walk back to Eden, sweetheart, so don't sweat the small stuff.”

S. King, Insomnia

TABLE OF CONTENTS

TABLE OF CONTENTS

ACKNOWLEDGMENT

First of all, I would like to thank my committee for taking the time to read this thesis.

I would also like to thank my PhD supervisor Prof. Dr. Wolfgang Meier who offered me the opportunity to do my doctorate studies in his laboratory at the department of physical chemistry, providing such a great working place to perform research at a high level.

I want to thank Prof. Dr. Cornelia G. Palivan, for her great advices and support throughout my PhD. I greatly appreciate all her effort.

I am very thankful to Prof. Dr. Corinne Nardin for agreeing to be my external co-examiner.

Prof. Dr. Catherine Housecroft is kindly acknowledged for being the chair.

I am also thankful to all my colleagues and friends in the group for their help. This work and other projects would have never been possible without them. Especially Ioana for her encouragement and Roland for his patience.

A special thank goes to Tomaž with who I spend so much time working together. I never met a more optimistic person regarding research and life.

On a personal level I thank my parents, who supported me during my studies in all aspects.

Finally, I am thankful to Julia who never stopped believing in me.

Thanks to all of you!

ABSTRACT

First in order to explore the possibilities of building a synthetic artificial cell following a biomimetic approach, we engineered synthetic polymer-based giant unilamellar vesicles (GUVs) with selective membrane permeability. Since the membranes of polymeric GUVs present a high impermeability compared to natural lipid membranes, membranes are selectively permeabilized in a biomimetic approach by the insertion of the small pore-forming peptide gramicidin (gA) as gA biopores are known to allow the transport of protons and monovalent ions. Whilst gA has been inserted in lipid membranes in numerous research studies, the challenge of inserting the bacterial pore into polymer membranes is greater because of the significant difference between the pore length and the thickness of the polymer membrane (more than 3.5 times). Confocal laser scanning microscopy (CLSM) was used to show that neither the size, nor the morphology of the GUVs was affected by successful insertion of gA and further to visualize the pH change inside the cavity of GUVs in real-time by recording videos. In order to demonstrate the successful insertion of gA, a pH-sensitive dye is encapsulated inside the cavity of GUVs and proton gradients between the environment of GUVs and their inner cavity serves to assess the exchange of protons across the membrane upon gA insertion. The results showed that gA was successfully inserted and remained functional in polymer membranes with thickness of 9.2–12.1 nm. Larger membrane thicknesses did not allow gA insertion, and 12.1 nm represents a limit for the mismatch between the pore length and the membrane thickness. Our gA-GUVs are therefore pH-regulating and maintain their integrity in different pH conditions in a cell-like manner. This bio-mimetic approach to use ion channels with specific selectivity for insertion in polymer membranes is an elegant strategy to develop mimics of biomembranes or for supporting the design of bioreactors.

Next, a functional cell mimetic compartment is developed by the insertion of the bacterial membrane protein (OmpF) in thick synthetic polymer membranes of an artificial GUV compartment that encloses the oxidative enzyme horseradish peroxidase. In this manner a simple and robust cell mimic is designed, that supports a rudimental form of metabolism. The biopore serves as a gate, which allows substrates to enter the cavities of the GUVs, where they are converted into the resorufin-like products by the encapsulated enzyme, and then released in the environments of GUVs.

ABSTRACT

Our bio-equipped GUVs facilitate the control of specific catalytic reactions in confined micro-scale spaces mimicking cell size and architecture and thus provide a straightforward approach serving to obtain deeper insights in the real-time of biological processes inside cells.

This elegant strategy of equipping both GUV membranes and GUV cavities with biomolecules, opens the way towards cell-like compartments as novel materials with bio-functionality is the combination of synthetic micrometer-sized giant unilamellar vesicles (GUVs) with biomolecules because it enables studying the behavior of biomolecules and processes within confined cavities.

Finally a visionary strategy for creating the first bioinspired molecular factory with functionality as a real cell-mimic based on micrometer-sized giant plasma membrane vesicles (GPMVs) is addressed. GPMVs are cell-derived giant vesicles consisting of an outer compartment architecture (membrane) and an inner composition, which both directly mirror the composition of cells from which they originate except the larger organelles like for example nuclei and Golgi apparatus making measurements easier and are the closest cell-mimic available on the market up to now. In a step towards the development of bioinspired molecular factories with functionality as cell mimics, we generate the next generation of cell mimics by the production of sophisticated hybrid molecular factories based on GPMVs, which are equipped with a synthetic molecular machinery inside their cavities that provides functionality. Such a hierarchical approach in compartmentalization allows the lower-level synthetic functional compartments encapsulated within the cavity of the GPMV to act as independent anatomically discreet units that specialize in their own function, making them nanoscale versions of nature own organelles.

Towards the first bioinspired molecular factory enzyme-equipped polymersomes with a reconstituted membrane protein (OmpF) are encapsulated inside the GPMVs as enzymatic nanocompartment spaces, where they retain their structure and functionality. When substrates were added to the outer solution of the GPMVs, it was shown that they could penetrate both the membrane of the GPMVs and the inner compartment membranes of the synthetic nanoreactors equipped with OmpF pores. In this respect the equipment of the catalytic nanocompartment spaces with OmpF was essential as it allowed the enzyme to perform in the inner cavities. Successful substrate conversion was visualized by following the fluorescent product of the enzymatic reaction (resorufin-like product), which could leave the polymersome and diffuse inside the GPMV cavity. Finally we demonstrate that equipped GPMVs can act as artificial cell mimics – retaining their membrane and inner composition if

they are injected into multicellular organisms – Zebrafish embryos. To the best of our knowledge, this is the first time that a molecular factory functioning as a cell-like mimic has been be constructed by using a top down-bottom up approach and has been tested in vivo by taking advantage of the fundamental nature of GPMVs.

Chapter 1

FUNCTIONAL BIOMIMETIC DESIGN OF GIANT UNILAMELLAR VESICLES (GUVS)

The first chapter of this thesis serves to familiarize the reader with the fundamental principles and the scientific interest of building synthetic cell-mimics. The reader is introduced to native cell membranes and the current state of the art of synthetic cell membrane mimics. Therefore, amphiphilic lipids and polymers, which are the central building blocks of synthetic membranes are explained first. Further the thermodynamically driven self-assembly and characterization methods of spherical membrane-based micro-sized vesicles -lipid, polymer and cell-derived GUVs are discussed, which are the basis/fundament used in the later chapters of this work, when designing different kinds of bioinspired cell mimics. Due to their size, cell-sized GUVs can give a deeper insight into biological processes and are therefore ideal candidates for biomimics. Finally, the approach of building molecular hybrids of cell membrane mimics by equipping them with biomolecules is presented.

This chapter is partially reprinted and has been published:
M. Garni, T. Einfalt, M. Lomora, A. Car, W. Meier*, C. G. Palivan*, Artificial Organelles: Reactions inside Protein–Polymer Supramolecular Assemblies, *CHIMIA International Journal for Chemistry*, Volume 70, Number 6, 2016, 424-427.
M. Garni, S. Thamboo, C. A. Schoenenberger, C. G. Palivan*, Biopores/membrane proteins in synthetic polymer membranes, *Biochimica et Biophysica Acta (BBA) - Biomembranes*, Volume 1859, Issue 4, 2017, 619-638.

ARTIFICIAL CELLS / CELL MIMICS

Since the discovery in 1838 that cells represent the basic structural and biological/ functional units of all known living organisms, the so called “building blocks of life” which contain the hereditary information have the necessary molecular machinery to support metabolism and are able to replicate independently, researchers had the dream to create a synthetic/artificial cell with all kinds of imaginable specific functionalities. Behind that dream, the fundamental motivation is that being able to create an artificial cell would help to answer essential questions of how non-living systems progressed from simple molecular organizational systems to living systems. Artificial cell mimics could ideally bring deeper insight into many fields such as cell biology, biochemistry, molecular biology, and systems biology[1] by studying cellular processes in an artificially created micro-environment that represents a real cell (Figure 1).

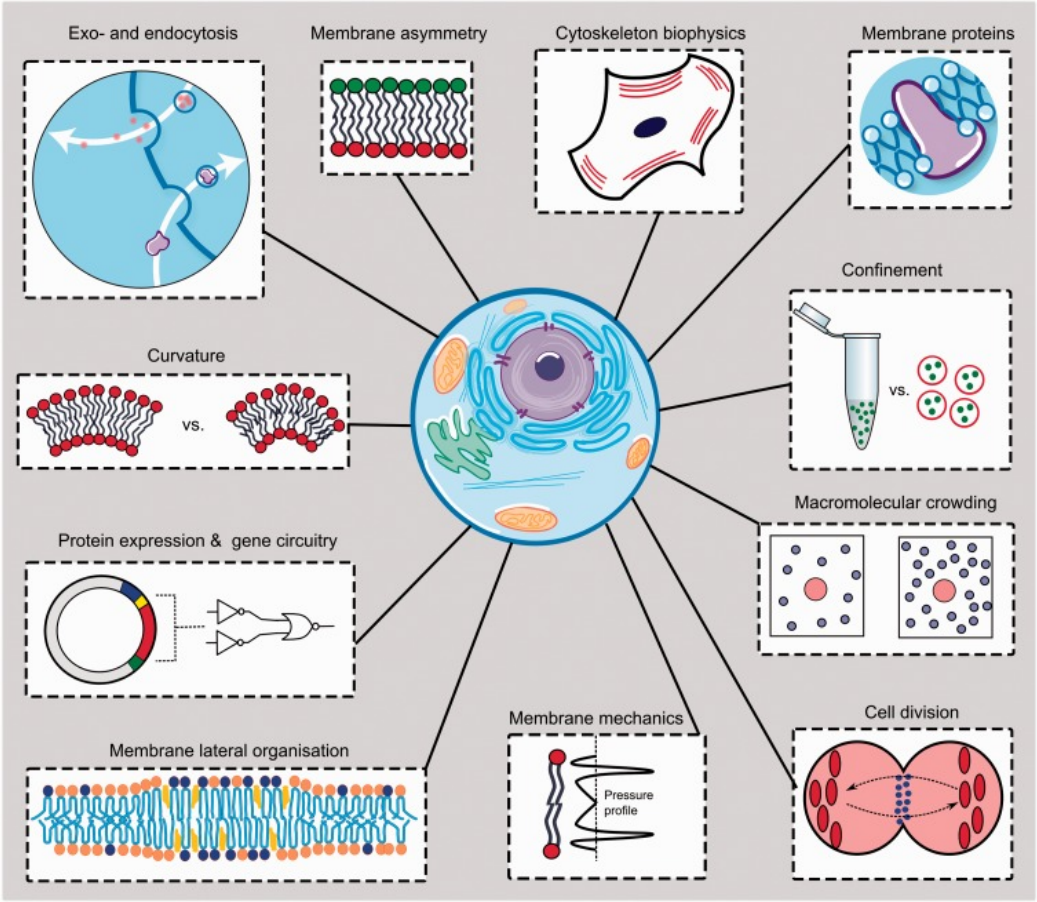

Figure 1. Artificial cell mimics *– A versatile platform that allows studying biological phenomena in a simplified manner. Adapted from Salehi-Rehyani with permission.*[1]

This technique is perceived as an 'understanding by building' approach. In a science-fiction scenario, the acquired knowledge could even lead to artificial cells, capable of producing synthetic biomacromolecules (i.e. genes, proteins), supporting independent metabolism, replication and differentiation – making them indistinguishable from cells found in living organisms. By appropriate vision and execution, researchers could build whole tissues, organs or organisms that could be later transplanted in our body as treatments for diseases and open the way towards longer lifespans. Two centuries after the discovery of living cells numerous achievements have step by step brought us closer towards the ambitious aim of designing an artificial cell mimic, becoming a rapidly growing area of research in the 21st century.[1]

Building an artificial cell – where to start?

Up to this point there are two established conceptual approaches that dominate the field of artificial cell mimics.

The first is based on genetic engineering techniques that allow reengineering and manipulation of an existing organism (i.e. stem-cell) with the help of well-developed tools and technologies in biotechnology. Currently this approach is more advanced, as it does not rely heavily on assembling the entire cellular machinery from scratch, but rather uses pre-existing organisms and modifies them. Top down designed cells embody the same complexity (i.e. intricate metabolic pathways) as the living cells they originate from. This complexity is advantageous when designing fully functional cells but hinders the use of top down cell-mimics to gain insight into singular processes within cells. As this thesis will focus primarily on cell-mimics as platforms for visualization of cellular processes, this approach is beyond the scope of this thesis and is discussed in detail elsewhere.[2]

The second approach is based on designing an artificial cell from the bottom up. In this way cell mimics are constructed on the molecular level by combining either synthetic, biological molecular building blocks or a combination thereof *in vitro*. The vast libraries of synthetic and biological molecules that have been discovered, isolated and studied in the previous century, give researchers an unprecedented freedom in choosing the material from which the artificial cell mimics are built. Specific molecular building blocks (i.e. lipids, polymers, DNA, proteins etc.) can be picked and combined in order to support a specific function (i.e. structural integrity or a specific chemical reaction), giving bottom up artificial cell systems an innate versatility. By using this approach, bottom up designed artificial cells are starting to

gain ground in applied sciences, for example as biosensing micromachines, and molecular systems that perform defined tasks, function / navigate autonomously and support a rudimental form of metabolism in the form of basic chemical synthesis.[3–7] Unquestionably, the most important application of bottom up designed cell mimics is in research areas where they are used as simplified mimics of real biological cells, giving insight into the complex cellular metabolism and the progression of non-living systems to living cells.

Finally, an unprecedented combination of bottom up and top down approaches is possible, where biological systems (i.e. eukaryotic cells) are used as a tool, to assemble individual molecular building blocks and produce artificial stand-alone systems on demand. To the best of my knowledge, this approach remains predominantly untapped and has not been used for the construction of a cell mimic by any other research group. The first proof of concept of a bottom up/top down designed cell-mimic is discussed in great detail in the last chapter of this thesis.

Building an artificial cell – the advantage

Both eukaryotic and prokaryotic cells are complex structures with well-organized molecular machineries that work with high precision and efficiency.[8] In order to develop artificial molecular systems with similar complexity and multifunctionality as is found in biological systems, it is necessary to understand and mimic at the molecular level the various reactions involved in cell metabolism.

The discovery of cell-free enzymatic reactions by Eduard Buchner in 1897[9] demonstrated that not all chemical reactions of biological systems require organized, living cells. In principle bottom up synthetic biology, is a contemporary application of this principle. In a bottom up approach of designing micro-sized vesicle-based cell mimics equipped with biomolecules, the latter have been shown capable of hosting a wide array of confined reactions[10] catalyzed by either inorganic catalysts or biomolecules. Examples of such reactions include the polymerase chain reaction[11], RNA polymerization[12], protein synthesis[13] and even coupled transcription and translation.[14]

Taking into consideration the fundamental complexity of the proteome found in eukaryotic cells, which covers over 20,000 protein coding genes in human DNA, the design of an ideal cell-mimic is still out of reach and demonstrates the enormous challenge bottom up synthetic biology faces.[15] In living cells there are various interactions between proteins and also between proteins and other biomolecules (i.e. DNA, lipids) that result in a complex network

capable of supporting all kinds of molecular interactions and signaling pathways. The challenge is to understand this complexity and to determine all the possible molecular parameters that play a role in supporting cellular metabolism in a quantitative manner. However, due to the overwhelming complexity a significant potential for redundancy is required, when studying cellular processes. Isolating the exact role that individual components play in cellular metabolism in a systematic way appears as a nearly impossible task when studying whole cells. Herein lies the key attraction of using bottom up designed artificial cells as models of their biological counterparts. Lab-created artificial cells come with a key advantage: simplicity. On the one hand, artificial cells are simple enough to experimentally give insight into fundamental processes of cell biology, and on the other hand they can still estimate aspects of biological processes, which otherwise only appear in more complex systems. Whereas biological cells require cell specific cultivation (i.e. temperature and CO_2 atmosphere) and essential nutrients, the designed artificial cells are independent of their external environment unless specified otherwise. By increasing the complexity of a simple artificial cell systematically using more and more components in a controlled manner, the construction of a cell mimic that represents almost a real cell could be realized in a not so far away future (Figure 2). Cell mimics previously arose in the form of biomolecule-loaded lipid- and polymer-based giant unilamellar vesicles (GUVs)[5,7,16–18] lipid coated porous silica nanoparticles[19], layer-by-layer capsules[20], membrane free microdroplets, and micro scaled proteinosomes.[21] This thesis will focus on giant unilamellar vesicles (GUVs) as their membranous hollow sphere structure makes them the closest cell mimics up to date.

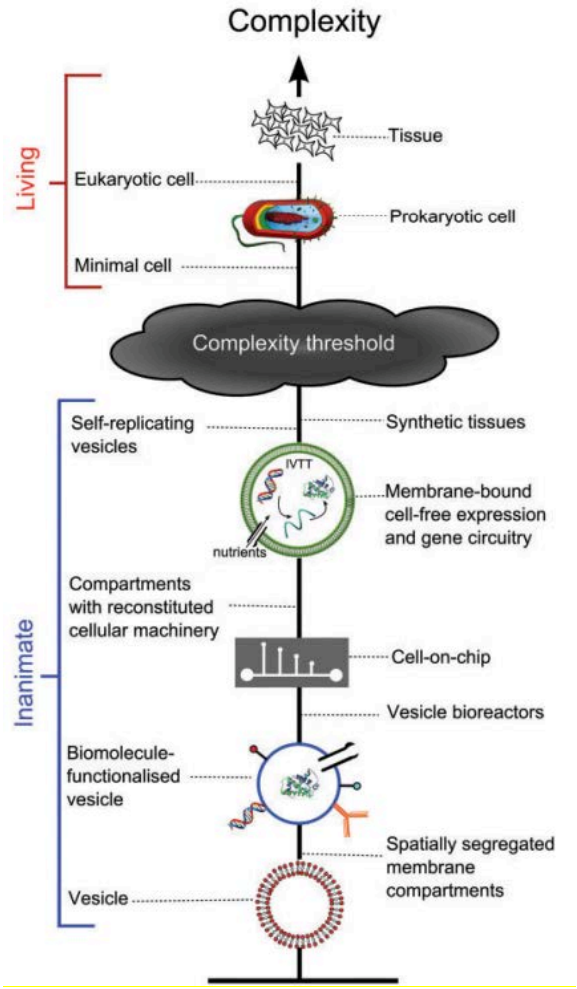

Figure 2. *Increasing complexity of artificial cell mimics, giving insight into the progression of non-living systems to living systems. Current artificial cell systems heavily rely on a bottom up or top down approach in design. Adapted from Salehi-Reyhani et al. with permission.*[1]

Previously, the most common approaches to produce membranous cell mimics were based on bulk self-assembly of molecular building blocks and emulsion-based techniques.[22,23] Contemporary approaches rely on the established microfluidics technologies, which allow a high degree of control with respect to size (micro- or nanoscale) and architecture (i.e. compartmentalization, connectivity within the mimic or membrane composition).[24–29] Due to the flexibility of the experimental approach, new ways are being opened in combining artificial cells with synthetic parts and therefore creating new hybrid materials. The above-mentioned techniques enable the controlled creation of artificial cells with defined functionalities working as complex self-organized systems and discussed along with the different types of molecular building blocks, later on in the subsequent chapters of the thesis.

ESSENTIAL BUILDING BLOCKS FOR CELL-LIKE MEMBRANE MIMICS: LIPIDS, POLYMERS AND CELL-DERIVED MATERIALS

Since many years, researchers study and mimic native biological cell membranes and further use them as a model to study various biological processes. When mimicking a cellular membrane in a laboratory environment many different factors have to be taken into account, such as lipid/polymer composition of the membrane[30–32], membrane asymmetry[33], degree of confinement and compartmentalization[34], as well as their intrinsic mechanical properties.[35,36]

Biomembranes

Analyzing native biological cell membranes resulted in a technological progress towards the generation of artificial membrane systems, which serve as the fundamental architecture of cell mimics. Biological membranes composed of a phospholipid bilayer are complex matrices which serve as a border between the inner cavity of a cell and the outside environment to protect the cell from its surroundings. The main components of cell membranes are phospholipids. Broken down, the phospholipid structure is composed of a hydrophilic head group (neutral, charged or zwitterionic) and a hydrophobic tail (saturated or unsaturated carbon chain).[37] Once in solution this leads to the molecular arrangement of phospholipid molecules into a thin two-dimensional double layer (bilayer), with hydrophilic head groups facing the water interfaces in order to reduce the total entropy.

The cell membrane controls the transport of substances through selective permeability towards ions and/or molecules and is involved in a variety of active cellular processes as for example cell adhesion, ion conductivity and cell signaling.[38] However, lipids alone cannot support complex function required from a cell. Biological cell membranes have a wide variety of different kinds of membrane proteins embedded within the lipid matrix in order to support cellular metabolism. In fact, membrane proteins are so important that they can contribute to 15-80% of the plasma membrane's dry weight and represent around 30% of the human cell genome, highlighting their importance.[39–41] Depending on their type, membrane proteins contribute to vital cellular functions or are involved in cell-to-cell communication. One of the major roles of membrane proteins is the translocation of substrates from the cellular environment across the plasma membrane into the cytoplasm and the excretion of metabolites or signaling molecules into the cellular environment. For this purpose biological

systems have evolved specific and non-specific membrane protein channels, which allow translocation of substrates or solvents across the phospholipid membrane with exceptional selectivity and at high transport rates.[30,41] In addition to membrane proteins relatively small molecular weight amphiphilic molecules, such as steroles (i.e. cholesterol) enhance membrane tensile strength and maintain membrane fluidity.[43] Once self-assembled, cellular membranes represent a dynamic mosaic of molecules where membrane proteins and lipids can diffuse freely in the two-dimensional space. The wide range of components found in eukaryotic and prokaryotic membranes, makes creating artificial membrane systems a great challenge. Simplifying membrane composition by narrowing down the components is the first step in obtaining a control over the self-assembly of the fundamental architecture of the cell mimic.

Lipid-based artificial membranes

With regard to composition, most cell mimics are composed of phospholipids, as they are readily available, well characterized and represent membranes that closely imitate the composition of the natural plasma membrane of cells. Phospholipids are abundant molecules in all biological membranes and at first seem to be the most suitable building blocks for the construction of membrane-based cell mimics. By definition, phospholipids are built of four components: a.) fatty acids (i.e. C18, C16, C12), b.) a platform to which the fatty acids are attached (i.e. glycerol or sphingosine), c.) a phosphate, and d.) an alcohol attached to the phosphate (i.e. serine, choline, ethanolamine).[44] This flexibility in phospholipid composition already gives us an idea into the variety of phospholipids that can exist by varying the different sub components of a phospholipid. In aqueous environments phospholipids can form many kinds of assemblies, such as micelles, vesicles and hexagonal phases, which are a result of the molecular conformations the phospholipids adopt (Figure 3).[44] The molecular shapes are a result of the individual phospholipid components. For example, non-bilayer forming lipids, such as the unsaturated phosphatidylethanolamine (PE) can be stabilized in a bilayer forming structure by the presence of a bilayer preferring lipid, such as phosphatidylserine (PS). A rule of thumb is that 20-50% of bilayer preferring lipids are required to maintain a stable bilayer. Further, the structural properties of lipid mixtures can be modulated by a range of parameters, like head group size, temperature, hydrocarbon saturation, ionic strength, pH or even the presence of divalent cations (i.e. Ca^{2+}).[44]

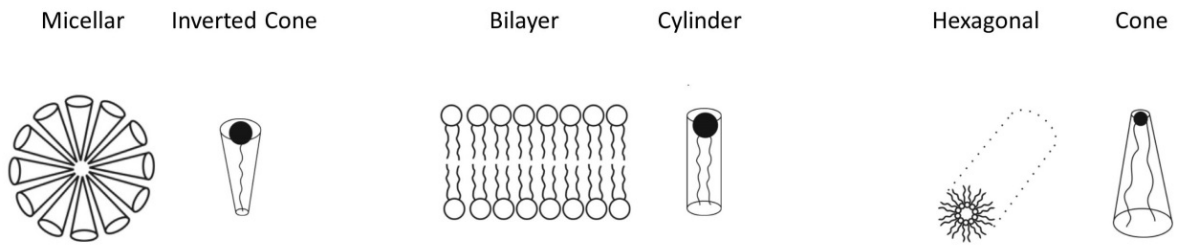

Figure 3. *Polymorphic phases and corresponding dynamic molecular shapes of component phosphoplipids. Modified from Li et al. with permission.*[44]

Ideally, by observing the composition of the plasma membrane – composed mainly of phosphatidylcholine (PC), phosphatidylethanolamine (PE), phosphatidylinositol (PI) phosphatidylserine (PS), sphingomyeline (SM) and steroles (i.e. cholesterol) – a formulation could be achieved in a laboratory environment, which would mimic the natural plasma membrane.[30]

Intuitively, phospholipids should represent an ideal platform for the reconstitution of membrane proteins[45], as the composition of the cell mimic membrane can be achieved close to that of cell membrane and various parameters of the membrane changed on demand by changing the lipid composition. The power to methodically change membrane lipid composition of the cell mimics has allowed researchers to study the effects of geometric membrane curvature on protein binding, activity, and function[46,47], in addition to protein-induced membrane deformation that is implicated in trafficking[48] and lipid and protein distribution.[49]

An important factor to consider when working with lipid-based artificial cell mimics is that amphiphilic molecules (i.e detergents) used in membrane protein isolation and purification might influence the GUV self-assembly. The task of membrane protein reconstitution is not trivial, as amphiphiles stabilizing membrane proteins outside their native environment heavily influence the self-assembly of the lipid bilayer.[45] Despite the recent advances, using lipid-based membranes to form artificial cell mimics comes with various disadvantages, such as a relatively high membrane permeability and low stability, which are both a direct result of the fluidity of the phospholipid bilayer.

Polymer-based artificial membranes

Amphiphilic block copolymers represent an alternative to lipids as building blocks for generating artificial cellular membranes. Due to their synthetic and rationally designed origin,

amphiphilic block copolymers offer a new dimension of bioinspired supramolecular assemblies. The large variety of chemical structures found in synthetic copolymers allows formation of membranes with tailored properties, which have several advantages over those of liposomes, especially in their mechanical and chemical stability.

The essential building blocks of synthetic membranes - synthetic polymers - most commonly categorized into homopolymers, copolymers and polyelectrolytes and can be obtained in a laboratory environment via different polymerization procedures.[50] Polyelectrolytes are a special group of polymers that present characteristic charged functional groups, which leads to the assembly of structures based on the opposite charges of the polyelectrolyte multilayers, however these are beyond the scope of this thesis.[51] As the name implies, homopolymers are composed of repeating units of relatively low molecular weight monomers connected by covalent bonds. Block-copolymers are composed of two, three or more different blocks of covalently linked homopolymers. Once homopolymeric blocks are synthetized, two, three or more different homopolymeric blocks are linked together in a final step in order to yield the desired block-copolymer. Amphiphilicity is an essential consideration when designing a membrane forming polymer. In this respect, the amphiphilic properties of the final polymer chain are the result of different hydrophilic and hydrophobic ratio of individual types of homopolymeric blocks composing the polymer. During self-assembly the amphiphilic properties of the block-copolymers alongside with the respective lengths of polymer chains and the method used in preparation of nanoarchitectures determine if the polymer will form a membrane. The molecular properties of individual blocks as well as of the entire copolymer chain, such as the specific molar mass and polydispersity, lead to the formation of various self-assembled structures in water, including spherical, cylindrical, gyroidal and lamellar structures.[52–54] The resulting morphology of self-assembling structures in solutions is dictated by the relative fraction of hydrophobic and hydrophilic block volumes, whereas the thickness of the membrane is controlled by the overall molecular weight of the amphiphilic block copolymer. In order to favor formation of spherical structures, called polymer nano-sized vesicles (polymersomes) or GUVs (Figure 4.), the hydrophilic to whole mass balance (*f*-value), the packing parameter ($p = v/a_0 l_c$), and the polydispersity index (PDI) of the amphiphilic block-copolymer are essential parameters, which determine how the self-assembly process will take place (v = volume of hydrophobic part, a_0 = contact area of head group, l_c = length of hydrophobic part).[55,56]. *f*-ratios in a range of 25 - 45% and *p* parameters between 0.5 and 1 and a PDI around 1 favor formation of hollow sphere vesicles (Figure 4). The chemical nature of the amphiphilic copolymers plays an essential role in providing the

artificial membrane with properties that are conducive to the integration of functional biomolecules. The most commonly used amphiphilic block copolymers consist of hydrophilic blocks such as poly(acrylic acid) (PAA), poly(ethylene oxide) (PEO), poly(ethylene glycol) (PEG), poly(2-methyl-2-oxazoline) (PMOXA), or poly[L-isocyanoalanine(2-thiophen-3-yl-ethyl)amide] (PIAT), in combination with a hydrophobic block, such as polystyrene (poly(1-phenylene-1,2-diyl), polybutadiene (PB; buta-1,3-diene), or poly(dimethylsiloxane) (PDMS).[57–59]

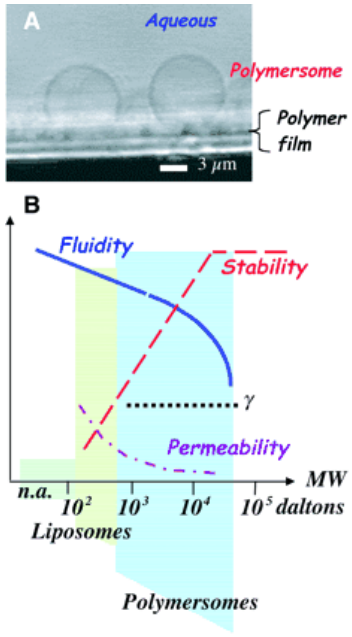

Figure 4. Polymersome formation and membrane properties. A) *Polymersome formation from a rehydrated thin polymer film.* ***B)*** *Schematic representation of membrane properties versus amphiphile molecular weight of polymers and lipids. Adapted from Discher et al. with permission.*[56]

General preparation methods of GUVs

Vesicular structures of sizes up to 1 µm self-assembled from amphiphilic phospholipids or polymers are termed liposomes or polymersomes, whereas larger cell-sized structures are termed giant unilamellar vesicles (GUVs). Because the architecture of supramolecular assemblies varies significantly with the method of formation, appropriate procedures need to be selected in order to obtain the desired structure. There are several different methods for the preparation of lipid or polymer-based GUVs (Figure 5).[60]

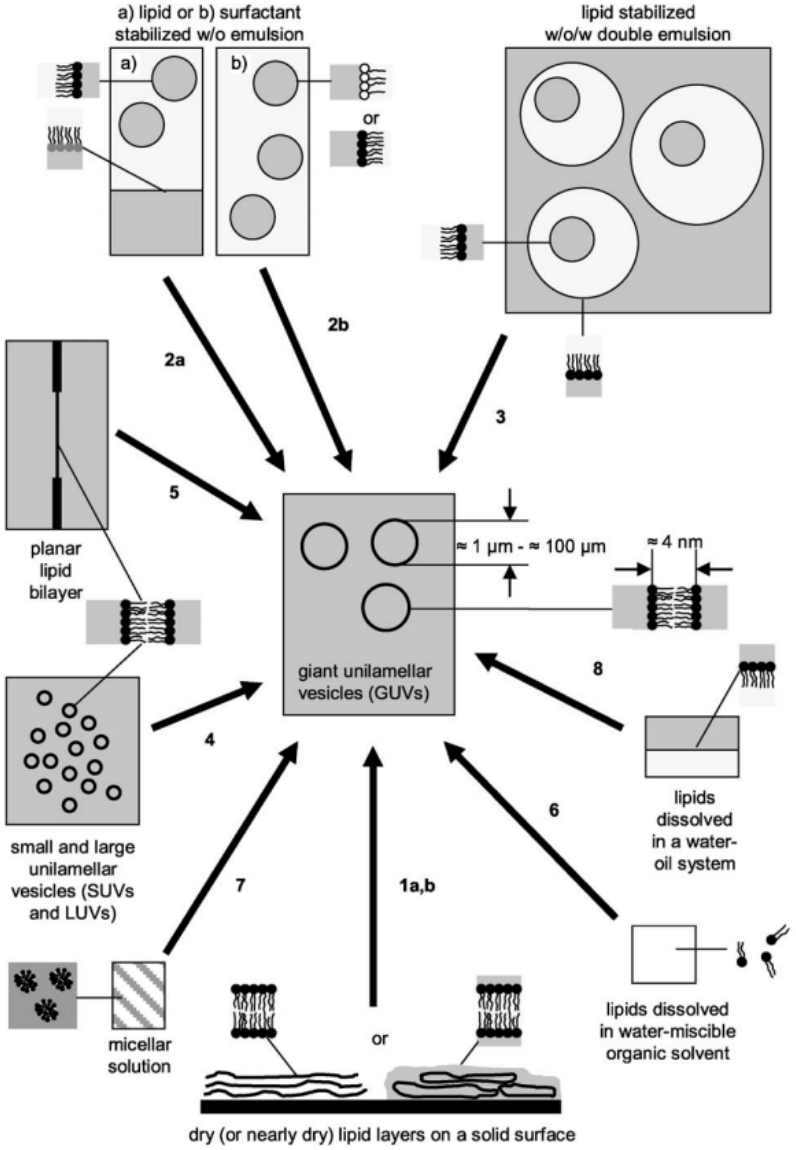

Figure 5. Commonly used lipid GUV formation methods. 1a. *Hydration of a dried thin lipid film deposited on a surface, or* ***(1b)*** *hydration in the presence of an electric field (electroformation),* ***2.*** *Conversion of a lipid-stabilized water in oil double emulsion or a surfactant-stabilized water in oil emulsion into giant vesicles,* ***3.*** *Transformation of a lipid-stabilized water/oil/water double emulsion into giant vesicles.* ***4.*** *Fusion of smaller, nano-sized liposomes into larger GUVs,* ***5.*** *Jet blowing onto a planar lipid bilayer kept between separate aqueous solutions,* ***6.*** *Mixing lipids in an organic solvent into water,* ***7.*** *Micelle formation method,* ***8.*** *Bilayer forming lipids that are present in a w/o two phase system. (Figure x). Figure and text adapted from Peter Walde et al. Chem Bio chem.*[60]

Here, the aim is to provide a general overview of the different GUV formation techniques. The conventional procedures for the formation of lipid GUVs can be easily adapted to polymer GUV formation. Although many of the methods for polymer GUV formation resemble those used for the preparation lipid GUVs, they need to be carefully adapted for

each amphiphilic block copolymer, as the thermodynamic self-assembly of polymers differs to that of lipids. Depending on the procedure and the amphiphiles (lipids / polymers), it is possible to obtain micrometer-sized GUVs that encapsulate small volumes of about ten picoliters.[55,61,62] Among other methods GUVs can be formed by the conversion of a lipid-stabilized water in oil double emulsion or a surfactant-stabilized water in oil emulsion into GUVs. More recently, microfluidic double emulsions have proven to be versatile for generating highly monodisperse GUVs.[63,64] Another emulsion-based technique is the transformation of a lipid-stabilized water/oil/water double emulsion into GUVs. Further, it is possible to fuse smaller nano-sized vesicles (liposomes / polymersomes) into larger GUVs.[60] A more straightforward approach is mixing lipids/polymers dissolved in an organic solvent into water and finally by assembly of amphiphile-based micelles into GUVs, when the co-solvent or solvent is removed or diluted.[65]

However, the two most widely used techniques that result in GUV formation involve swelling of the amphiphilic film in an electrical field (electroformation) or spontaneous swelling (film hydration). In the electroformation approach, dry polymer films (such as PMOXA–PDMS diblock copolymer and PMOXA–PDMS–PMOXA triblock copolymer films) deposited on conductive indium tin oxide glass slides form GUVs when rehydrated with 300 mM sucrose solution in an alternating sine-wave current.[66,67] If charged amphiphiles are used this method is not favorable due to the electrostatic interactions. A more suitable technique to circumvent this problem is film rehydration, where the amphiphile is first dissolved in an organic solvent, which is subsequently removed by using a rotary evaporator or high vacuum pump to yield a dry thin polymer film. Rehydration takes place by adding an aqueous solution to the dried film that leads to the detachment of the film from the substrate. Because self-assembly does not have a strong size selection regarding GUV radius, a mixture of GUVs in the size range from 1 to 40 μm is formed.

Based on their size, GUVs closely reflect cellular membrane properties and behavior, particularly with respect to membrane curvature. Similar to lipid-based GUVs, block copolymer GUVs are well suited for characterizing the mechanical and rheological properties of single- or multi-component membranes, as well as for investigating bilayer interactions. They are also easily visible under an optical microscope, and offer the possibility of directly visualizing certain interactions of encapsulated solutes and/or structures in real-time. Hybrid phospholipid/block copolymer vesicles,[67,68] in which the polymeric membrane is blended with phospholipids, combine the robustness and chemical versatility of polymersomes with

the softness and biocompatibility of liposomes. Such structures can be conveniently characterized by preparing hybrid GUVs.[69]

Cell-derived architectures

Maybe the most innovative option in constructing an artificial cell mimic is exploiting nature itself to build the cell mimic. Cell-derived vesicles (CVs) are lipid-based hollow sphere structures, shed by cells under both physiological and pathological circumstances. CVs can also be referred to as natural liposomes, consisting of a bilayer membrane that is derived directly from the cell. In this respect, various different kinds of CVs exist and range from nanometer-sized exosomes - derived from endosomal membranes of donor cells, and larger micrometer-sized giant plasma membrane vesicles (GPMVs) – derived from the plasma membrane cells.[70]

GPMVs present a particularly interesting platform, whose potential has surprisingly been left predominantly untouched.[71,71] These cell-derived micro vesicles can be produced and isolated in high quantities by chemical, salt or laser treatment of donor cells[71–73] and are formed by a local delamination of the plasma membrane from the underlying cytoskeleton, which leads to filling of the expanding area within the GPMV via a passive flow of the cytoplasm[74] (Figure 6).

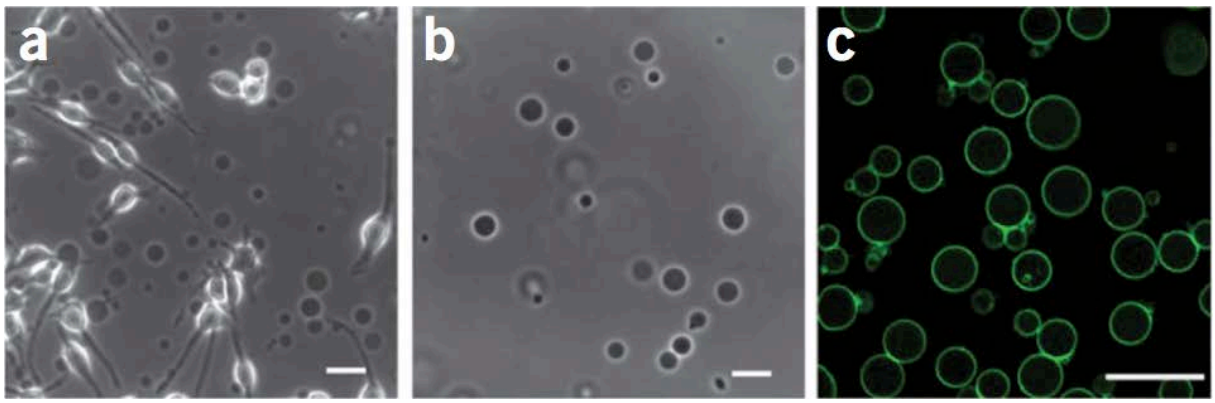

Figure 6. GPMV visualization. ***(a,b)*** *GPMVs are visualized by bright-field microscopy directly after formation* ***(a)*** *or after isolation* ***(b)****.* ***(c)*** *Fluorescence microscopy allows direct visualization of GPMVs after labeling the membranes with a fluorescent amphiphilic dye (FAST-DiO). Scale bars, 20 µm. Adapted from Sezgin et al. with permission.*[74]

Hence, both the outer membrane architecture and the inner composition of GPMVs directly mirror the composition of the cells from which they originate, but without the larger cellular organelles (i.e. nuclei, Golgi apparatus) making them the closest cell-mimic available on the

market up-to now.[75] Previously these characteristics made GPMVs improved membrane models to study the lipid composition of the plasma membrane, the behavior of functional membrane proteins within the GPMV membrane, and membrane interaction with external compounds.[76] Even more recently GPMV applications have been extended from biophysical model[77,78] to bioinspired drug delivery agents by making use of the host-cell membrane functionality.[79,80] However, up to date there no reports of studies that take advantage of the complexity of the GMPVs membrane and its compartment architecture in order to create molecular factories that act as artificial mimics of cells.

Subcompartmentalization within cell mimics

In biological cells, evolution has developed the system of subcompartmentalization (cellular organelles) within individual cells in order to allow specific reactions to take place in a spatially defined manner. This is a powerful solution, as many reactions (i.e. protein lysis, electron transport) need very specific conditions (i.e. low pH, proton gradient) to take place. When designing an artificial cell mimic, this concept has been realized by constructing synthetic multicompartmentalized sytems. The most prominent examples were based on smaller nano-sized liposomes within a larger lipid-based GUV[58], liposomes within a larger polymer-based GUV and finally smaller nano-sized polymersomes within a polymer-based GUV (Figure 7).

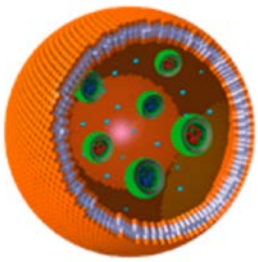

Figure 7. Subcompartmentalization within artificial cells. *Smaller polymersome sub-compartments encapsulate enzymes and diffuse freely within the cavity of a larger polymer GUV. Adapted from Peters et al. with permission.*[16]

By applying the principle of multicompartmentalization *in vitro* an artificial cell mimic is created with artificial organelles – successive enzymes of an enzymatic cascade reaction are separated within different sub-compartments in a larger polymeric GUV. This facilitates the diffusion of reagents and products between the sub-compartments, while confining the enzymes to their individual subcompartments. However, for the creation of an artificial cell

mimic by multicompartmentalization, every membrane of the different compartments has to be selectively permeabilized. This would allow a higher control of the diffusion of substrates and products across all involved membranes. To realize this, the knowledge of membrane protein reconstitution in artificial membranes is required.

Characterization of cell mimics

Because of the great variability of structural materials used in the construction of cell mimics (amphiphilic block copolymers, lipids or cell-derived materials) careful characterization of the system is required with respect to membrane properties, size, structure and functionality. Membrane properties, such as permeability, elasticity, and surface charge, are especially important parameters in many applications. Several methods are commonly applied to characterize vesicular structures (liposomes, polymersomes, lipid/polymer GUVs and GPMVs)[81,82] including various electron microscopy (EM) techniques, which allow direct visual inspection of these structures. In particular, cryo-EM, which avoids the drying and staining artifacts associated with conventional transmission or scanning EM, provides information on size, morphology, and membrane thickness of the vesicular assemblies.[83] Atomic force microscopy (AFM) measurements reveal mechanical characteristics in addition to morphology.[84] Light/fluorescence/confocal laser scanning microscopy can be used to visualize GUVs and follow their integration *in vivo*. Fluorescence correlation spectroscopy (FCS) can be utilized to analyze fluorescently labeled structures (i.e. lipids, polymers or proteins), providing data on lateral diffusion coefficients and molecular organization in GUV membranes[83], and on the number of antibodies coupled to artificial membranes.[85] Due to their cell-like size, GUVs can be subjected to flow cytometry analysis and analyzed in terms of size and fluorescent properties.[86] The whole-cell patch clamp technique also applies to GUVs and can be used to measure current and voltage of intact GUVs (Figure 8).[87]

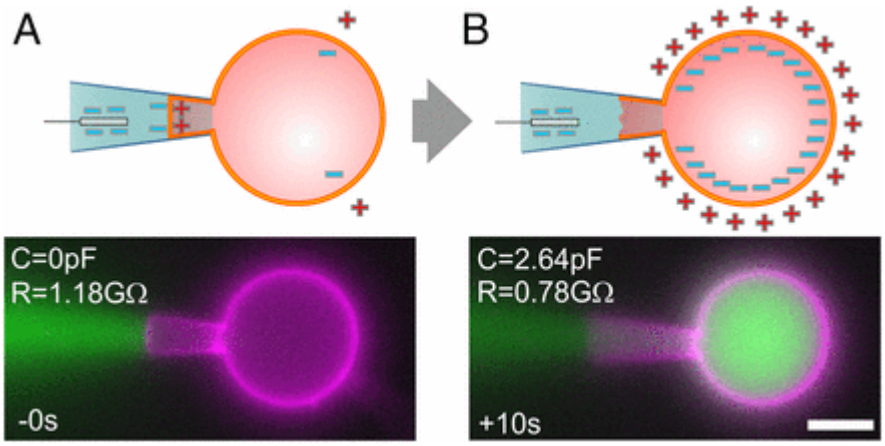

Figure 8. Whole GUV Patch-clamp technique. A) *GUV-Attached method: The adhesion between the GUV membrane and micropipette inner surface leads to an electrical seal (R> 1GOhm).* ***B)*** *Whole-GUV method: To access the GUV interior while establishing the electrical seal resistance the pipette pressure is adjusted before breaking the membrane patch with a voltage pulse. A low molecular weight fluorescent dye (Carboxyfluorescein – Green) can enter the GUV from the pipette. The capacitance increases, since the micropipette now controls the transmembrane voltage, current and tension of the whole GUV membrane. Adapted from Garten et al. with permission.*[87]

Among the diverse scattering methods, static and dynamic light scattering (SLS, DLS) are predominantly employed to assess molecular mass and radius of gyration (SLS), and hydrodynamic radius and size distribution (DLS) of nano-sized polymersome samples, but are not suitable for GUVs, due to their size and subsequent sedimentation behavior. Zeta potential measurements provide information about the surface charge of artificial membranes under various conditions.[88] Artificial cell mimics may be characterized with respect to their membrane permeability[89–92], or responses to various external stimuli such as temperature, pH, redox potential, or the presence of biomolecules (e.g., saccharides, nucleotides).[93–96] Moreover, if endowed with biological functions by the insertion of membrane proteins, artificial cell mimics can be characterized by functional assays related to the embedded proteins.

HYBRID SYSTEMS – ARTIFICIAL CELLS EQUIPPED WITH BIOMOLECULES

In order to increase the functionality of the cell mimic lipid- and polymer-based artificial membrane systems have previously combined with numerous different biomolecules (proteins, DNA, polysaccharides or their combinations.[1,62]

Lipid-based biomimics

Lipid-based systems have previously spearheaded the field of biomolecule equipped artificial cells, due to the relative accessibility of lipids to several research groups in the world and maybe even more significantly due to the proximity of lipid membranes to biological cell membranes. As this thesis focuses primarily on synthetic membranes equipped with biomolecules and cell-derived structures, only the most prominent examples of lipid structures equipped with biomolecules are presented here. The first report of a functionally reconstituted membrane protein in lipid membranes dates back to 1971 where the transmembrane ATP-Pi exchange was catalyzed by the mitochondrial proton translocating ATPase in artificial lipid membranes.[97] Since then established techniques of membrane protein reconstitution have been improved and new, more sophisticated methods developed (Figure 9).[98,99]

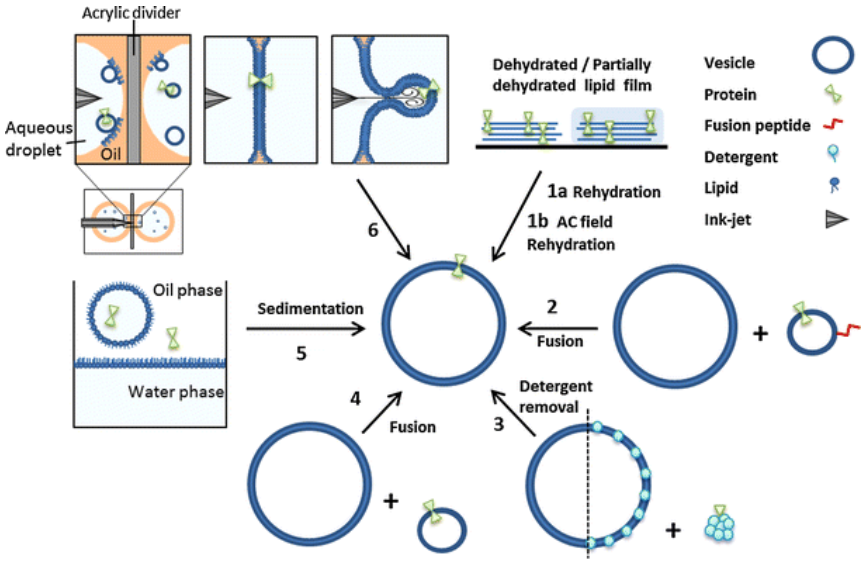

Figure 9. Schematic representation of the methods used for preparation of proteo-GUVs *(not to scale).* ***(1a) Spontaneous swelling:*** *Dehydrated or partially dehydrated biological membranes, proteoliposomes or lipid/protein solutions are rehydrated.* ***(1b) Electroformation:*** *Dehydrated or partially dehydrated biological membranes,*

proteoliposomes or lipid/protein solutions are rehydrated under the influence of an AC-electrical field. ***(2) Peptide-induced fusion:*** *Fusion of preformed GUVs and proteoliposomes are induced by a fusion peptide conjugated to the liposomes.* ***(3) Direct (detergent-mediated) reconstitution:*** *Purified and detergent solubilized protein is added to preformed GUVs prepared from lipids or lipids and detergent.* ***(4) Spontaneous fusion:*** *Preformed GUVs are incubated with proteoliposomes.* ***(5) Droplet transfer method:*** *Droplets coated with a lipid monolayer are formed and sedimented through a water phase lined with a lipid monolayer, resulting in bilayer GUVs. Protein is either added to the intra-vesicular or extra-vesicular solution depending on the desired protein orientation.* ***(6) Microfluidic jetting:*** *Two aqueous droplets are introduced in an oil-filled custom chamber divided by an acrylic spacer. Lipid monolayers form at the oil-water interfaces with protein and lipids deriving from proteoliposomes. When the spacer is removed, the monolayers merge into a planar lipid bilayer from which GUVs are blown using the nozzle of an ink-jet printer. Text and figure adapted from Jørgensen et al. with permission.*[99]

For the incorporation of transmembrane proteins in GUVs, main methods involve the assembly of GUVs from a dried film of lipid and proteins by spontaneous swelling or by electroformation.[98] For this technique to work, relatively "robust" proteins are required that retain function and structure after drying. Further only membrane proteins, which do not need a specific orientation can be applied, because during the self-assembly process of GUVs the protein orientation is lost and likely symmetrical.

A very promising approach towards the design of cell membrane mimics was shown by the direct incorporation of solubilized membrane proteins in preformed GUVs. GUVs containing complex, biologically relevant internal solutions are formed in the presence of a subsolubilizing concentration of detergent. Next, membrane proteins can be unidirectionally inserted in these GUVs, followed by the detergent removal step.[100] Despite the higher success rates of the incorporation of proteins by this technique, there is the disadvantage that some of the proteins aggregate during the reconstitution process due to the low amount of detergent or more critically that the detergent molecules used in the reconstitution effect the GUV architecture.

Applying the latest mentioned technique allowed the development of lipid GUVs with the reconstituted membrane protein bacteriorhodopsin (BR), a light-induced proton pump that produces a transmembrane-stable and light-switchable electrochemical gradient of protons.[112,113] To visualize the functionality of BR, lipid GUVs with an encapsulated pH-responsive dye (pyranine) were produced. After the incubation with fluorescently red-labeled BR micelles, the detergent was removed. The internal pH variation due to the proton transfer

across the lipid membrane could be measured with the help of the pH sensitive pyranine dye (Figure 10).[100]

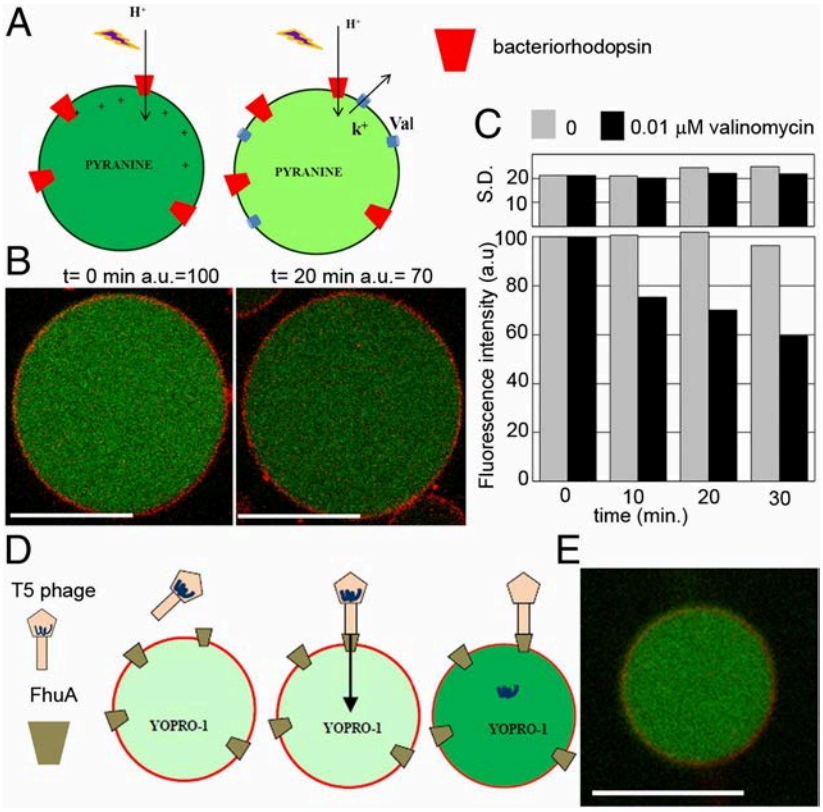

Figure 10. Direct incorporation of solubilized transmembrane proteins in GUVs. *Reconstitution of red-labeled bacteriorhodospin, a photoactivable proton pump, in DOTM destabilized EPC–EPA GUVs.* ***(A and B)*** *After detergent removal, light-induced proton pumping induces an internal acidification of GUVs.* ***(C)*** *Normalized pyranine fluorescence intensity and variance in the presence (black columns, n = 350) and in the absence (gray columns, n = 440) of valinomycin.* ***(D)*** *Schematic representation of the reconstitution of FhuA, a T5 phage receptor, in red-labeled EPC GUVs encapsulating YOPRO-1, a green fluorescent DNA probe.* ***(E)*** *After binding of T5 phage to FhuA, DNA is injected inside GUVs (Scale bars: 10 µm). Text and figure adapted from Dezi et al. with permission.*[100]

A more complex reconstitution example was shown with the *Escherichia coli* outer membrane protein FhuA. This receptor was functionally reconstituted into lipid GUVs even though there are several partners needed for the functional assay. Starting with the encapsulation of a green fluorescent probe, with enhanced fluorescence after binding to DNA, into lipid GUVs, followed with the incorporation of FhuA into the membrane, followed by the incubation with T5 phage, a large increase of the green fluorescence inside the cavity of GUVs could be observed. This proved the functional reconstitution with a defined orientation.[100]

Another strategy for the reconstitution of transmembrane proteins in GUVs was achieved by fusion of native membranes or proteoliposomes with lipid GUVs.[100] This detergent-mediated fusion resulted in GUVs with incorporated membrane proteins (Figure 11). Interestingly the orientation of the membrane proteins reconstituted in the membrane of GUVs stays the same as in the native vesicles.[101]

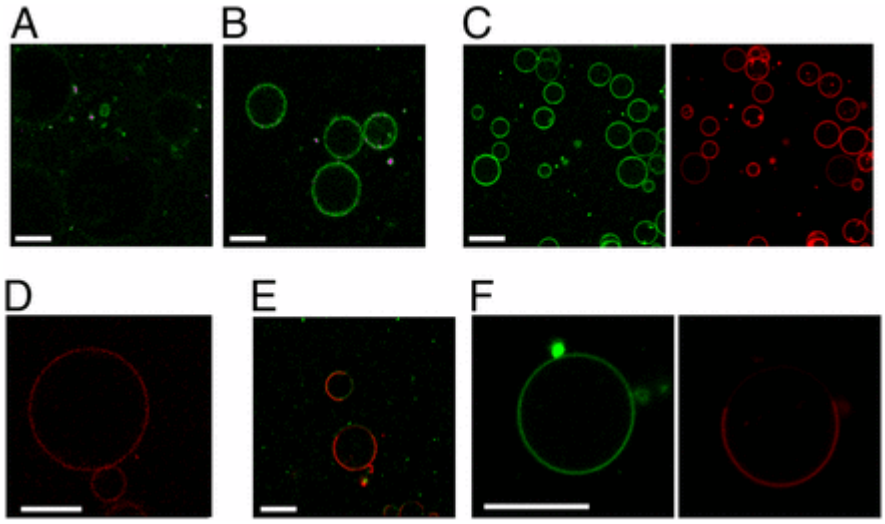

Figure 11. Incorporation of transmembrane proteins by fusion of native membranes with GUVs. *Fusion of green-labeled inverted inner vesicles (IMVs) of E. coli containing overexpressed BmrC/BmrD, a multidrug resistance transporter to nonlabeled EPC–EPA GUVs in the absence* ***(A)*** *or the presence* ***(B)*** *of 300 μM Triton X-100.* ***(C)*** *Fusion of green-labeled chromatophores to DOPC/DOPE GUVs containing Tx-red–labeled lipid.* ***(D)*** *Fusion of proteoliposomes containing red-labeled bacteriorhodopsin to unlabeled DOPC/DOPE GUVs in the presence of 300 μM Triton Xk00.* ***(E and F)*** *Fusion of green E. coli IMVs to red-labeled GUVs containing lipid domains of DOPC/sphingomyelin/cholesterol, in the absence* ***(E)*** *or in the presence* ***(F)*** *of 300 μM Triton X-100 (Scale bars: 10 μm). Text and figure adapted from Dezi et al. with permission.*[100]

To prove the functionality of membrane proteins, which are reconstituted via this fusion technique, the bacterial heterodimetic ATP-binding cassette efflux transporter BmrC/BmrD was incorporated into membranes of GUVs after DNA was encapsulated in their cavities. The addition of ATP to the external solution induced the transport of ethidium bromide to the inner cavity of the GUVs, where it could bind to DNA resulting in an enhancement of its fluorescence (Figure 12).[100]

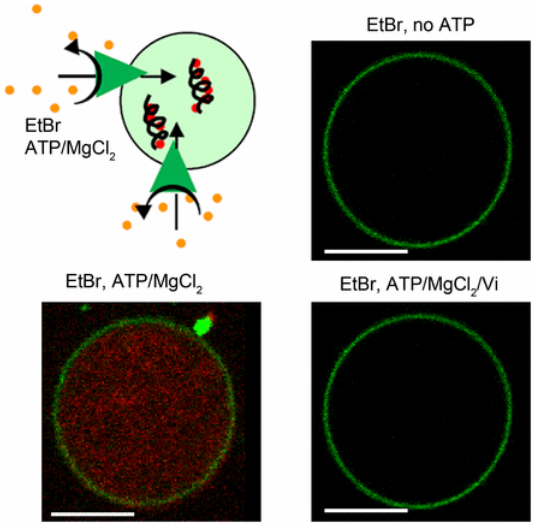

Figure 12. Drug transport by BmrC/BmrD, a bacterial ABC transporter in GUVs. *EPC/EPA GUVs are grown encapsulating DNA before incorporation of BmrC/BmrD by fusion of green E. coli IMVs. Addition of ATP induces the translocation of ethidium bromide (EtBr) and its binding to DNA induces an enhancement of its fluorescence. The transport is inhibited by addition of orthovanadate (Vi), a specific inhibitor of BmrC/BmrD (Scale bars: 10 μm). Text and figure adapted from Dezi et al. with permission.*[97]

Recent advances have lead towards GUV systems with complex lipid compositions and controlled lipid asymmetries that enabled detailed studies of membrane protein structure and function in cell-like model membranes.[102]

The final example presented in the chapter of functional membrane protein reconstitution into GUVs deals with the ATP synthase (F1F0-ATPase), which is a rotating transmembrane protein complex. Reconstituted into lipid GUVs, it synthesizes ATP through proton-pumping activity across the lipid membrane. The proton outward translocation through F1F0-ATPases could be visualized by encapsulating a pH-sensitive fluorophore (pyranine) within the GUVs, which allows a change of pH to be detected as a change in fluorescence signal. Therefore, the insight of the GUV cavities shows an increased fluorescence when proton pumping takes place (Figure 13).[103]

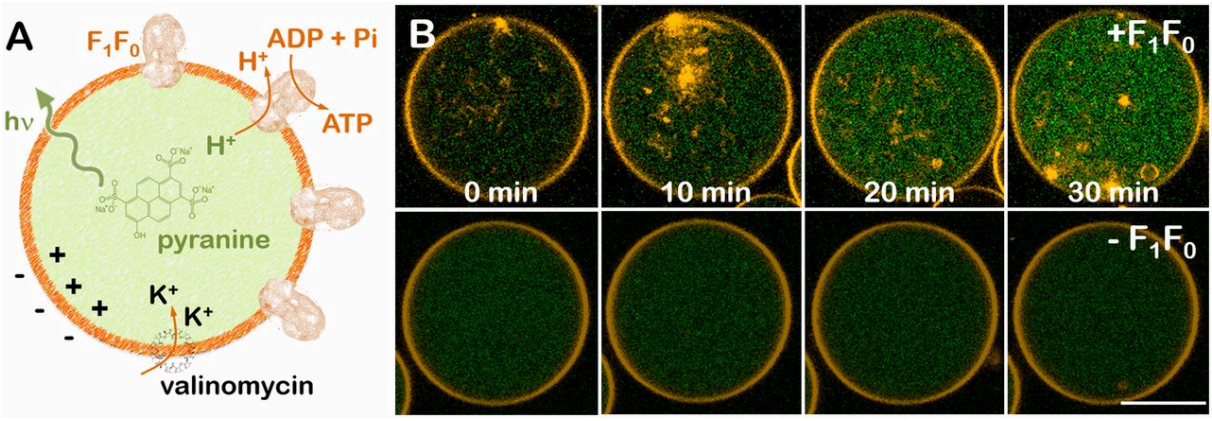

Figure 13. ***Reconstitution of the E. coli F1F0-ATPase in GUVs. A)*** *Schematic cartoon of F1F0-ATPase reconstitution into giant vesicles (Left). ATP synthesis is triggered on valinomycin incubation that creates a membrane potential, positive in the lumen of the vesicle. Proton outward translocation through F1F0-ATPases is monitored by the pH-sensitive fluorophore pyranine (green). The lipid bilayer was doped with 0.5% mol RhPE (orange dye).* ***B)*** *Proton efflux kinetics of E. coli GUVs on valinomycin incubation as observed under fluorescence microcopy, in the presence (Top) and in the absence (Bottom) of F1F0-ATPases (Scale bar: 10 microns). Text and figure adapted from Almendo-Vedia et al. with permission.*[103]

In addition, it was obtained that ATP synthase rotates at a frequency of about 20 Hz. The rotation of F1F0-ATPase promotes fluctuations at certain parts of the GUV membranes. This phenomena was observed as a reduction in the bending stiffness and the associated lowering of its surface tension of the GUV membrane, establishing that there is a direct link between microscopy protein activity, supramolecular organization, and macroscopic mechanics of the GUV membrane.

All these examples of the shown methods for the reconstitution of membrane proteins into the membranes of lipid GUVs should apply to a wide variety of membrane or peripheral proteins for producing more complex biomimetic GUVs.

Polymer-based biomimics

Using synthetic polymer membranes as a platform for the incorporation of biomolecular gateways has gained considerable interest since the first polymersomes were published in 2000.[104] Selective permeability of artificial membranes, most importantly the exchange of energy, solutes and molecules across the membrane, is a prerequisite for many technological, bioengineering, and biomedical applications. Although by themselves, polymer membranes exhibit lower permeability compared to lipid membranes, it is possible to modify molecule

transport through them by choosing appropriate polymers that favor porous membrane formation, or by chemical modification of the artificial membranes to induce pore formation. More significantly, functional insertion of ion-channels, transporters and pore-forming peptides and membrane proteins into synthetic polymer membranes presents a biomimetic strategy for membrane permeabilization.[66]

Even though, numerous protein reconstitutions have been successfully implemented with lipid membranes of GUVs, these methods are not readily applicable to synthetic copolymer membranes. A reason for this is the different physicochemical properties of polymer membranes, such as flexibility and fluidity, strongly affect membrane-protein-detergent interactions.[34,55] Polymer GUVs are more sensitive towards disruption by detergents used in membrane protein reconstitution methods. In addition, a key parameter for protein functionality is the lateral mobility within membranes, which largely depends on the flexibility and fluidity of the membrane.[105]

Further, compared to lipid membranes, synthetic polymer membranes have a much higher molecular mass and therefore a considerably thicker membrane, which results in a mismatch in length between the hydrophobic domain of the copolymer membrane and the membrane-spanning hydrophobic domain of the biomolecule.

Smaller nano-sized polymersomes are the preferred nano-objects for the development of pilot polymer-based bio hybrids because they are significantly more stable than GUVs, due to their smaller size and resulting higher surface tension.

Significant progress in understanding the mechanisms of reconstituting membrane proteins in nano-sized polymersome membranes and developing corresponding procedures have been reported recently, thus improving the success rate for preparing polymer membranes with functional protein entities.[106] Nevertheless, optimal reconstitution procedures for GUVs still have to be established empirically for each membrane protein and polymer membrane, and this is often a painstaking endeavor. A substantial mismatch has been overcome in specific conditions of synthetic membranes, resulting in successful insertion of various biopores and membranes proteins.

Interestingly, incorporation of biomolecules can influence the morphology of the synthetic supramolecular assembly. For example, increasing the concentration of the water channel Aquaporin 0 (Aqp0) leads to a change in morphology from spherical structures to planar membranes with PEO-PB or PMOXA-PDMS-PMOXA membranes, which can be 10 times thicker than lipid membranes (Figure 14). These functional Aqp0 molecules remained active up to a 1:1 protein to polymer ratio where initiation of crystallization was observed.[107,108]

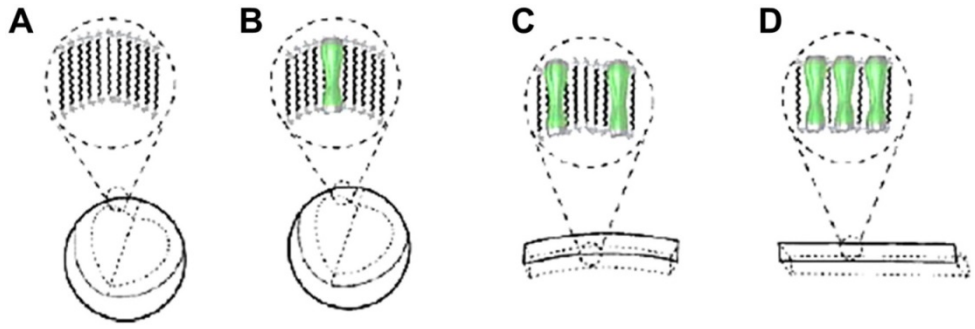

***Figure 14**. **A model illustrating the behavior of Aqp0 in PEO-PB polymer membranes.** The concentration of Aqp0 (ABA42) affects the membrane morphology. **(A)** In the absence of ABA42, **(B)** 15.5 M ABA42, **(C)** 3.9 M ABA42, **(D)** 1.3 M ABA42. Increasing the amounts of protein in the polymer membrane (left to right) leads to changes in the structure from spherical (vesicle) to planar membranes, and ultimately to a crystalline structure. Adapted from Kumar et al. with permission.*[108]

In order to understand the molecular factors that affect the mobility of membrane proteins within synthetic membranes, the lateral diffusion of both the polymer chains and the membrane proteins have been investigated using a small library of diblock and triblock copolymer membranes based on PMOXA as hydrophilic block and PDMS as hydrophobic block (Figure 15).[83,109] A number of fluorescently labeled membrane proteins (AqpZ, OmpF and prokaryotic K+ ion channel (KcsA)) were successfully reconstituted in PMOXA-PDMS and PMOXA-PDMS-PMOXA GUV membranes, where they exhibited a lateral diffusion similar to that of the polymer chains in the membrane, but an order of magnitude slower than in lipid membranes.[83,109] This study revealed that a significant flexibility of the membrane is necessary to overcome the high hydrophobic mismatch between the membrane thickness (9–13 nm) and the 3.5–5 times smaller proteins (3.3–7.1 nm) to allow successful insertion of membrane proteins. Owing to the PDMS flexibility, such synthetic polymer membranes provide a fluid environment that can adopt conformational changes in order to incorporate the proteins in a functional state.[83,110]

Despite the proof that all these membrane proteins (KcsA, AqpZ and OmpF) were successfully reconstituted into triblock copolymer membranes of GUVs, the functionality of the reconstituted membrane proteins was not addressed in this study.

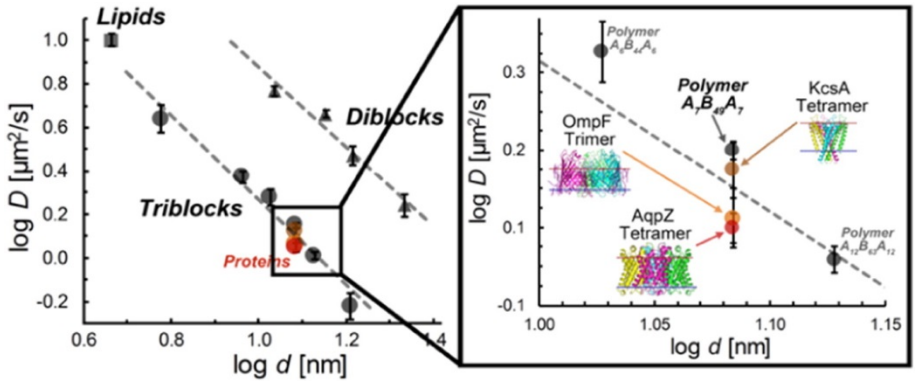

Figure 15. Log − log plots displaying the diffusion coefficient D relative to membrane thickness d. *Lipids are shown as squares and triblock copolymers as circles. The membranes self-assembled from different triblock copolymer have different molecular weights and thus different membrane thicknesses. The dashed line represents the power law dependence of the diffusion coefficient in relation to the membrane thickness as D ∼ d− 1.25. The zoomed area illustrates diffusion coefficients for KcsA (green), AqpZ (red), and OmpF (blue) within the three different ABA membranes (ABA34, ABA49, ABA63). Text and figure adapted from Itel et al. with permission.* [83,109]

Functional reconstitution of biomolecules in the membrane of GUVs

Insertion of biopores into polymer membranes of GUVs induces permeability to specific ions/molecules, i.e. renders the GUVs selectively permeable. The first example of a PMOXA-PDMS-PMOXA-based GUV (1–2 μm dimensions) membrane that was permeabilized for Ca^{2+} ions was obtained by inserting an unselective ionophore, Lasalocid A, and the highly selective ionophore N,N-dicyclohexyl-N′,N″-dioctadecyl-3-oxapentane-1,5-diamide.[90] In addition, the channel forming peptide alamethicin that transports cations and anions unselectively was inserted into PMOXA-PDMS-PMOXA membranes of GUVs.[90] The spontaneous insertion of these three ionophores was achieved by adding the ionophores in ethanol to the preformed GUVs, which led to ion carrier-assisted precipitation of calcium phosphate inside their cavities. This concept of combining synthetic membranes with natural membrane proteins can serve as a new platform for biomimetic mineralization. Calcium carbonate precipitation induced within polymer GUVs was triggered by the calcium-selective ionophore calcimycin, which induced a calcium influx into carbonate-containing GUVs and opened the way towards the development of efficient microreactors.[111] However, systems based on GUVs in general cannot be used for medical applications because of the size and instability of these cell-sized polymer structures.

Functional reconstitution of membrane proteins in polymer membranes of nm-sized vesicles

Despite the number of examples of lipid GUVs equipped with membrane proteins, there is no study regarding the functionality of a reconstituted membrane protein into polymer GUVs. However, it was possible to reconstitute membrane proteins with preserved functionality in the polymer membranes of nanometer-sized vesicles. For example the 26 kDa alpha-helical model membrane protein bacteriorhodopsin (BR), a light-driven proton pump, that depends on a specific orientation for functionality. It generates an electrochemical proton gradient by converting the potential energy of incident photons and is usually found in two-dimensional crystalline patches known as "purple membrane" (PM). Its functional reconstitution into PEtOz-*b*-PDMS-*b*-PEtOz (PEtOz, poly(2-ethyl-2-oxazoline) polymersome membranes, allowing transmembrane proton pumping, has been achieved during the polymer membrane self-assembly step.[112,113] The simultaneous embedding of BR and F0F1-ATP synthase has been proposed to convert photon energy to chemical energy in response to external illumination.[112] In a cascade of orchestrated reaction steps, BR generates a pH gradient across the membrane, and together with the molecular motor protein F0F1-ATP synthase, this proton gradient is used to drive the conversion of ADP and inorganic phosphate into ATP (Figure 16).[113] Because of its high photochemical efficiency, thermal stability and cyclicity, BR is of great interest for the development of bioelectronics devices, such as photonic materials in optical memories, drug delivery, biocatalytic reactors, fuel cells, and nanomachines.[114]

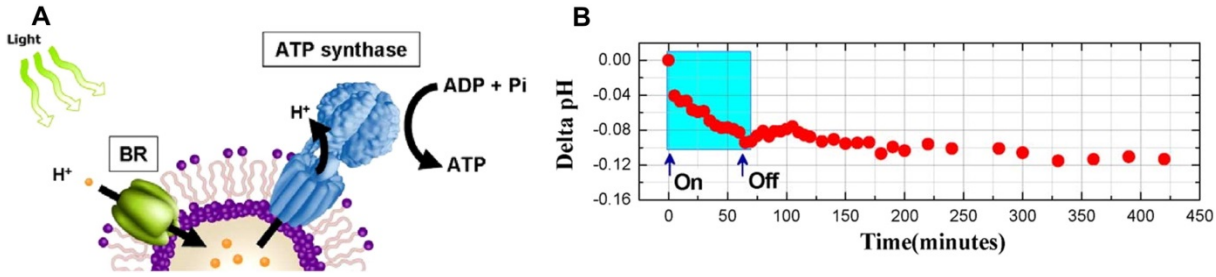

Figure 16. (A) *Schematic representation of bacteriorhodopsin (BR) and F0F1-ATP synthase reconstituted in a proteopolymersome.* ***(B)*** *Photoresponsive behavior of BR-ATP synthase-proteopolymersomes: pH change during and after illumination. Adapted from Choi et al. with permission.*[113]

This example shows that in general the functional membrane protein reconstitution in polymer membranes can be realized. Even further, it was possible to create small nanoreactors, meaning membrane protein equipped polymersomes with ecapsulated enzymes. Substrates can enter their cavities, react with the enzyme and the product converted by the enzyme can be released afterwards.

This concept was realized by building a tuneable catalytic compartment space, developed by the encapsulation of horseradish peroxidase (HRP) in PMOXA-PDMS-PMOXA polymersomes with a membrane containing a pore (OmpF) that was chemically modified with a pH-responsive molecular cap. Opening the OmpF "gate" by a change in pH led to the influx of Amplex UltraRed and induced peroxidase activity (Figure 17).[115] Catalytic compartment spaces with trigger-based activity represent ideal candidates when a specific step in the flow of an artificial cell requires a reaction activated "on demand", i.e. by the presence of a specific stimulus.

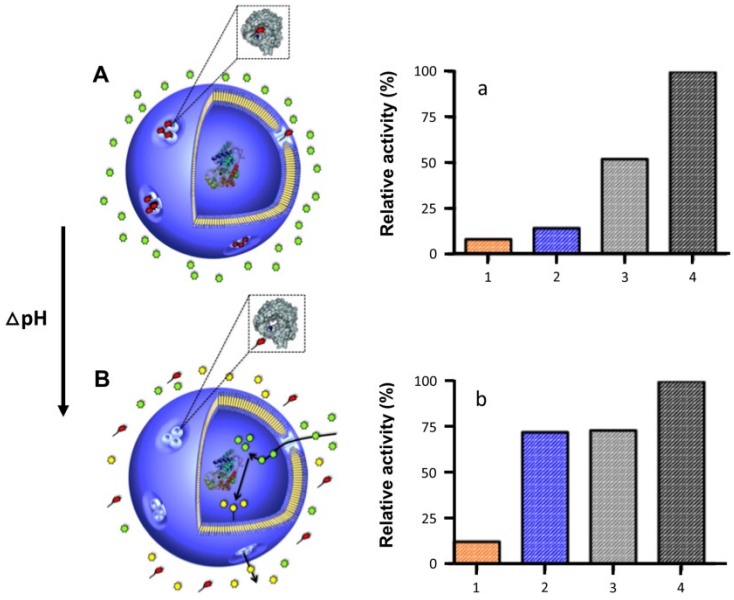

Figure 17. A) *Concept of a catalytic compartment space with activity triggered by a chemically engineered protein "gate" inserted in the synthetic membrane of a polymersome. A change in pH induces the release of the sensitive molecular cap (red dots) from the protein "gate", allowing substrates (green dots) to enter, and the products of the enzymatic reaction (yellow dots) to be released.* ***B)*** *Substrate Amplex UltraRed conversion kinetics of catalytic compartment spaces equipped with different OmpFs: OmpF blocked with a pH-responsive molecular cap (blue), OmpF with pH-responsive molecular cap released (grey), Ompf-WT (black), and unpermeabilized catalytic compartment spaces (orange) at pH 5.5, at time 0* ***(a)*** *and after 1 h* ***(b)****. Text and figure adapted from Einfalt et al. with permission.*[115]

GAP IN KNOWLEDGE

The possibility to use GUVs with functional reconstituted membrane proteins as cell-mimics appears as a realizable vision considering the state of the art for reconstitution of membrane proteins into nano-sized polymer vesicles. Previous research demonstrated that the mismatch between the thick polymer membrane (di- or triblock) and the small membrane proteins, can be overcome if the polymer membrane has a high flexibility and fluidity. The latter allows entanglement, integration and protection of the membrane proteins within the synthetic membrane, while at the same time stretching and compressing in the area of a small biomolecule to preserve its active conformation should be possible. Unfortunately, reconstitution methods for membrane proteins used for polymer vesicles in the nanometer range (polymersomes) are not easy adapted to polymer GUVs, even if the same polymer is used. A reason for this are the GUV formation techniques. Whereas polymersome membranes can be stirred, disrupted, reassembled and further purified with the help of dialysis and filtration, these techniques are limited in the case of GUVs. The major cause for this is that their membrane thickness versus their total size ratio (keep in mind by using the same polymer the membrane thickness is not changing, only the size of the total compartment and therefore the inner cavity). This is also the reason why smaller compartments are always more stable than bigger ones and stirring (applying mechanical stress) rapidly decreases the amount of GUVs in solution.

Another reason which makes the work with GUVs more complicated is that several measurements or treatments are not useful at all as for example extrusion to get a homogeneous size distribution, which is quite often used in the case of polymersomes, it would not make sense to use this technique for GUVs. GUVs with homogeneous sizes can only be achieved with the microfluidic technique for GUV formation, which is a very new and not so well-established method. Regarding purification methods, techniques that allow the separation of nano-sized polymersomes from GUVs are scarce and rudimental. Therefore, measurements and techniques used for cells are more useful when working with GUVs, due to the comparable sizes and morphologies of GUVs to cells. This brings us back to lipid GUVs, where a lot of membrane proteins could be functionally reconstituted into their membranes - the measurement techniques used in lipid GUV characterization can be directly applied on polymer GUVs. However, the lipid membranes are orders of magnitude thinner and more robust against detergents, used in membrane protein reconstitution, than membranes of polymer GUVs. Approaches of membrane protein reconstitution cannot be

easily adapted for polymer GUVs. Nevertheless, by combining the knowledge of membrane protein reconstitution into membranes of both, lipid GUVs and nanometer-sized polymersomes, the design of polymer GUVs with functional reconstituted membrane proteins or biopores may/could be realized. Finally, cell-derived giant plasma membrane vesicles (GPMVs) are promising candidates towards the design of artificial cells due to their native cell membrane and the cell plasma inside their cavities. By modifying membranes of GPMVs by genetic modification of donor cells we can equip them with specific functional membrane proteins and at the same time encapsulate functional nano-sized compartments (i.e. membrane protein equipped polymersomes with encapsulated enzymes) inside their cavities the design of the closest cell mimic up to now may/could be created.

Chapter 2

AIM OF THE THESIS

The aim of this thesis is to advance the state of the art in development of cell mimics, with the focus on designing giant unilamellar vesicles (GUVs and GPMVs) with inserted functional biomolecules or membrane proteins used as a platform to get a deeper insight into biological processes. Due to their size in the micrometer range, which corresponds to the size of native cells, GUVs have the unique advantage that they can be visualized and analyzed by microscopy techniques thereby allowing insight into compartmentalized processes in real-time. Besides GUVs formed out of synthetic lipids there are only a few examples/studies done in the direction towards using synthetic polymer GUVs with reconstituted biomolecules inside their synthetic membrane. In Nature, biomolecules (transmembrane proteins, pores, etc.) are well adapted for the native cell membranes in which they are present with preserved functionality. An environment, which is only slightly different from the biological one can lead to the denaturation of the biomolecule or the disruption of the environment into which the biomolecule is inserted. This makes the insertion of biomolecules into artificial membranes so difficult. Nevertheless, a great scientific interest remains, as especially membrane proteins play a crucial role in fundamental cell processes, which are up to now unknown. However, there are many unanswered questions in this research field like: How do biomolecules (enzymes, proteins, substrates) behave inside confined compartments with sizes that mimic cells? Is there any interaction between encapsulated compounds and compartment membranes? Do encapsulated compounds diffuse freely inside the cavities, or are they attached to the membrane? If so, does this possible interaction affect the activity and stability of the encapsulated compounds? Development of advanced functional compartments requires detailed responses to such questions in order to understand the complexity and specificity of natural bio-compartments. These questions are addressed in this work by using cell-sized GUVs for the visualization of interactions and diffusion behavior of encapsulated compounds, further membrane interactions in real-time with the help of microscopy techniques. Therefore pores and membrane proteins are inserted into the membranes of polymer GUVs to visualize their functionalities. In addition cell-derived micrometer-sized giant plasma membrane vesicles (GPMVs) present a particularly interesting platform,

because both the outer compartment architecture of GPMVs (membrane) and the inner composition of GPMVs directly mirror the composition of cells from which they originate, but without the larger organelles like for example nuclei and Golgi apparatus making measurements easier and the closest cell mimic available up to now. By using these GPMVs, a strategy for creating the first bioinspired molecular factory with functionality as cell mimic is introduced and executed.

Chapter 3

SYNTHETIC GUVS WITH ENGINEERED PROTON SELECTIVE PERMEABILITY AS STIMULI-RESPONSIVE COMPARTMENTS

Following a biomimetic approach, we present here in this first chapter synthetic giant unilamellar vesicles (GUVs) with proton selective permeability, achieved by inserting gramicidin (gA) biopores in their polymer membrane. Encapsulation of a pH-sensitive dye inside the cavity of GUVs was used to assess the proper insertion and functionality of gA inside the synthetic membrane. Confocal laser scanning microscopy (CLSM) was used to show that neither the size, nor the morphology of the GUVs was affected by successful insertion of gA. Interestingly, proper insertion and functionality of gA were demonstrated for membranes with thicknesses in the range 9.2–12.1 nm, which are significantly greater than membrane lipid counterparts. GUVs with inserted gA exhibited efficient time response to pH-changes and therefore are ideal candidates for designing bioreactors or biosensors for a variety of applications in which changes in the environment, such as variations of ionic concentration or pH, are required.

This study has been published: Mihai Lomora, Martina Garni, Fabian Itel, Pascal Tanner, Mariana Spulber, Cornelia G. Palivan*. Polymersomes with engineered ion-selective permeability as stimuli-responsive nanocompartments with preserved architecture, Biomaterials, (2015), Volume 53, pages 406-414.
DOI: 10.1016/j.biomaterials.2015.02.080

MOTIVATION AND PROBLEM DEFINITION

Compartmentalization is crucial for biological systems as it allows spatial localization of molecules within defined spaces. Furthermore an eukaryotic cell has the majority of its volume retained by intracellular membranes in discrete compartments known as cell-organelles, an essential feature for cellular metabolism.[38] Compartmentalization through confinement of compounds can be achieved using nanoscale and microscale synthetic structures. These have previously been used to transport sensitive molecules in conventional drug delivery approaches[93,116], function as nanoreactors[117], biosensors[118], or artificial organelles[119]. Synthetic nanocompartment spaces with encapsulated catalytically active compounds (i.e. enzymes) in their inner cavities have been shown to increase efficacy of polymerization reactions[120] and catalysis[121,122] offer protected space for consecutive enzymatic reactions[16], serve as source of reactive oxygen species, or provide twofold functionality (oxygen storage and detoxification of peroxinitrites)[117]. Polymeric vesicles (polymersomes, polymer giant unilamellar vesicles) have spearheaded the field of artificial compartmentalization and have found numerous applications in different scientific fields, because they are more robust and versatile than their lipid analogs.[123] An additional advantage of polymeric vesicles is the possibility to regulate their properties (size, morphology) by changing the polymer composition, functionalizing the polymer end groups for targeting approaches, or introducing stimuli-responsiveness. Especially GUVs are very appealing platforms for the construction of rudimental cell mimics due to their micrometer sizes, which allow us to visualize them by microscopy techniques. Therefore, they are a useful platform to get a deeper insight into biological processes in real-time.

As described in the introduction of this thesis, most of the advances in designing custom-made polymer vesicles have been made on assemblies in the nanometer ranges, due to their relatively high stability when compared to microscale systems. Among others, these have been designed to respond to specific stimuli, such as pH[124], temperature, light[125], enzyme[16,126] or a combination of thereof[127,128]. Responsive polymeric assemblies can be created by numerous approaches: (i) selection of responsive homopolymers, (ii) selection of copolymers with stimulus-responsive blocks (for example polydimethylaminoethyl methacrylate PDMAEMA[129]), and (iii) use of responsive groups on the main chain, on side chains of polymers, or as linkers between different blocks.[130–132] For example, responsiveness of compartments towards pH-changes, because a pH-change is an essential signaling factor accompanying pathological conditions.[133] pH-responsive assemblies have been designed by

using a pH-responsive polymer, such as PDMAEMA[129] or 4-vinylbenzyl)-pentane-1,5-diamine dihydrochloride (VBPDA)[133], and introducing amino acids (histidine)[134] or carboxyl groups in the polymer main- or side chains.[128] Most of pH-responsive 3D polymer assemblies are aimed to dissociate or degrade into polymer chains or small molecules in order to discharge their molecular cargo.[135–137] Although polymersomes and polymer GUVs have lower membrane permeability compared to their lipid counterparts.[138,139] There are various possible approaches for increasing it, such as: (i) selection of polymers that intrinsically form porous membranes for example poly(styrene)-block-polyisocyanoalanine(2-thiophene-3-yl-ethyl)amide[118] or boronic acid-based block copolymers[140], (ii) chemical modification of the membrane with a hydroxyalkylphenone[141] and (iii) insertion of channel proteins.[57,104,139] There are only rare examples of pH-responsive 3D polymer assemblies capable of maintaining their structural integrity during their response to stimuli.[142,143] Most of them are obtained by using a cross-linked homopolymer PDMAEMA but they have lack controlled permeability and limited stability.[143]

One aspect that needs to be considered is that preservation of the compartment integrity is necessary if polymer vesicles are to serve as bioreactors, biosensors or artificial organelles. To the best of our knowledge, none of these examples were reported on polymer GUVs with selective membrane permeability, where pores could allow an exchange of small molecular weight molecules with a defined cut-off depending on the pore size.

Here we describe the design of GUVs with membranes capable of permitting proton exchange without changing their hollow-sphere architecture (Figure 18). Selective permeability of GUV membranes was achieved by inserting biopores. We selected as a biopore model the bacterial ion channel gramicidin (gA), which allows a controlled passage of protons and ions.[144] This biopore was selected, due to its simplicity (only 15 amino acids in its compositions), and versatility. In previous studies, gA has been well characterized in lipid membranes[145–148], surfactants mimics of unsaturated lipids[149,150], and liposomes[150,151], in which a successful insertion was favored by a reduced thickness mismatch between gA size and the model membranes. However up till now, there is only one report on the insertion of gA in synthetic membrane arrays, which gave shallow insight into the influence of the membrane thickness, the number of inserted gA pores or their localization inside the membrane.[152]

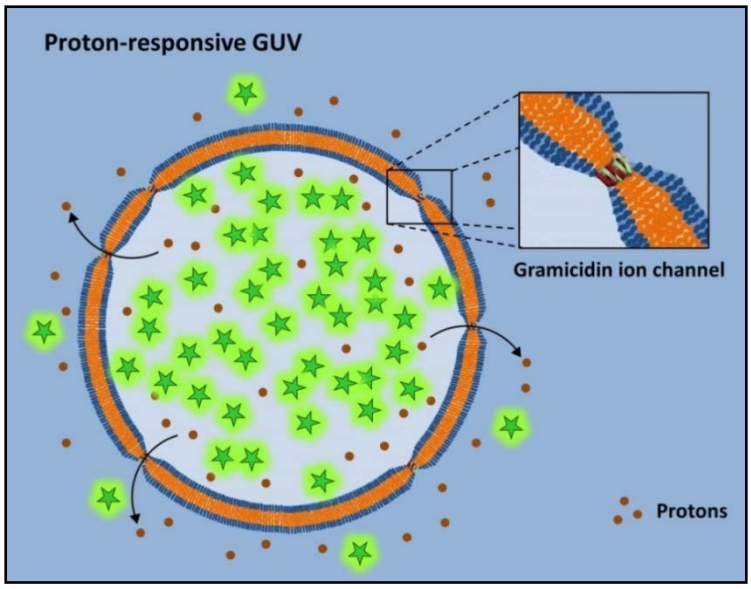

Figure 18. *Design of a GUV engineered for proton-selective permeability based on gramicidin (gA) biopore insertion.*

In order to study and understand the effect of membrane thickness on the functional insertion of the gA pore we have used a library of poly(2-methyloxazoline)-block-poly(dimethylsiloxane)-block-poly(2-methyloxazoline) (PMOXAx-PDMSy-PMOXAx) triblock copolymers, capable of self-assembly into GUVs with membrane thickness ranging from 9.2 to 16.2 nm. Depending on the hydrophilic-to-hydrophobic ratio, this type of amphiphilic polymer self-assembles in dilute solutions, and generates vesicles with sizes in the micrometer range (GUVs), with high mechanical stability and flexibility.[104] In previous studies, PMOXAx-PDMSy-PMOXAx membranes have been shown to be permeable only to reactive oxygen species and oxygen[153], whereas presenting high impermeablity to ions, and low molecular mass molecules.[138,139] Confocal laser scanning microscopy was used to analyze the functional insertion of gA in the polymer membrane of GUVs and if its insertion affects their architecture and size. GUVs without inserted gA were used for control experiments. The encapsulation of a pH-sensitive dye inside the cavities of the GUVs enables monitoring proton exchange across the GUV membranes due to the fluorescence intensity change as a result of pH.

Therefore, gA was inserted in individual giant unilamellar vesicles (GUVs), and the change of fluorescence intensity of the encapsulated dye was visualized in real-time (gA insertion is described in detail in material and methods, chapter 3). The design of GUVs with membranes permeable to protons represents a new approach for creating compartments with specific responses, whilst preserving their morphology, and therefore the encapsulated active

compounds. They represent ideal candidates for developing applications in which specificity and responsiveness are key factors, as for example in biosensors.

PROTON OUTFLUX THROUGH SYNTHETIC MEMBRANES OF GUVS

Polymer membranes present characteristic bilayer thicknesses, which are significantly higher compared to lipid membranes. This leads to a higher degree of hydrophobic mismatch between the polymer membrane and the protein size, as compared to lipid bilayers with thicknesses of 3 to 5 nm. Especially for shorter membrane proteins or biopores, their incorporation into membranes with increased thicknesses is a challenging task.

gA which has a length of ≈2.6 nm forms a pore with an inner diameter of 0.4 nm.[154] It should be tested if gA can be functionally inserted into the membranes of GUVs with thicknesses ranging from 9.2 to 16.2 nm which are significantly larger than the biopore.

A membrane thickness larger than the size of the gA has been reported to be correlated with a dimeric stretched active conformation of the biopore with preserved functionality in the case of lipid membranes.[155] However, as polymer membranes have a significantly larger thickness than those formed from lipids, the difference between the polymer membrane and the size of the gA channel is large. Therefore, we were interested to see whether gA insertion is affected or even blocked as predicted by modeling the insertion of membrane proteins in polymer membranes.[110] Triblock copolymers resulting in GUVs with membrane thickness between 9.2 and 16.2 nm were chosen (Table 1).

Polymer composition	Molecular weight (Mw) [g/mol]	Membrane thickness (d) [nm]	Successful gA reconstitution
$A_6B_{34}A_6$	3800	9.2	Yes
$A_7B_{42}A_7$	4500	10.3	Yes
$A_6B_{44}A_6$	4500	10.7	Yes
$A_7B_{49}A_7$	5100	12.1	Yes
$A_{12}B_{63}A_{12}$	6900	13.4	No
$A_{12}B_{87}A_{12}$	8700	16.2	No

Table 1. *gA reconstitution as a function of membrane thickness.*

Owing to their large dimensions, we used giant unilamellar vesicles (GUVs) as a tool to visualize gA insertion and activity by testing all six triblock copolymers (Table 1). First, we verified the GUV membrane integrity by adding Bodipy 633, a fluorescent hydrophobic dye known to directly insert into the hydrophobic part of the membrane (Figure 19A, Figure S1). Then, a gA labeled with a green fluorophore (gA-OG488) was added to the GUVs (Figure 19B). The similar fluorescence intensities of both components (Figure 19C) indicate that neither the insertion of gA nor the addition of the solvent affects the shape/architecture of the GUV membrane.

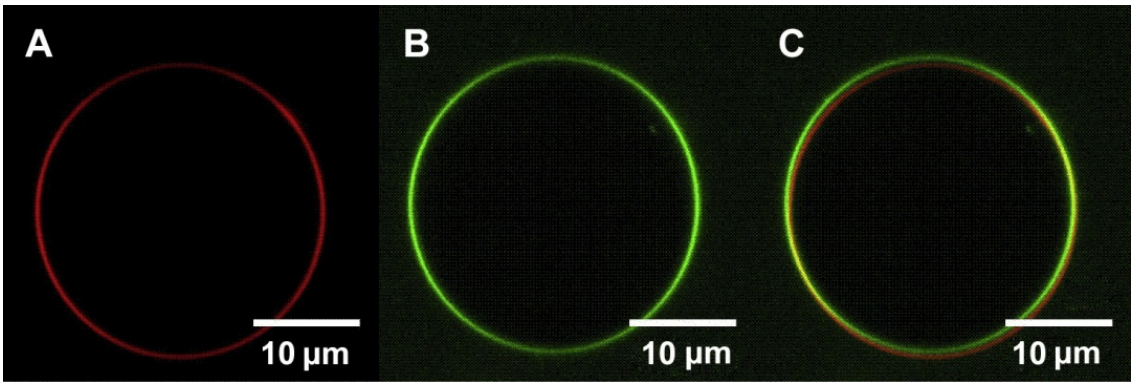

Figure 19. *CLSM images of a giant unilamellar vesicle (GUV) composed of $A_7B_{49}A_7$ triblock copolymer in the presence of:* ***(A)*** *Bodipy (red),* ***(B)*** *labeled gA-OG488 (green),* ***(C)*** *Overlay of A and B (red and green).*

In order to verify the functionality of gA when inserted into GUV membranes, 5(6)-carboxyfluorescein (CF), a pH-sensitive fluorescent dye with reduced fluorescence intensity at low pH, and high fluorescence intensity at high pH, was encapsulated in GUVs.

GUVs were formed in presence of CF at pH = 5.5 (Figure 20). At this pH the fluorescence of the dye is quenched, therefore CLSM micrographs show low fluorescence intensity inside GUVs (Figure 20A, inset). It has to be noted that the CF concentration inside the GUVs is higher due to dilution of the GUV solution into the LSM observation chamber that is already filled with a CF-free buffer (see experimental section). Therefore, at the beginning of the experiments, the fluorescent intensity inside the GUVs was always higher than the outside solution. In order to prove that GUVs membranes are impermeable to protons, the pH of the outer solution was increased from 5.5 by the addition of NaOH. The higher pH increases the fluorescent intensity of the background solution significantly, but the fluorescent intensity of the inner cavity of the GUVs remained unchanged, indicating that the block copolymer membrane does not allow diffusion of protons (Figure 20A, inset). The change of

fluorescence intensity outside the cavities of GUVs upon gA insertion was also confirmed by plotting the fluorescent intensity over time (Figure 20A). Even after several additions of NaOH, no response of the fluorescent intensity inside the GUVs was observed until the particular GUV ruptured and released its encapsulated CF, shown as a sudden intensity increase (Figure 20A). GUVs tested in presence of pure solvent (DMSO:EtOH (1:1)) were observed to have a membrane still impermeable to protons (Figure S2) showing that the solvent affects neither the GUV membrane stability nor its permeability properties, which is an important fact when performing the experiments with gA.

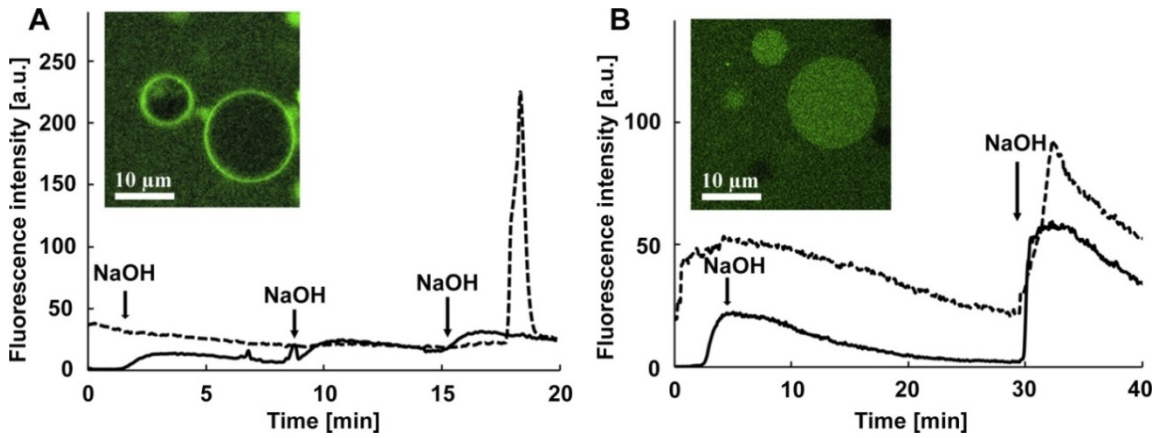

Figure 20. *Fluorescent intensity change over time of 5(6)-carboxyfluorescein (CF) inside and outside of polymer GUVs ($A_7B_{42}A_7$) in absence* ***(A)****, and in upon insertion of gA* ***(B)****. Insets: representative LSM images showing the principle of blocking the membrane to protons* ***(A)*** *and permeability of the membrane to protons by insertion of gA* ***(B)****. Fluorescence intensity inside GUVs (dotted line), and outside GUVs (solid line).*

In contrast, when gA was added to the GUVs solution and the pH was increased, the fluorescent intensity inside the GUVs increased immediately after the higher pH reached the GUV membrane, shown by the higher fluorescent intensity of the outside solution. The increase in the fluorescence intensity inside GUVs clearly indicates permeability of the membrane because of a successful insertion and functionality of gA (Figure 20B).

INFLUENCE OF POLYMER MEMBRANE THICKNESS ON gA INSERTION

Successful incorporation of gA with preserved functionality was achieved for GUV membranes based on $A_6B_{34}A_6$, $A_6B_{44}A_6$, $A_7B_{42}A_7$, and $A_7B_{49}A_7$ block copolymers with thicknesses ranging from 9.2 to 12.1 nm. These GUVs showed a significant fluorescence intensity increase inside their cavities whereas GUVs without incorporated gA showed no fluorescence change. The increase in fluorescence indicates that gA is functional incorporated into thick polymer membranes and proton outflux across the membrane takes place. The preserved functionality for gA inside membranes with thicknesses ranging from 9.2 to 12.1 nm can be explained by a bilayer compression which exists due to an energetic balance between the surface tension at the hydrophobic/hydrophilic interface and the chain configurations to match the biopore length. Bilayer compression results in an increase of the surface tension energy and a decrease in stretching energy. Protein insertion reduces the system free energy compensating for thickness mismatches.[110]

A modulation of membrane protein activity has been reported for Complex I when inserted in PMOXAx-PDMSy-PMOXAx membranes, the hydrophobic block being the key domain, which provided the necessary flexibility to accommodate the significantly smaller size of the hydrophobic part of the protein.[156]

The functional insertion of gA in GUV membranes of $A_{12}B_{63}A_{12}$ and $A_{12}B_{87}A_{12}$ block copolymers with thicknesses $\geq$13.4 nm showed no fluorescent intensity change inside the cavity of GUVs (Table 1, Figures S3–S7) meaning there is no outflux of protons across the membrane taking place. This leads to the assumption that there is a limit regarding thickness mismatch for which the membrane perturbation energy becomes a barrier for protein insertion.[110] In this case the thickness mismatches between the synthetic membrane and the biopore which is higher than 12.1 nm can not be compensated via the bilayer compression anymore.

The successful insertion of other membrane proteins (e.g., OmpF, AqpZ, and Complex I) in PMOXAx-PDMSy-PMOXAx GUV membranes can be explained by similar compensation in thickness mismatches, whereas in these examples the functionality of the reconstituted membrane proteins was not studied .[104,156–158] The hydrophobic mismatch of membrane proteins/biopores reconstituted into polymer membranes which is significantly higher compared to lipid membranes together with the higher mechanical stability of synthetic

membranes makes the design of polymer GUVs with equipped membrane proteins/biopores quite challenging.

Nevertheless the insertion of biopores with preserved functionality into polymer membranes could be realized by choosing polymers with sufficient intrinsic flexibility regarding the hydrophobic domain even when the mismatch between the membrane protein/biopores and the thickness of the membrane was more than 3.5 times higher.

In summary GUVs obtained by electroformation technique, proved successful insertion and functionality of gA in block copolymer membranes with thicknesses ≤12 nm.

CONCLUSION

GUVs with selective membrane permeability by inserting gramicidin biopores, which allowed proton transport could be engineered. Whilst there are numerous research studies showing the successful incorporation of this biopore into lipid membranes, its insertion intointo the membrane of polymer GUVs is more challenging due to the significant mismatch between the pore length and the thickness of the polymer membrane (more than 3.5 times). By using a small library of PMOXAx-PDMSy-PMOXAx copolymers, which self-assemble in giant unilamellar vesicles (GUVs) with membrane thickness ranging from 9.2 to 16.2 nm, the conditions in which gA can be inserted and remains functional inside the synthetic membrane, whilst preserving the GUV architecture could be analyzed. By the encapsulation of a pH-sensitive dye inside the cavities of GUVs proton gradients between the environment of GUVs and their inner cavity served to assess the exchange of protons across the membrane upon gA insertion. It could be shown that gA was successfully inserted and remained functional in polymer GUV membranes with thicknesses in the range of 9.2–12.1 nm. Larger thicknesses did not allow gA insertion, and therefore 12.1 nm represents a limit for the mismatch between the pore length and the membrane thickness. Our gA-GUVs are therefore pH self-regulating compartments, which maintain their integrity in different pH or ion gradient conditions.

Our bio-mimetic approach to insert proton channels with specific selectivity into the polymer membranes of GUVs is an elegant strategy towards the development of micrometer-sized cell mimics or to design bioreactors in which biopore functionality is combined with preserved membrane architecture.

Chapter 4

LIVE FOLLOW-UP OF ENZYMATIC REACTIONS INSIDE THE CAVITIES OF SYNTHETIC GIANT UNILAMELLAR VESICLES (GUVS) EQUIPPED WITH MEMBRAN PROTEINS MIMICKING CELL ARCHITECTURE

Compartmentalization of functional biological units, cells and organelles serves as an inspiration for the development of biomimetic materials with unprecedented properties and applications in biosensing and medicine.
Due to the complexity of cells, the design of ideal functional materials remains a challenge.
An elegant strategy to obtain cell-like compartments as novel materials with bio-functionality is the combination of synthetic micrometer-sized giant unilamellar vesicles (GUVs) with biomolecules because it enables studying the behavior of biomolecules and processes within confined cavities.
Here in this second chapter, we introduce a functional cell mimetic compartment by inserting the model biopore bacterial membrane protein (OmpF) in thick synthetic membranes of an artificial GUV compartment that encloses – as a model – the oxidative enzyme horseradish peroxidase. In this manner a simple and robust cell mimic is designed: the biopore serves as a gate, which allows substrates to enter cavities of the GUVs, where they are converted into products by the encapsulated enzyme, and then released in the environments of GUVs.
Our bio-equipped GUVs facilitate the control of specific catalytic reactions in confined micro-scale spaces mimicking cell size and architecture and thus provide a straightforward approach serving to obtain deeper insights in the real-time of biological processes inside cells.

This study has been published: Martina Garni, Tomaz Einfalt, Roland Goers, Cornelia G. Palivan*, Wolfgang Meier*. Live follow-up of enzymatic reactions inside the cavities of synthetic giant unilamellar vesicles (GUVs) equipped with membrane proteins mimicking cell architecture, ACS Synthetic Biology, (2018), 7 (9), 2116-2125.

MOTIVATION AND PROBLEM DEFINITION

Cells, as complex assemblies with highly defined structures based on organelles, and a cytoplasm with a variety of biomolecules enclosed by the cellular plasma membrane, serve as an inspiration for the development of new functional systems.[8] In this respect, the bottom up approach to mimic the hierarchical organization and functionality of various cellular structures or even of entire cells[1] is the focus for producing new functional materials with a large variety of applications, such as therapeutics[159], catalysis[160], biosensing, and surface technology.[161] Biomimetic materials are created by combining synthetic assemblies with active biomolecules or complexes (proteins, enzymes, DNA).[162] Self-assembly processes that take place in biological systems can be used to obtain biomimetic materials in which the biomolecule induces functionality, whilst the supramolecular assemblies (micelles, nanoparticles, tubes, liposomes, polymersomes, planar membranes[162,163] or micrometer-sized giant unilamellar vesicles (GUVs)) serve as stable matrices.[164] The development of functional biomimetic systems requires an understanding of the various reactions that occur within the cellular microenvironment and at cellular interfaces.[165,166] In this respect, synthetic compartments are very appealing supramolecular assemblies, because their architecture offers well defined and protected reaction spaces for encapsulated catalytic compounds (enzymes, proteins) similar to the compartmentalization of cells or natural organelles. Polymer compartments (polymersomes with nanometer sizes and synthetic GUVs with micrometer sizes) self-assembled from amphiphilic block copolymers[55,56], have become an elegant solution for the development of functional compartments with various advantages over lipid compartments (liposomes and lipid GUVs), such as an improved stability, the possibility to functionalize their external interface with specific molecular groups, and the huge variety of polymers whose chemistry can be tailored to achieve specific properties (stimuli-responsiveness, flexibility, crystallinity).[56] Polymersomes have been developed for various applications, such as conventional drug delivery systems[93,116], catalytic nano-compartments named nanoreactors[117], biosensors[118], and even artificial organelles that act as simple mimics of cellular organelles.[119] Interestingly, the study of enzymatic reactions taking place inside polymersomes as confined reaction spaces with sizes less than 300 nm indicated that in specific conditions it was possible to induce an increase in the bioactivity of encapsulated enzymes[167], whilst the presence of crowding agents (i.e. PEG) inside the cavity induced a decrease in bio-activity.[167] Despite the use of polymersomes in various applications, there are still important unanswered questions, such as: How do biomolecules

(enzymes, proteins, substrates) behave inside confined compartments with sizes that mimic cells? Is there any interaction between encapsulated compounds and compartment membranes? Do encapsulated compounds diffuse freely inside the cavities, or are they attached to the membrane? If so, does this possible interaction affect the activity and stability of the encapsulated compounds? Development of advanced functional compartments requires detailed responses to such questions in order to understand the complexity and specificity of natural bio-compartments.

To answer such questions, polymer GUVs can serve as a platform that allows a deeper insight into the molecular processes (reactions, interactions) that take place inside confined cavities, in their membranes, and at the interface, by real-time visualization using microscopic techniques. In comparison to GUVs nano-sized polymersomes can only give an indirect insight into membrane protein reconstitution and localization of enzyme reactions. GUVs can be measured directly by established microscopic techniques as their sizes match cell dimensions, and reactions or interactions can now be visualized. Thus, they represent a simple model system for studying the above mentioned processes and interactions in a cell-like manner. In this respect, polymer GUVs are of particular interest because their higher mechanical stability than lipid-based GUVs allows these processes to be studied for longer periods of time. Unlike lipid-based GUVs, there are currently only a few examples of polymer GUVs being used as functional platforms.[18] For example, synthetic GUVs based on poly(butadiene)-b-poly(ethylene oxide) (PBut2.5-b-PEO1.3) loaded with hydrophilic dyes, liposomes (DPPC) and polymersomes (PBut1.2-b-PEO0.6) allowed a fast selectively triggered release due to a light-induced increase in the osmotic pressure, which resulted in rupture of the GUVs.[168] Despite the potential application of this system for directed delivery and controlled local dosing of active compounds, applications of this approach are limited by the fast-irreversible decomposition of the GUVs.

PB-*b*-PEO polymer GUVs can mimic structural and functional eukaryotic cells by encapsulating enzyme-filled intrinsically porous PS-*b*-PIAT polymer nanoreactors with free enzymes and substrates to fulfil a three-enzyme cascade reaction inside the multicompartmentalized structures.[16] However, that work provided no information about the localization of the enzymes, and only the fluorescence product was observed by spinning disk confocal microscopy. Furthermore, the transmembrane exchange of substrates and products occurred because of the intrinsic permeability of the membrane, and unlike in cell membranes was not mediated by membrane proteins.

Proton transport through polymer polyethylene oxide polybutadiene (PEO-PBD) GUVs membranes has been achieved by incorporating two different synthetic pores, self-assembled from either a dendritic dipeptide or a dendritic ester. However, assembly of dendrimers into stable helical pores was not possible in the case of poly(2-methyloxazoline)-block-poly(dimethylsiloxane)-block-poly(2-methyloxasoline) (PMOXA-PDMS-PMOXA)-based GUVs, either because of the significant solubility difference between PBD and PDMS, or the differences between di- and triblock architectures.[169]

A more challenging approach for development of cell mimics based on synthetic GUVs is to insert biopores and membrane proteins into their membranes to induce enhanced permeability to specific ions or molecules, or to support in situ reactions while preserving the 3D architectures of the GUVs. This approach gives the possibility of understanding the biological function of the biopores or membrane proteins, and the visualization of transmembrane processes in real-time. An example is GUVs based on the rendering of PMOXA-PDMS-PMOXA triblock copolymer permeable for Ca^{2+} ions by inserting an unselective ionophore, Lasalocid A, and a highly selective ionophore N,N-dicyclohexyl-N′,N′-dioctadecyl-3-oxapentane-1,5-diamide[90] whilst insertion of the channel forming peptide alamethicin allowed unselective transport of cations and anions.[90] The insertion and functionality of the small pore-forming peptide gramicidin (gA) in synthetic PMOXA-PDMS-PMOXA GUVs membranes was visualized in real-time by the fluorescence change of the encapsulated dye inside inner cavities.[164] Interestingly, functional insertion of gA could be achieved in thick membranes up to 5 times greater than the size of gA.[164] The ability of synthetic membranes, to allow insertion of biopores and membrane proteins (KcsA, OmpF and AqpZ) that are several times smaller than the membrane thickness is the result of its intrinsic fluidity, which overcomes the significant hydrophobic mismatch, if the copolymers are appropriately selected chemically, as in the case of diblock and triblock PMOXA-PDMS-PMOXA copolymers.[18,83,109] However, to the best of our knowledge, the proof of a functional reconstitution of membrane proteins in synthetic GUVs with cell-like membranes has not yet been established.

Here we present the functional reconstitution of a membrane protein in thick and stable synthetic membranes of GUVs, in order to support cell-like functionality - an enzyme reaction that takes place within a GUV micro-sized cavity (Figure 21). Membrane protein functionality inside GUV membranes represents the key factor for enabling diffusion of the substrates/products of the reaction, and therefore supporting the in situ reaction in a cell-like manner.

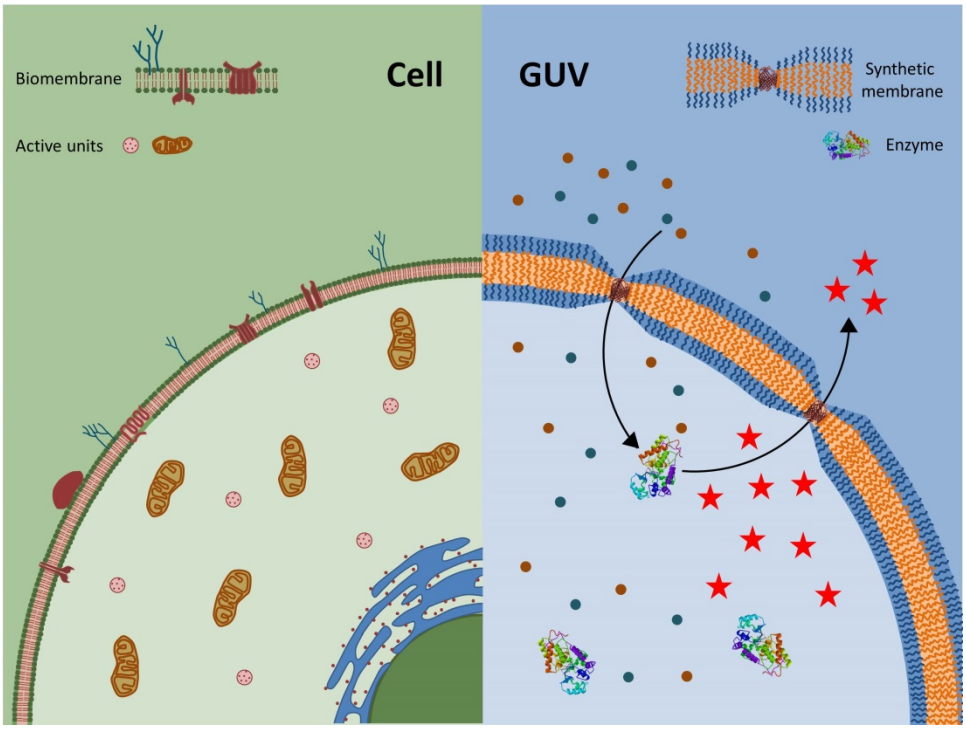

Figure 21. *Design of a natural cell* ***(left)*** *and a synthetic giant unilamellar vesicle (GUV) with encapsulated enzymes engineered for selective permeability to substrates and products based on reconstitution of the Outer membrane protein F (OmpF) to visualize a model enzymatic reaction inside the cavity* ***(right)****.*

We selected a cysteine double mutant of the bacterial outer membrane porin F (OmpF) as the model membrane protein, because it has various advantages, such as well-known stability and a pore size, which allows diffusion of molecules up to 600 Da. The controlled labelling of the cysteine residues within the OmpF backbone by fluorophores allows the OmpF reconstitution to be monitored.[115] In addition, OmpF has already been inserted into PMOXA-PDMS-PMOXA polymersome membranes with sizes around 200 nm, either as wild type[115], or as a mutant[170], and demonstrated to allow molecular diffusion. Therefore, we chose this type of amphiphilic copolymer to generate GUVs. The crucial step in our approach was to simultaneously encapsulate an enzyme inside GUVs and insert the OmpF double mutant to provide the trans-membrane exchange of substrates and products for the in situ enzymatic reaction. The molecular cut-off of OmpF pores plays a dual role: i) it prevents the model enzyme horseradish peroxidase (HRP) from escaping from the cavity of the GUVs, and ii) it allows diffusion of the substrates (H_2O_2, Amplex UltraRed (AR)) and the fluorescent product of the enzymatic reaction (resorufin-like product). The reaction has been characterized on whole GUV populations by flow cytometry, whilst conversion into the fluorescent product

inside individual GUVs has been detected by confocal laser scanning miscroscopy (CLSM) in real-time by time-lapse recording. Real-time visualization allows a deep insight regarding the membrane protein and enzyme localization, synthetic membrane permeability, and calculation of the conversion rate. Membrane protein functionality in the synthetic membranes of GUVs together with the in situ enzymatic reaction represents a necessary step towards the production of more sophisticated reactions inside functional compartments. Such synthetic GUVs equipped with membrane proteins represent robust functional assemblies that benefit from the stability of the synthetic membrane and the activity of the biomolecules: they open the opportunity of providing detailed insight into the design of multifunctional systems that serve as simple models of artificial cells.

INSERTION OF THE CHANNEL PROTEIN OMPF

An essential step towards the production of synthetic GUVs with controlled membrane permeability and a confined space for enzymatic reactions is the reconstitution of the double mutant of the channel porin OmpF, OmpF-M. In order to visualize OmpF-M reconstitution in the $PMOXA_7$-$PDMS_{49}$-$PMOXA_7$ polymer membrane of GUVs by CLSM, 300 mM sucrose was used as a default rehydration solution, since it allows GUVs to settle once they are dispersed in PBS (150 mM PBS). The cysteine residues replacing the native amino acids K89 and R270 in OmpF-M were conjugated with a fluorophore (Atto 488 Maleimide)[170], and non-reacted Atto 488 Maleimide was removed by filtration and dialysis. Atto 488 modification of OmpF-M has been evaluated by fluorescence correlation spectroscopy (FCS) and gel electrophoresis. FCS allows the determination of the diffusion time for fluorescent molecules through the confocal volume of the confocal laser scanning microscope (CLSM), and thus their binding to compounds/assemblies with significantly higher molecular weights by measuring the respective diffusion times.[171,172] By comparing the molecular brightness (counts per molecule, CPM in kHz) and diffusion times of Atto 488 in PBS (pH 7.4) (3.1 ± 1.23 kHz) and Atto 488 maleimide bound to OmpF-M in 1% n-octyl-β-D-glucopyranoside (OG) PBS (pH 7.4) (4.5 ± 0.3 kHz), a labelling efficiency of an average of 2 Atto 488 molecules per OmpF-M monomer was obtained. No residual fluorescence was observed when Atto 488 was added to wild type OmpF in 3% OG, or to 3% OG alone, thus proving that the maleimide fluorophore binds specifically to the cysteine residues of OmpF-M (Figure 22A, Figure S8).

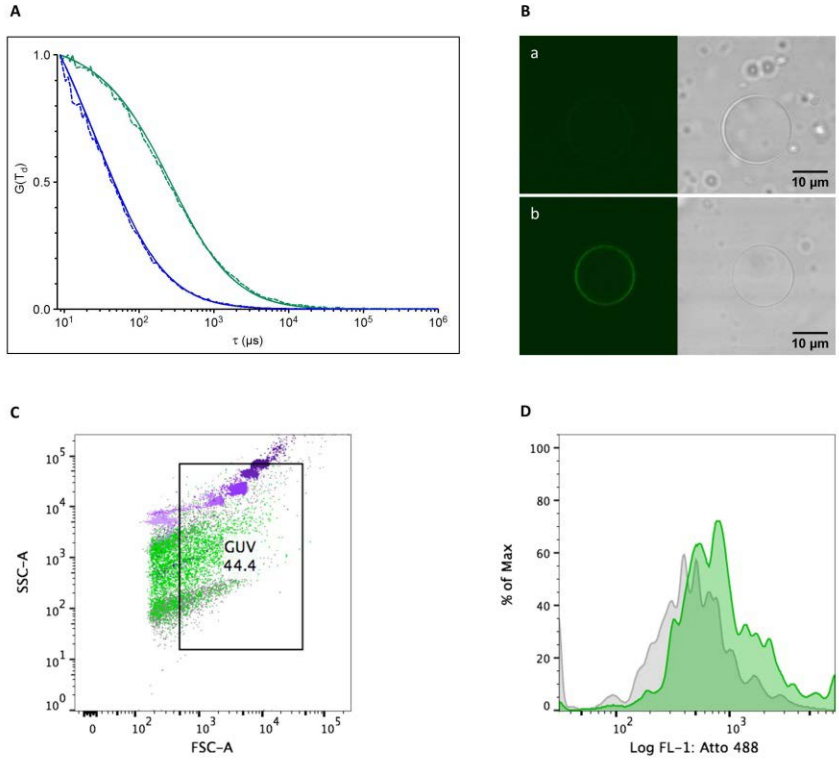

Figure 22. Atto 488 conjugation of OmpF-M. A: *FCS autocorrelation curves of Atto 488 in PBS (Blue), and OmpF-Atto 488 in 3% OG (Green). Dotted line – experimental auto correlation curves, Full line – fit. Curves normalized to 1 to facilitate comparison.* ***B:*** *CLSM micrographs of GUVs: without labeled OmpF-M (a), and with labeled OmpF-M (Atto 488) reconstituted into the synthetic membrane (b).* ***C:*** *Flow cytometry analysis of HRP-loaded GUVs containing OmpF-M (green), HRP-loaded GUVs without OmpF-M (grey), and polystyrene latex beads with diameters 2µm, 3µm, 5µm, 7µm s, and 10µm (visualized in increasing size from light purple to dark purple).* ***D:*** *Flow cytometry analysis of PMOXA-PDMS-PMOXA GUVs with OmpF-Atto 488 (green) or without OmpF-Atto 488 (grey).*

To determine whether OmpF was inserted in GUV membranes, CLSM measurements were carried out by using GUVs prepared in the presence of Atto 488 labeled OmpF-M (Atto 488-OmpF-M), and compared with GUVs in the presence of unlabeled OmpF-M (Figure 22B). Membranes of the GUVs with unlabeled OmpF-M remained dark, whilst those of GUVs with Atto 488-OmpF-M presented a distinct fluorescent membrane (shown in green in Figure 22B), which clearly indicates successful insertion of Atto 488 OmpF-M. In addition to CLSM measurements, insertion of Atto 488-OmpF-M was evaluated by flow cytometry, which has previously been used for analysis of lipid GUVs.[21] First, the sizes of the GUVs were calibrated using the forward scattering (FSC-A) of polystyrene latex beads in the size range of 2-10 µm (Figure 22C). Taking into account the GUV population between 3 – 10 µm, a

significant shift in fluorescence was observed in the population for GUVs that contained Atto 488-OmpF (Figure 22D, Figure S9). The GUV population smaller than 3 μm was discarded in line with CLSM measurements where GUVs in this size range were too small for precise measurements inside their cavities.

ENZYME ENCAPSULATION INSIDE THE CAVITIES OF GUVS

We were interested in encapsulating enzymes within the cavities of GUVs and analyzing how they behave inside a cell-like confined space, lacking the crowded environment of the cytoplasm. In addition, the enzymatic reaction was used to verify diffusion of the substrates through the OmpF-M pores.

In order to follow the encapsulation of the model enzyme horseradish peroxidase (HRP) in GUVs, lysine residues of HRP were conjugated with Atto 488 succinimide ester, and the unreacted fluorophore was removed by filtration and dialysis. The conjugation and purity of the Atto 488-HRP conjugate was established with FCS (Figure 23A) and SDS-PAGE (Figure S10). Atto 488 in solution had a typical diffusion time $\tau D = 44.3 \pm 17$ μs and molecular brightness of 4.4 ± 0.3 CPM, whereas the Atto 488-HRP presented a significantly longer diffusion time $\tau D = 252 \pm 43$ μs with a molecular brightness of 3.4 ± 0.5 CPM. The free fraction of Atto 488 in the HRP-Atto 488 solution was determined with a two component fit of the autocorrelation curve to be 15% ± 11% (Figure 23A).

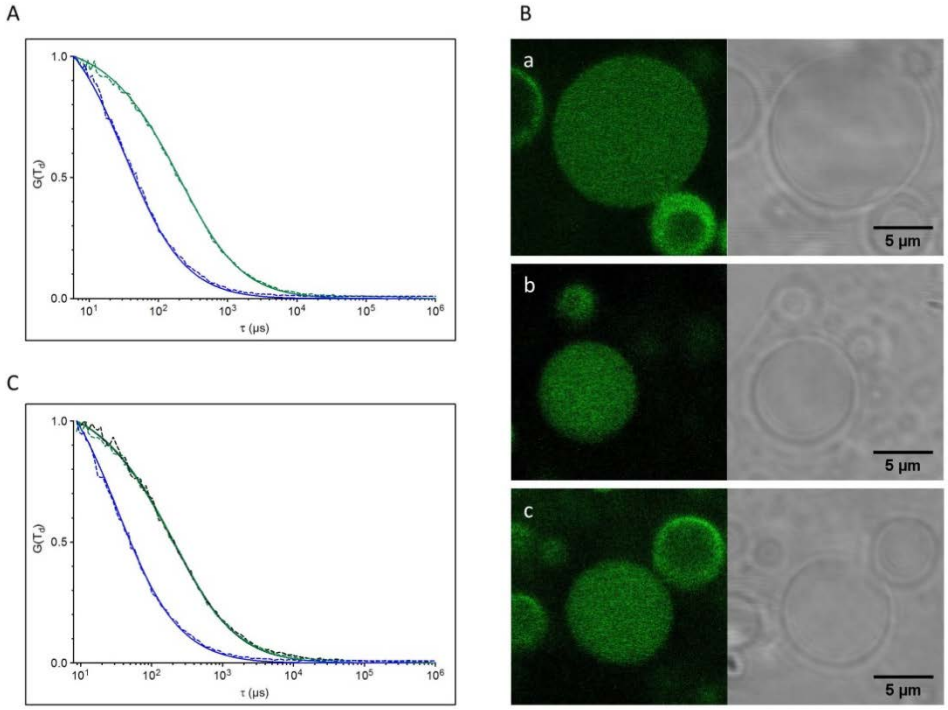

Figure 23. A: *FCS autocorrelation curves for Atto 488 in sucrose (Blue), and HRP-Atto 488 in sucrose (Green). Dotted line – experimental auto correlation curves, Full line – fit. Curves are normalized to 1 to facilitate comparison.* ***B:*** *a,b,c: CLSM images of polymer GUVs with labeled HRP (Atto 488) encapsulated. In each image: left: fluorescence channel, right: transmission channel.* ***C:*** *FCS autocorrelation curves for Atto 488 in sucrose (Blue), HRP-Atto 488 in sucrose (Black), HRP-Atto 488 in GUV (Green). Dotted line – experimental auto correlation curves, Full line – fit. Curves normalized to 1 to facilitate comparison.*

After encapsulation of Atto 488-HRP in 300 mM sucrose solution, and settling of the GUVs to the imaging chamber surface (SI), most of the GUVs measured by CLSM showed fluorescence inside their cavities (Figure 23B), indicating successful HRP encapsulation and free diffusion of the enzyme. In addition, GUV membranes presented only low fluorescence intensity, due to the reflection of fluorescent light between the GUV membrane / cavity interface, and a minor enzyme-membrane interaction. No fluorescence was observed outside the GUVs, which demonstrates successful purification of the GUVs after enzyme encapsulation (purification procedure is described in material and methods, chapter 4) . Self-assembly of the GUVs with encapsulated enzyme is a statistical process, meaning not all GUVs have the same amount of Atto 488-HRP present inside their cavities. To visualize in more detail the dynamics of enzyme encapsulation in the GUVs, we performed FCS measurements inside the cavites of Atto 488 labeled HRP-loaded GUVs (Figure 23C). As the

encapsulated HRP molecules have similar diffusion times (273 ± 144 μs) to the free HRP in sucrose (252 ± 43μs), it confirms a successful enzyme encapsulation (at least 10 GUVs were measured by FCS), and no change in the dynamics of the enzyme inside the confined space of the GUVs (Figure 23C).

ENZYME REACTION INSIDE GUVS CAVITIES

To address the question of enzyme functionality within GUV cavities, the rate of oxidation of Amplex UltraRed by HRP in the presence of H_2O_2 was first studied in solution by fluorescence spectroscopy and the enzyme activity for HRP in PBS pH=7.4 compared to that for HRP in 300 mM sucrose, which was used for GUV formation (Figure S11). There was no evident difference between the two media. Furthermore, without H_2O_2 as a co-substrate, there was barely any conversion of Amplex UltraRed into the fluorescent resorufin-like product. Similarly, there was no substrate conversion if no substrate Amplex UltraRed or no enzyme was present in solution (Figure S11).

This model enzyme reaction has been recently studied in synthetic compartments with sizes in the nanometer range, namely polymersomes equipped with OmpF-M. As we modified this method for the formation of OmpF-M equipped polymersomes by using sucrose solution for GUVs preparation instead of PBS pH=7.4, and the addition of OmpF-M in bidistilled water instead of PBS pH=7.4 (since the presence of salts disturbed the GUV formation), we were interested in determining whether these modifications affect the OmpF-M reconstitution and further enzymatic reactions. Therefore, we compared the enzymatic reaction inside polymersomes under the above mentioned conditions used for GUVs with those previously reported for polymersomes by fluorescence spectroscopy. For this, OmpF equipped polymersomes loaded with HRP were prepared and characterized (Figure S12, S13). As the *in situ* enzymatic reaction was not affected, this result indicates that the sucrose solution together with the addition of the OmpF-M in bidistilled water used for the GUVs experiments (see below) does not affect the functional reconstitution of OmpF or the activity of the encapsulated enzyme within polymersomes (Figure S14). This information tells us that the OmpF-M reconstitution together with the enzyme reaction should not be hindered by the conditions used for preparing the GUVs.

By monitoring the enzymatic reaction by CLSM for up to 12 min, it was demonstrated that the membrane protein OmpF is fully functional in the synthetic membrane of GUVs and that

it renders the membrane permeable to the substrates and products. We produced videos with an image recording time of 15.7 s/image and 1 s delay. To establish a starting point (t=0), the first image was recorded before addition of the substrates. Then, the enzymatic reaction was initiated by adding substrates (Amplex UltraRed and H_2O_2) to the external solution, and the increase in the fluorescent signal associated with the product of the reaction was visualized by CLSM (Figure 24). The same procedure was carried out for HRP-loaded GUVs without inserted OmpF-M (Figure 24).

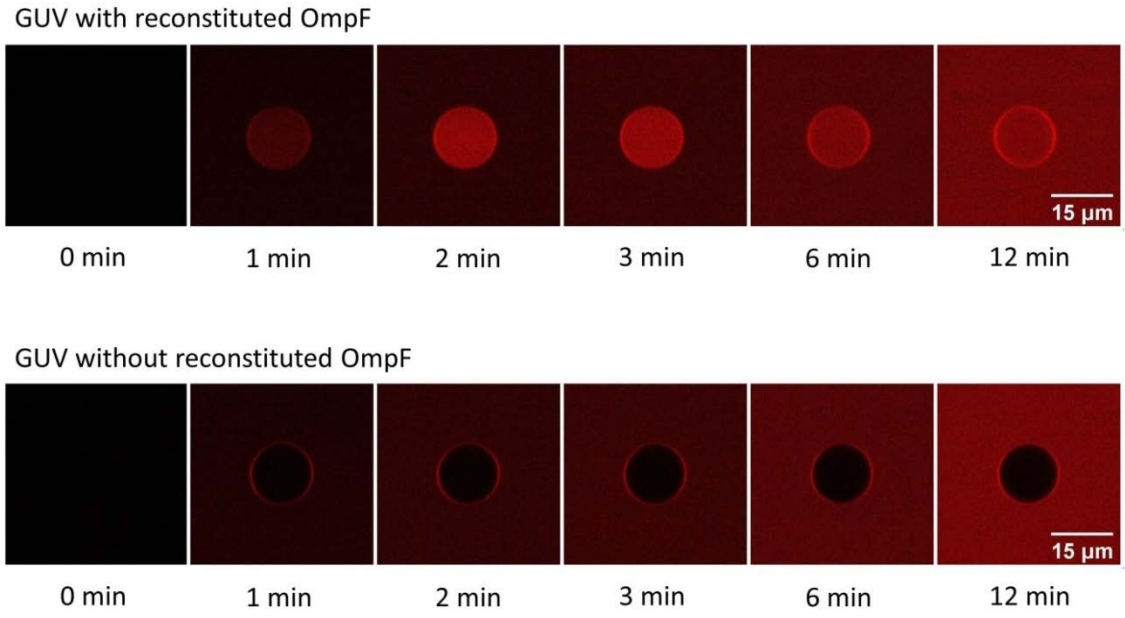

Figure 24. *CLSM Fluorescence micrographs of single GUVs obtained over time, by recording images at certain time points after initial addition of the substrates H_2O_2 and Amplex UltraRed.* ***Top)*** *GUV with reconstituted OmpF-M.* ***Bottom)*** *GUV without OmpF-M.*

The increase in the fluorescence intensity within GUVs equipped with OmpF-M results from the formation of the fluorescent resorufin-like product, and proves the functional insertion of OmpF-M that permits molecular transport through the synthetic membrane of the GUVs. On the contrary, there was no increase in fluorescence intensity inside GUVs without inserted OmpF-M, since the substrates were unable to pass through the synthetic membrane. Over time, the fluorescence inside the cavity of the OmpF-equipped GUVs decreased slightly (see the change from 165s to 6 min in Figure 24), because the resorufin-like product of the enzyme reaction diffuses out of the GUVs through the OmpF-M pores. As expected, after a certain time, the fluorescence inside the cavity of OmpF-equipped GUVs becomes equal to the fluorescence intensity of the environment of the GUVs, which is not the case for GUVs without OmpF-M, where there was almost no fluorescence signal inside the GUVs (dark core

of GUVs). Both GUVs with OmpF-M inserted and without OmpF showed a fluorescent membrane over time due to small amounts of HRP interacting with GUV membranes and being exposed at the exterior of GUVs even after several washing steps. In addition, a second factor, which causes the membrane to appear fluorescent, is the scattering and reflection of fluorescent light between the GUV membrane / cavity interface. Note, that in the following data assessment, the fluorescence intensity of the membrane of the GUVs has not been taken into account. The passive accumulation of the fluorescent resorufin-like product in the background was used as a criterion to determine whether the enzyme reaction has taken place within the cavity of the GUVs. The reaction occurred only if the fluorescence intensity was higher inside the GUVs than in the background. Both phenomena were considered in the data assessment, and consequently the membrane fluorescence was disregarded and the fluorescence intensity of the background was subtracted.

For each image of the sequences, the mean fluorescence intensity of a region of interest (ROI), depending on the individual size of the GUVs, both inside the cavity of each GUV (Figure S15) and outside the GUVs (background) was calculated using the program ImageJ. The mean fluorescence intensity values of the background over time were subtracted from the values inside GUVs cavity (Figure 25 A and C, Figure S16). Around 70% of the GUVs with reconstituted OmpF-M showed fluorescence higher than the background inside their cavities indicating that the enzyme reaction occurred, whereas the fluorescence intensity inside the cavity of ~ 70% of the GUVs without OmpF showed less fluorescence intensity than the background (Table S2).

In order to estimate the conversion rate, *k,* for the GUVs with and without OmpF, a linear regression of the fluorescence increase within the first 120 s was performed on all the curves, where each curve corresponded to a single GUV with background fluorescence intensity subtracted. Only GUVs with fluorescence higher than the background in case of the OmpF-M equipped GUVs (70%) were taken into account and vice versa for the GUVs containing no OmpF. A conversion rate of $k \approx 0.011\ s^{-1}$ was obtained for GUVs with reconstituted OmpF-M (Figure 25 B). In contrast, for GUVs without OmpF the negative conversion rate was an order of magnitude lower with $k \approx -0.0036\ s^{-1}$ (Figure 25 D). The increase in the relative fluorescence intensity for OmpF-equipped GUVs clearly indicates successful *in situ* bio-activity of HRP (Figure 25 A and B), whilst the decrease towards negative values of the curve for the GUVs without OmpF is due to an increase in the fluorescence intensity of the background that results from the HRP activity at the exterior of the GUVs (Figure 25 C and D).

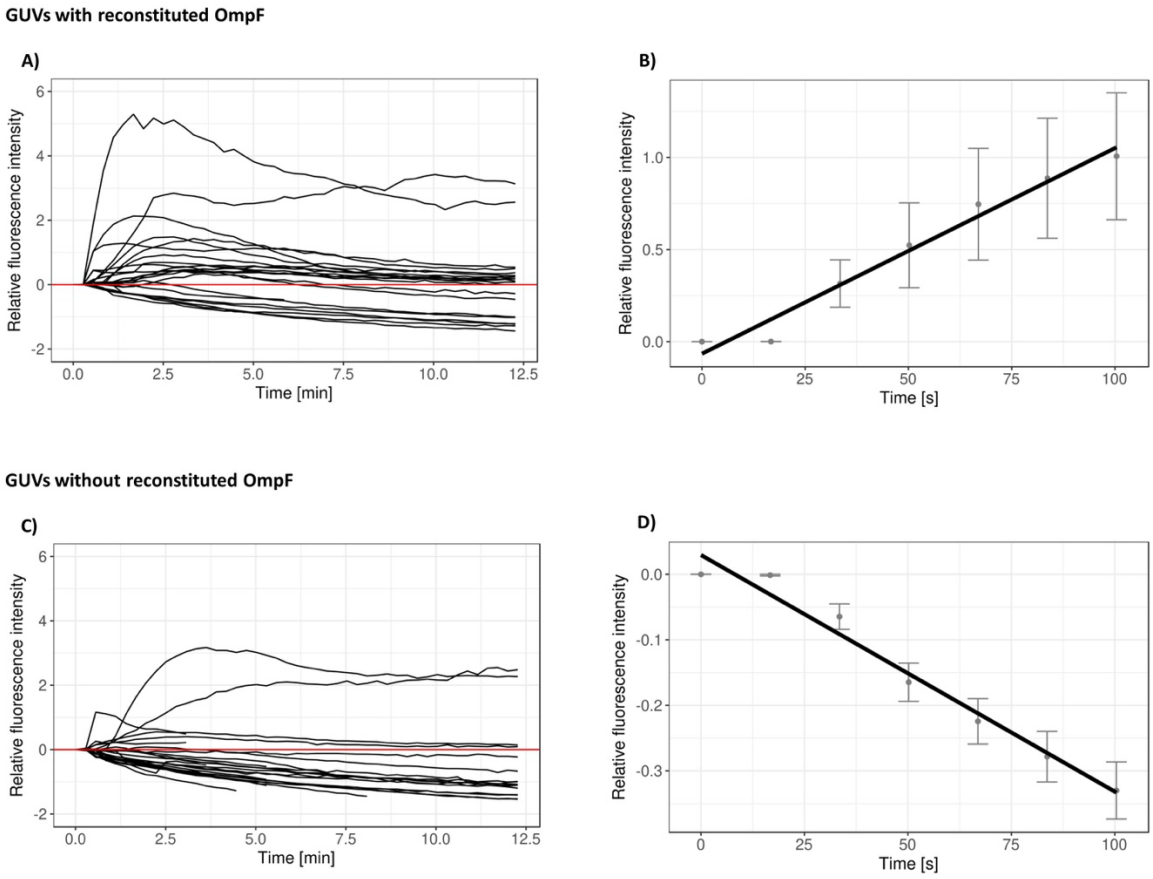

***Figure 25. Top**: GUVs with reconstituted OmpF-M. **Bottom:** GUVs without reconstituted OmpF-M **A and C:** Temporal variation in the relative fluorescence intensity of the resorufin-like product inside the cavities of single GUVs after addition of the reagents H_2O_2 and Amplex UltraRed after background subtraction. Each curve represents one GUV. **B** and **D**): Linear regressions of change of the fluorescence intensity over time. Shown are the mean values with standard error of the mean (sem). n = 18 – 25.*

To gain further information on the membrane permeabilization by insertion of the OmpF-M pore, the Amplex UltraRed enzymatic assay was applied in combination with flow cytometry analysis. Oxidation of Amplex UltraRed was observed inside the cavities of HRP-loaded GUVs equipped with OmpF-M, in agreement with the results obtained by CLSM, and the significant shift of the fluorescence for HRP-loaded GUVs equipped with OmpF-M compared to HRP-loaded GUVs without OmpF-M clearly proved that the porins allow substrates to efficiently diffuse into the cavities of the GUVs (Figure 26, Figure S17).

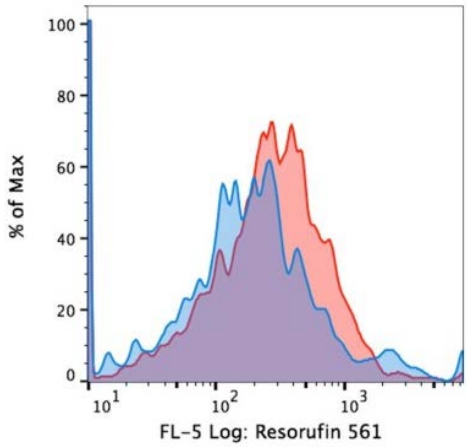

Figure 26. Flow cytometry analysis *- Amplex UltraRed enzymatic assay of OmpF equipped (red) or unequipped $PMOXA_7$-$PDMS_{49}$-$PMOXA_7$ GUVs (blue).*

Thus these CLSM and flow cytometry results confirm the necessity of functional membrane protein reconstitution inside polymer GUV membranes for production of the fluorescent product by the enzyme confined inside the GUV cavities.

GUV SIZE DISTRIBUTION

Next, we were interested in assessing whether the size of GUVs affects the enzymatic reaction that takes place within their cavities. To determine the corresponding sizes of the GUVs for a comparison between the dataset from GUVs with reconstituted OmpF-M and GUVs without OmpF-M, it was necessary to investigate whether these two populations showed size differences. First, the diameters of GUVs (both OmpF-equipped GUVs, and GUVs without OmpF) were measured using ImageJ and plotted (Figure S18); a Welch Two Sample t-test showed no significant difference between the OmpF-equipped GUVs and GUVs without OmpF (p-value = 0.27, $\alpha = 0.05$) (Figure S19).

To carry out a more detailed comparison, the fluorescence intensity of each individual vesicle was taken 260 seconds after the reaction was initiated to ensure a stable signal. A significant difference in fluorescence intensity was observed between the averages of OmpF-equipped GUVs and GUVs without OmpF (Figure S20 A) ($p \approx 0.024$ ($\alpha = 0.05$)).

Further details of the *in situ* enzymatic reaction were revealed by dividing the GUVs into 4 groups, namely from 6 to 9 µm (A), 9 to 11 µm (B), 11 to 13 µm (C) and 13 to 16 µm (D) (Figure S13 B). The difference in intensity of the two GUV populations was less pronounced

in the range of 6 to 9 µm, but the median intensity differed clearly between OmpF equipped GUVs and non OmpF equipped GUVs within the size ranges 9 to 11, 11 to 13 and 13 to 16 µm, and was most pronounced with the higher sizes. This is in good agreement with the expectation that larger GUVs should contain more dye molecules and thus have a higher overall intensity. Even though a slight decrease was observed from group C to group D, it was not statistically significant ($p \approx 0.344$).

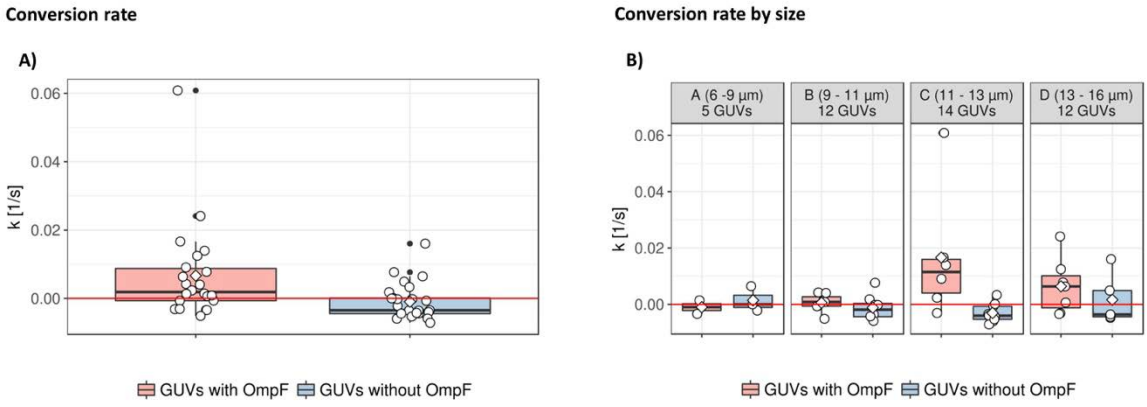

Figure 27. A) Conversion rate, k, of two populations of GUVs with and without reconstituted OmpF-M. *Each GUV was fitted independently.* ***B)*** *Variation of conversion rate, k, with GUV diameters. The black line = median, white square = average value, white points = data points.*

The conversion rate, was further calculated for each individual GUV. Again, there were significant differences between GUVs with and those without inserted OmpF (Welch Two Sample t-test, p-value ≈ 0.025, $\alpha = 0.05$) (Figure 27A). Classification of GUVs into the same size clusters as above shows a similar behavior to that described in the previous paragraph (Figure 27B). Overall, the difference in the median conversion rate, *k*, is marginal for group A, but there is an obvious difference in group B, and this increased in groups C and D. Since there was a constant enzyme concentration in the rehydration solution, the number of enzymes present in a GUV's cavity should depend only on its size, and therefore volume. Thus, with increasing GUV sizes, the volume and the number of enzymes per cavity should increase, and explains the lower conversion rate that was observed in group A. Furthermore, larger sizes have more membrane surface, which allows a higher number of OmpF pores to be present. This then results in increased substrate diffusion rates, and a steady stream of substrates and product can be achieved. It appears that the closer the physical characteristics (e.g. size and volume) are to a natural cell, the higher the performance of the system.

CONCLUSION

This is the first time that a membrane protein (OmpF) has been reconstituted into synthetic polymer membranes of giant unilamellar vesicles (GUVs) with preserved functionality, and is instrumental in initiating an *in situ* enzymatic reaction by allowing diffusion of substrates and products. The model enzyme reaction inside the GUV cavities was monitored in real-time and gave insight into both the substrate conversion rate by the encapsulated enzyme and the reconstitution of the functional membrane protein (OmpF) in synthetic GUV membranes. The large cavities of GUVs allowed free diffusion of the encapsulated enzyme, as proven by FCS. Furthermore, there appears to be a size-dependent trend in enzyme conversion rate in respect of GUV diameters. Also, whereas direct observation of internal reactions in established nano-compartment platforms, such as liposomes and polymersomes, are limited by the resolution barrier, GUVs provide a unique opportunity for observing the behavior of biomolecules within defined confined spaces. The combination of biomolecules and synthetic materials found in membrane protein-equipped polymer GUVs not only offers the advantages of increased stability and lower membrane permeability than lipid GUVs, but together with an encapsulated enzyme makes the micro scale compartment platform relevant for various applications, as for example a research tool to study biomolecule behavior within these cell-like compartments or as biosensors.

Our simultaneous encapsulation and insertion of biomolecules in GUVs allows a thorough understanding of biological processes in real-time, and represents a useful platform to study reactions inside confined spaces or interactions of biomolecules with membranes by a straightforward change of enzyme type. As GUVs have sizes similar to those of cells, they allow the relevant study of bio-processes *in vitro* in a simple manner. Thinking even further ahead, molecular factories and advanced cell mimics could be developed by encapsulating in cell-sized GUVs various polymersomes loaded with different types of enzyme inside their cavities.

Chapter 5

STRATEGY FOR CREATING BIOINSPIRED MOLECULAR FACTORIES WITH FUNCTIONALITY AS CELL MIMICS

The final experimental chapter of this thesis builds on the knowledge of cell-biology in order to create the first cell-like molecular factory. In this respect, micro-sized giant plasma membrane vesicles (GPMVs) are chosen as a fundament on which the cell mimic is constructed. These cell-derived vesicles present an ideal material as they are produced and isolated in high quantities by chemical, salt or laser treatment of donor cells, presenting themselves as a molecular material that has a potential, which has surprisingly left untouched. During their formation, GPMVs acquire both the outer compartment architecture of the donor cell (plasma membrane) and the inner composition of cells (cytoplasm). In this way GPMVs composition directly mirrors the composition of cells from which they originate with the exception of the larger organelles like for example nuclei and Golgi apparatus - making them the closest cell-mimic available on the market up to now. The possibility of designing molecular factories by manipulating cellular material (cytoplasm and plasma membrane) by genetic modification together with the encapsulation of solid sphere structures nanoparticles / vesicular structures (liposomes, polymersomes) in the cytoplasm-like cavities of the GPMVs represents the basis of these molecular factories. To develop bioinspired molecular factories with functionality as cell mimics, we propose a new approach for the generation of cell mimics by the production of sophisticated hybrid molecular factories based on giant plasma membrane vesicles (GPMVs) equipped with the necessary molecular machinery inside their cavities that provides function. When encapsulated in GPMVs, solid sphere and vesicular structures can further be used as sensors when there are active objects on their surfaces (i.e. fluorophores), but can also provide a mean of spatial localization of molecules within the GPMVs (i.e. attached on the surface or encapsulated). Towards the first bioinspired molecular factory enzyme-equipped polymersomes with a reconstituted membrane protein (OmpF) are encapsulated inside the GPMVs as enzymatic nanoreactors where they retain their functionality. Successful substrate conversion was visualized by the fluorescent product (resorufin-like product), which could leave the polymersome and diffuse inside the GPMV cavity, which thus allowed the substrates to be transported to the inside and the product to diffuse out of these polymersomes. Finally, we demonstrate that equipped GPMVs can act as artificial cell mimics.

This study has been published: T. Einfalt[x], M. Garni[x], D. Witzigmann, S. Sieber, N. Baltisberger, J. Huwyler, W. Meier*, C. G. Palivan*. Bioinspired molecular factories with architecture and in vivo functionalities as cell mimics, Advanced Science, (2019). (in press)
[x] Both authors contributed equally.

MOTIVATION AND PROBLEM DEFINITION

Innovative molecular concepts that closely imitate natural cellular compartmentalization currently appear to be in high demand as they represent first stepping stones towards the production of life-like micro- and nano scale biomimetic system.[165,173,174] The bottom up approach used in designing artificial biomimics is based on the combination of specific molecular building units (natural or synthetic) to form a hybrid hierarchically organized framework with a distinct architecture and functionality.[16] This modular design makes hybrid systems very appealing both in research and industry[175], where their applications are starting to play a major role as biosensors[176], sophisticated therapeutic or diagnostic tools[177], and even cross over in the field of electronics.[178] Especially in fundamental research, cell-like biomimetic compartment systems imitating cellular or subcellular structures prove themselves as excellent models of pro and eukaryotic cells and have previously given insight of the progression from non-living materials to a living organism.[16,173,179]

In the game of cellular imitation, substantial advances in developing nanoscale systems capable of functioning within the intracellular environment of viable cells have been achieved by the contribution of several groups, where nanomimics mimicked subcellular structures (i.e. organelles) in the form of artificial organelles (AOs).[119] However, despite advances in developing artificial cellular sub-compartments, a decade after the first notion of an artificial cell was introduced in synthetic biology the design of a functional stand-alone cell mimic, available to any laboratory in the world, continues to remain one of the most elusive and challenging concepts to realize. This is primarily as designing a life-like cell mimic requires the bottom up construction of system that possesses a confined molecular machinery, which can function in a highly controlled manner.[62] To achieve a cell-like organization a complex molecular factory needs to be designed, ideally capable of adapting to specific tasks and environmental conditions - a microscale compartment system that is adept to engineering and processing molecules (i.e. proteins, RNA, DNA) in a life-like manner. Previously there have been several attempts to design an artificial cell. These arose in the form of biomolecule-loaded lipid- and polymer-based giant unilamellar vesicles (GUVs)[5,7,16–18], lipid coated porous silica nanoparticles[19], layer-by-layer capsules[20], membrane free microdroplets, and micro-scaled proteinosomes.[21] However, existing synthetic compartment systems predominantly fail to meet the complexity found in nature, especially in relation to the diverse lipid and biomolecule composition that is inherent to the cellular architecture. In this respect, not only compartment barriers (i.e. membranes)[21] but

also the mainly used buffer-solutions[62] encapsulated within the cell mimics are far away from the cellular structures. Up till now cell mimics are designed by combining few isolated biomacromolecules (i.e. enzymes, membrane proteins) with a certain type of synthetic material (i.e. coacervates, droplets, liposomes, proteinosomes, polymers, porous silica particles) in order to construct a cell mimic with a very specific function.[18–21,180–182] The precisely defined composition of current "cell-mimics" makes it easier to define their function and characterize the role of individual building blocks, however it also represents a fundamental barrier, as the rudimental diversity in materials means that individual "cell-like" compartment systems cannot get near the complexity found in living organisms and are limited by the materials used in construction. This has led to the development of very group specific cell mimics, that cannot be easily adapted by other laboratories, due to the materials (i.e. polymers) used in their design. Another issue in designing cell mimics is that all modifications to the fundamental architecture (i.e. membrane and inner cavity) have to be inserted by crude self-assembly, which especially true for modifications done to the membrane. Membrane protein reconstitution has presented a challenging task since years, because the formation of membranous structures is based on spontaneous self-assembly processes, which can be rapidly disrupted during the process of protein reconstitution, due to the presence of amphiphilic molecules used in membrane protein isolation, purification and stabilization.[45,183] There have been significant advances in controlling the self-assembly process of cell-mimics by means of microfluidics, however the complexity of the resulting systems is still minimalistic and leaves room for improvement.[182] As a result of having to tightly control the self-assembly parameters, current synthetic systems are composed of only one, two, or as seen in only rare cases more types of synthetic materials, complemented by a narrow selection of biomolecules.[184] This inadequate material diversity of present biomimics is a feature that makes them largely fail to imitate the structure and metabolism found in natural cellular structures, where complex function is supported by an array of different biomolecules involved in fine-tuned internal reactions.

When designing a system that is closer to nature in terms of complexity and function compared to present cell-mimics, the organization and composition of the most basic structural and functional units found in eukaryotic organisms (i.e. cells and their subcellular compartments) offers inspiration as to how an archetype of a compartment-based molecular factory should be built. In this respect, in order to closely imitate cellular structure, molecular factories should be based on a versatile membranous outer compartment barrier complemented with different kinds of membrane proteins, which at the same time envelops

and holds in place an inner aqueous molecular machinery that is composed of membranous active sub compartments each containing biomolecules/active substances.[1]

Hierarchy in compartmentalization (compartments in compartments) is essential as multi- and sub-compartments allow molecules (i.e. enzymes or inorganic catalysts) to function in a spatially controlled manner and allow exchange of substrates/products between different sub-compartments.[185,186]

When choosing the starting material to build a cell-like molecular factory giant plasma membrane vesicles (GPMVs) present a particularly interesting platform, whose potential has surprisingly been left predominantly untouched.[71,187] These cell-derived micro vesicles (GPMVs) can be produced and isolated in high quantities by chemical, salt or laser treatment of donor cells[71–73] and are formed by a local delamination of the plasma membrane from the underlying cytoskeleton, which leads to filling of the expanding area within the GPMV via a passive flow of cytoplasm.[74] Hence, both the outer compartment architecture of GPMVs (membrane) and the inner composition of GPMVs directly mirror the composition of cells from which they originate, but without the larger cellular organelles (i.e. nuclei, Golgi apparatus) making measurements easier and are the closest cell-mimic available on the market up-to now (Figure 28).[75] Previously these characteristics made GPMVs improved membrane models to study the lipid composition of the plasma membrane, the behavior of functional membrane proteins within the GPMV membrane, and membrane interaction with external compounds.[76] Even more recently GPMV applications have been extended from biophysical models[77,78] to bioinspired drug delivery agents by making use of the host-cell membrane functionality.[79,80] However, up to date there are no reports of studies that take advantage of the complexity of the GMPVs membrane and its compartment architecture in order to create molecular factories that act as artificial mimics of cells.

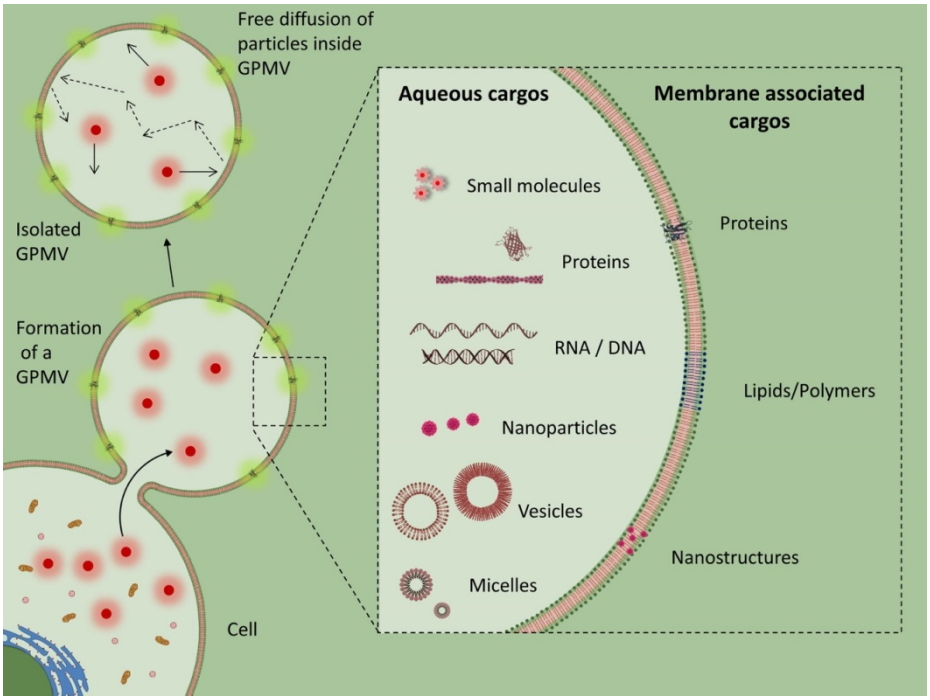

Figure 28. Schematic illustration of GPMV molecular factories, presenting the different types of molecular cargo that can be incorporated in the GPMV structure*. Small molecular weight molecules (i.e. salts, fluorophores, chemotherapeutics), biomacromolecules (i.e. proteins, DNA), solid sphere nanostructures (i.e. quantum dots and nanoparticles) and hollow sphere nanostructures (i.e. liposomes, polymersomes) are integrated into the cytoplasmic cavities of GPMVs to form a complex molecular machinery. Loading of GPMV cavities is achieved through transfer of material from the donor cell cytoplasm during GPMV formation, whilst in addition the membrane associated cargo is transferred from the cell to the plasma membrane of GPMVs during vesicle formation.*

Here, we propose a new approach for the generation of artificial cell mimics by the production of sophisticated hybrid molecular factories based on giant plasma membrane vesicles (GPMVs) equipped with the necessary molecular machinery that provides function (i.e. catalyst equipped nanocompartments). In our opinion, the cellular origin of GPMVs has an untapped potential for developing a cell mimic, because the composition of GPMVs membrane is not restricted by a limited library of lipidic or synthetic amphiphiles and in addition avoids the reconstitution of membrane proteins characteristic for lipid or polymer compartment systems. Transfer of the contents of cytoplasm and membranes from donor cells to GPMVs occurs spontaneously during GPMV formation and offers the opportunity to build a cell-like molecular factory by a straightforward engineering, which combines well-established techniques of GMPVs formation, with an elegant selection of components that are incorporated through the cell during their formation.[71,73,79,188]

In the strategy we present here, eukaryotic cells are used to i) manufacture GPMVs (top down approach), and ii) simultaneously equip GPMVs with a large variety of structural and functional units (enzymes, proteins, nano-objects, catalytic compartments) by pre modifying cell composition (bottom up approach). Design of GPMV-based molecular factories through this combination of a bottom up and top down approach utilizes the fundamental architecture of GPMVs - a cytoplasm-like core that is surrounded by a versatile plasma membrane - and a functional unit with plasma membrane-based outer barriers and inner molecular machinery that is constructed during plasma membrane vesiculation of donor cells pre-loaded with a molecular cargo of interest (i.e. small molecular weight molecules, biomacromolecules or larger nano-sized assemblies) , which can be activated “on demand” (Figure 28).

Such a molecular factory opens up the possibility to reproduce and study biological processes in a real cell-like environment with defined components and less crowding agents. As both, the compartment core and structural membrane of a GPMV unit are directly derived from the cell, it implies that they can both be modified on demand by modifying the cellular composition, either by genetic modification or integration of molecular building blocks into the cytoplasm / plasma membrane. In addition, GPMV-based cell mimics not only have similar sizes to eukaryotic cells, but they also present a spherical shape that allows exact surface and volume determination, and therefore access to concentration-calculations that are important for precise kinetic studies.

The ability to manipulate membrane composition represents a key advantage of GPMV-based artificial cells, since membrane protein reconstitution in synthetic polymer / lipid GUVs is always a time-consuming and challenging task.[45,183] Genetic modification and subsequent cell membrane alteration of the GPMVs represent a fast, robust and flexible alternative to current approaches.

ENGINEERING GPMV MEMBRANE AND POSSIBLE MODIFICATIONS

In order to develop a functional compartment, modifications done to its fundamental structure, the load bearing membrane, have to be addressed first. Customization of the cell mimics outer barriers - the plasma membrane – is important, as both lipid and protein components of the membrane play essential roles in compartment permeability, functionality, stability. In addition, membrane composition predominantly determines how the compartment will interact with the environment (i.e. protein binding, immune response) – an important consideration for future *in vivo* and *in vitro* applications.[177,191] As the GPMV material composition directly mirrors that of the donor cell, we have investigated the extent to which the GPMV membranes can be modified on demand in a streamlined approach by modifying the lipid, protein and polymer composition of the donor cell. In this respect, we were interested to determine the effect of outfitting apical membranes of cultured model human cells (HepG2 liver carcinoma) with highly lipophilic molecules (such as the membrane tracer DiD[46], fluorescently-tagged amphiphilic lipids e.g. DOPE-Rhodamine and DOPE-FITC[192] or polymers e.g. Cholesterol-PEG-5000-FITC[193]) on the composition of GPMVs. Customized integration of lipids, as reported here by integration of a combination of DOPE-Rhodamine and DOPE-FITC into GPMVs, is central to the design of a GPMV-based cell mimic, as it allows combining molecules in the GPMV membrane that can act in tandem. We confirm that incubation of the model HepG2 cell line with DOPE-Rhodamine and DOPE-FITC micelles leads to integration of the fluorescently tagged lipids in the cell, and once the vesiculation process is induced, the introduced lipids are transferred to the membranes of the GPMVs (Figure 29). Due to their fluorescent nature these types of modifications done to the plasma membrane not only provide a way to manipulate the structural properties of GPMVs but also allow following membrane fluidity, integrity and architecture (possible domain building) directly, through the use of fluorescence techniques. We further demonstrate that the customized equipment of GPMVs is not limited by integration of lipids by successful integration of membrane tracers, such as DiD (Thermofischer) (Figure 29) or polymer modified cholesterol (Cholesterol functionalized polyethylene glycol 5000-FITC). The latter is especially important for future *in vivo* applications of GPMVs as artificial cells, as it demonstrates that GPMV membranes can be equipped with polymer macromolecules such as PEG, which prevent unspecific protein

binding, shield the membrane charge and provide steric stability through presence of PEG chains on the apical surface of membranes[194](Figure 29). Yet modifying GPMV membranes with only relatively small molecular weight molecules is not sufficient to design a functional cell mimic, since active processes taking place at biological compartment interfaces are mostly governed and regulated by numerous bio-macromolecules, such as membrane associated proteins[188]. For this purpose, we further engineered HepG2 cells to overexpress a plasma membrane associated protein GFP tagged leucocyte specific (Lck) tyrosine kinase using baculovirus gene transfer (BacMam 2.0).[195] Upon inducing vesiculation in donor cells we demonstrate that in addition to modifying the composition of the GPMV the plasma membrane forming the compartment barriers can also be manipulated and equipped on demand with functional membrane associated proteins (Figure 29).

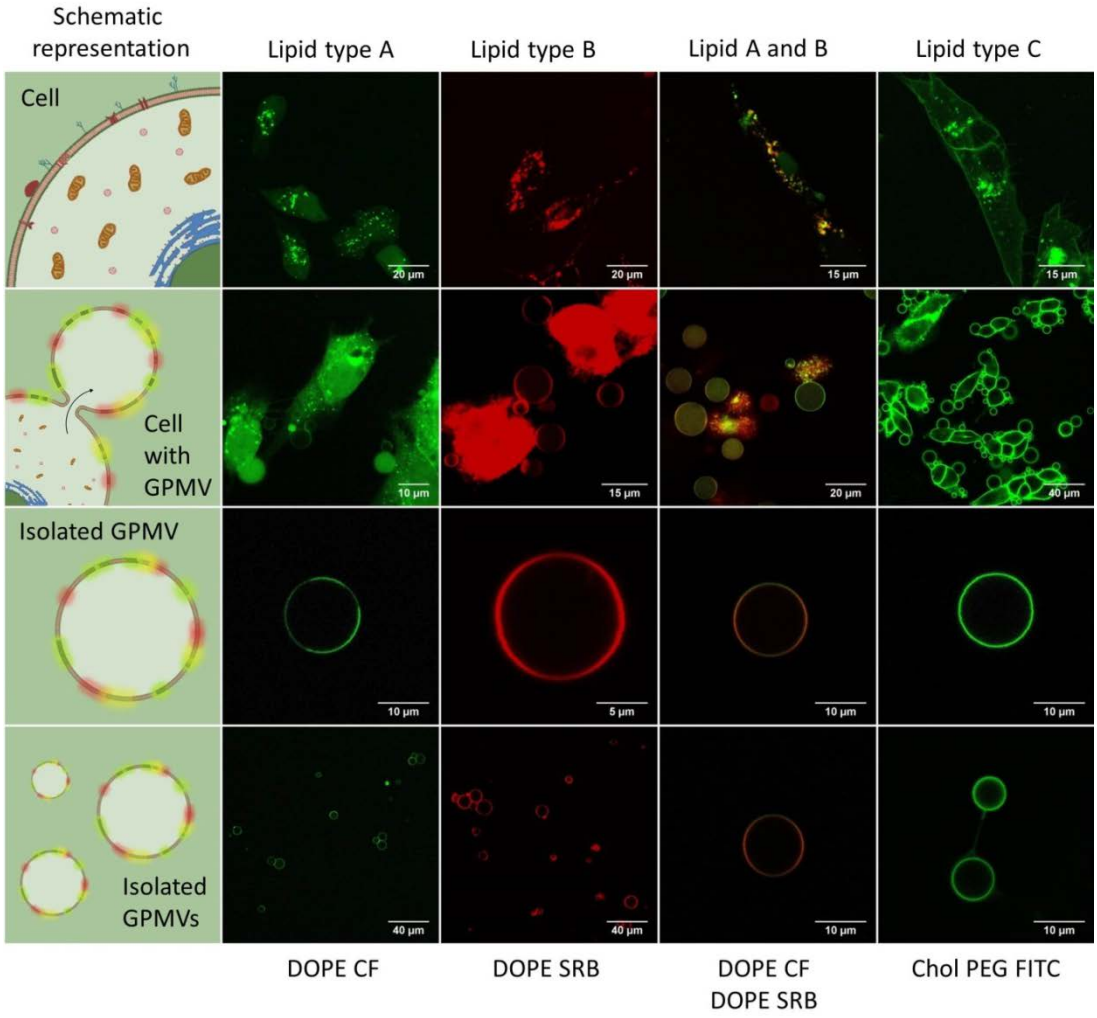

Figure 29. GPMV membrane modifications Top: *HepG2 cells.* ***Middle:*** *HepG2 cells after vesiculation.* ***Bottom:*** *Isolated GPMVs. Carboxyfluorescein (CF, FITC) (green) Sulforhodamine (SRB) (red).*

Besides modifying the membrane of the cell mimic, it is also necessary to customize the composition of the cytosolic cavity within the GPMV and thereby introduce the crucial molecular machinery that will support function of the cell mimic. During the vesiculation process part of the donor cell cytoplasm is transferred directly into the GPMV cavity, therefore the cavity of GPMVs contains a cell-like composition by default, which represents an essential step in complexity compared to all other reported systems proposed as artificial cells.[1] To develop a customized molecular machinery, it is necessary to enhance the inner composition of a cell mimic with a unique blend of small molecular weight molecules and proteins, which mimic the cytoplasm and support the function and performance required for a specific molecular machinery to work. By preloading the model HepG2 cell line with a small molecular fluorophore (CellTracker™ DeepRed Dye)[196] and then inducing the GPMV vesiculation process, we demonstrate and confirm previous findings that low molecular weight compounds abundantly present in the cytoplasm of donor cells are transferred into GPMVs during a passive flow of cytoplasm into the expanding cavity (Figure 30).[79] The same transfer of material is also observed for GPMV formed by HepG2 cells genetically modified to over-expressed larger water soluble cytosolic proteins (>20 kDa), such as RFP-Actin and water soluble e-GFP (Figure 30), confirming the high degree in which the local environment within individual GPMVs can be controlled in a straightforward manner by the manipulation of the donor cell composition. In addition to encapsulation of a single molecular species within GPMVs, a combination of biomolecules (water soluble RFP and enhanced GFP (eGFP)) can also be achieved (Figure 30), leading to an even more complex inner environment. This implication of co-encapsulation remarkably important, since existence of different types of biomolecules within a single GPMV opens a possibility of combining classes of biomolecules that act in tandem (i.e. enzymes) within a confined space and thereby designing an environment where molecular interactions within the cell mimic can take place and be studied in a defined manner.

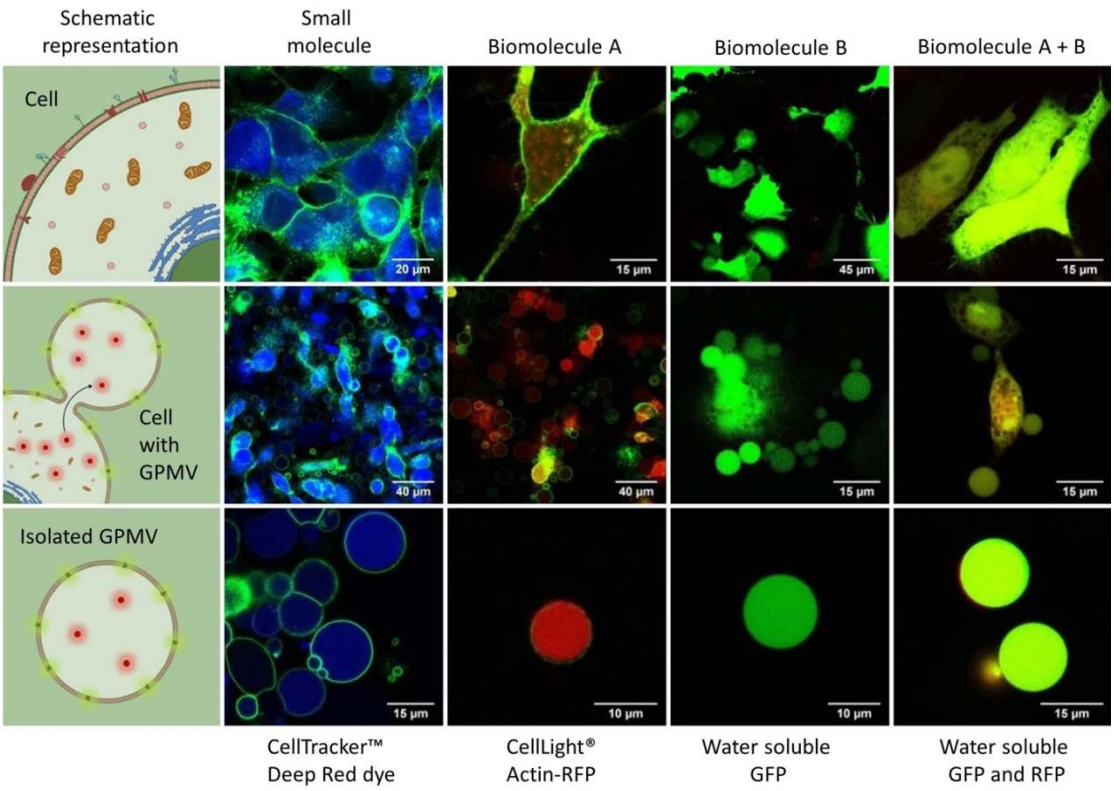

Figure 30. Building the outer compartment architecture of molecular factories. Top: *HepG2 cells after uptake.* ***Middle:*** *HepG2 cells after vesiculation.* ***Bottom:*** *Isolated GPMVs. CellTracker™ deep red dye (blue) and e-GFP tyrosin kinase (Green). Actin-RFP (Red) and GFP-tyrosin kinase (Green), water soluble e-GFP (green) and water-soluble e-GFP (green) and RFP (red).*

FUNCTIONAL COMPONENTS WE NEED FOR MOLECULAR FACTORIES

Besides having a customizable membrane and cytoplasm filled cavities, GPMVs are required to contain active compounds inside their cavities in order to support the function of a cell-like molecular factory. In nature, processes taking place within cellular compartments show significantly increased turn-over and efficiency as a result of spatial localization and multi-compartmentalization[165]. Prime example are enzymes involved in cellular metabolism, which are able to run highly efficient and complex cascade reactions due to their confinement within the space of specific organelles (e.g. the extensive range of respiratory enzymes that are confined to mitochondria Structure and function of mitochondrial membrane protein complexes). Accordingly, the next step in designing a molecular factory that mimics cellular function, herein referred to as e-GPMV, is the introduction of multi-compartmentalization.

The robust and solid sphere characteristics of nanoparticles (e.g. polystyrene, silica and gold nanoparticles) makes them valuable tool for imaging/visualization, and fluorescently-labeled nanoparticles encapsulated within the cavities of GPMVs can be used to study diffusion (Brownian motion), interaction processes inside the cytosol-filled GPMVs, or potential plasma membrane interactions. Further they can serve as biological sensors in the confined spaces of the GPMVs, if for example antibodies or enzymes are bound to particle surface. [197,198] However, one of the most interesting aspects of nanoparticle encapsulation in GPMVs is that of providing a mean for spatial localization of active molecules (i.e. enzyme, catalysts) on particle surfaces or encapsulation of the latter within particles (e.g. porous silica nanoparticles), opening the way to multi compartmentalization.[199]

We have attempted to mimic cellular multi-compartmentalization by introducing solid-sphere nanostructures in the size ranges 1-2 nm (carboxylated quantum dots), 40 nm and 0.5-1 μm (polystyrene beads) in GPMV cavities. Since cellular uptake of colloidal objects with sizes between a few nanometers and 1μm in diameter has been observed in non-phagocytotic cell lines[200] (Figure 31), we loaded cells with solid sphere nanoparticles (carboxylated quantum dots, polystyrene beads) to study how nanoscale assemblies are transferred from the cytosol of human-derived cells into GPMVs (Figure 31). During the process of GPMV formation, colloidal assemblies abundantly present in HepG2 cytoplasm are transferred to the cytosolic environment within GPMVs and are able to diffuse freely in GPMV cavities where, serving as autonomous islets. This bottom up approach of outfitting the fundamental molecular factory with nano-assemblies opens the way for spatial localization and sub-compartmentalization, thereby fulfilling a crucial requirement for the construction of complex biomimetic molecular machinery, which would allow chemical reactions to take place in life-like conditions.

We have observed that the process by which solid sphere particles are transferred from the HepG2 cytoplasm into GPMVs is governed by object size, and that for our model cell line a size-dependent cut-off into GPMVs appears around 1000 nm. However, efficient transfer of nanometer-sized particles was found for objects up to 500 nm in diameter, which filled about 25% of the GPMV cavities produced by a single cell with at least 1 colloidal object per GPMV. The likelihood of colloidal nanoassemblies being transferred from the cytoplasm of donor cells to GPMVs appears to be highly size-dependent with the smaller q-dots and 40 nm solid spheres being more abundant in GPMVs of a single cell than the larger 500 nm polystyrene latex beads. This is most likely in relation with the rate of nanoparticle uptake by cells – smaller nanoparticles reach higher intracellular concentrations faster, and will be

addressed in further studies. The uptake and subsequent transfer of nanoparticles in GPMVs could possibly be improved by choosing a phagocytotic cell line (i.e. THP-1 macrophages). Objects that were transferred into the GPMV interior retained their size and fluorescent properties, and showed no signs of aggregation or degradation (Figure 31). Free diffusion of objects in sizes up to 500 nm was observed within the cytosol-filled cavities of GPMVs. Observed by CLSM diffusion was primarily size dependent (bigger objects diffused slower) in agreement with the Brownian motion of colloidal assemblies in solution. Sedimentation of the larger 1 μm or 2 μm polymer beads occurred rapidly after they were added to the cellular culture, thus limiting their uptake and transfer into GPMVs. We observed a singular 1 μm particle bouncing on a GPMV, which showed the robustness of the GPMV membrane towards rupturing.

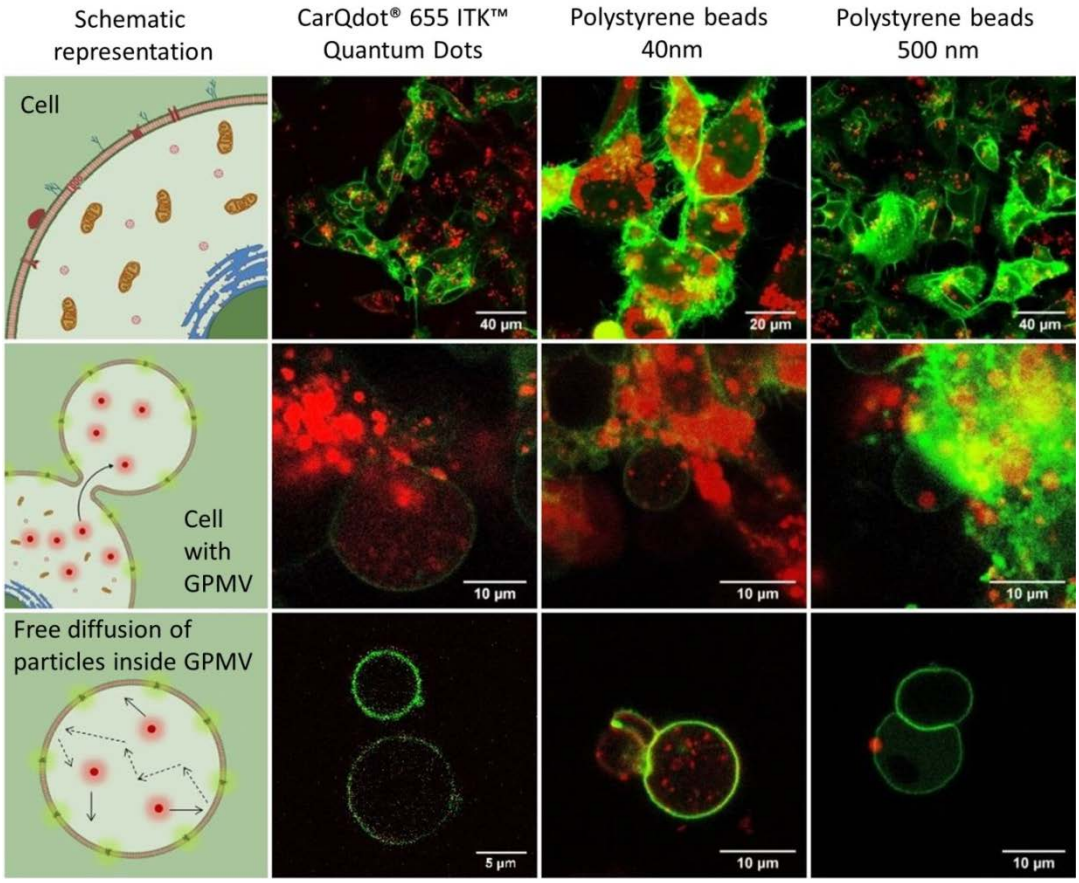

Figure 31. Transfer of artificial solid sphere objects from the HepG2 cytoplasm into GPMV. Top: *HepG2 cells loaded with nano assemblies.* ***Middle:*** *Cells after vesiculation.* ***Bottom:*** *GPMVs after isolation. Quantum dots and e-GFP tyrosine kinase. 40 nm-sized polystyrene beads and e-GFP tyrosine kinase. 500 nm-sized polystyrene beads and e-GFP tyrosine kinase. Quantum dots and polystyrene beads:Red and GFP:Green.*

VESICULAR STRUCTURES INSIDE GPMVS

The indication that 500 nm-sized solid sphere objects can be transferred from the donor cell cytoplasm into the GPMV interior opens a unique possibility of implementing a type of sub-compartmentalization in which smaller hollow-sphere vesicular structures (liposomes, polymersomes) are confined within GPMV cavities. The successful implementation of this principle is important as it allows a higher degree of sub-compartmentalization of active molecules within nano-sized cavities of GPMVs, and thus shows the properties of a molecular factory.

In order to achieve sub-compartmentalization within GPMVs, it is first necessary to have abundant lipid- or polymer-based vesicular compartments (i.e. liposomes or polymersomes) in the cytoplasm of the HepG2 cells. For this purpose, we incubated HepG2 cells with vesicles (liposomes and polymersomes) encapsulating sulforhodamine B (SRB) and carboxyfluorescein (CF) - hydrophylic trackers as markers for the integrity of aqueous cavities of the nano-sized compartments. SRB- and CF-loaded poly(2-methyloxazoline)-block-poly(dimethylsiloxane)-block-poly(2-methyloxasoline) ($PMOXA_{44}$-$PDMS_6$-$PMOXA_{44}$) polymersomes and two types of SRB-loaded liposomes composed of DSPC:cholesterol:DSPE-PEG (48:42:10 %mol) / DSPS:cholesterol:DSPE-PEG (53:42:5 %mol) were prepared in the size ranges of 100 - 200 nm, as determined by DLS, TEM and Cryo TEM (Figure S21-S27). Efficient loading of SRB into the cavities of negatively charged DSPS-PEG (-3.5 +/- 0.5 mV) and net neutral-charged DSPC-PEG (0.507 +/- 0.1 mV) sterically stabilized liposomes and $PMOXA_{44}$-$PDMS_6$-$PMOXA_{44}$ polymersomes was confirmed by fluorescence correlation spectroscopy (FCS) (Figure S28-29). After separation of polymersomes and liposomes from non-encapsulated SRB, FCS was further applied to determine the absence of non-encapsulated SRB, which could potentially co-diffuse into GPMVs (Figure S28-29). Once cells were loaded with the vesicular cargo of choice, as determined by CLSM, the GPMV vesiculation process was induced.

Liposome-based sub-compartments

As with solid sphere particles, we observed transfer of liposomes to the GPMV cavities, and the formation of spherical sub-compartment spaces within individual GPMV units (Figure 32, Figure S32). The negative charge of DSPS liposomes and the PEG chains present on the surface of both DSPS and net neutrally charged DOPC liposomes were selected specifically

to promote free diffusion of objects within the GPMVs, since electrostatic or steric repulsions are known to reduce interactions with the negatively charged plasma membrane.[201]

Encapsulated SRB remained confined to the liposome structure and did not distribute evenly through the GPMV cavities, as observed with the small molecular weight fluorophore loaded in GPMVs (Figure 30). Upon vesiculation, liposomes within GPMVs retained their fluorescence and exhibited similar free diffusion behavior to the encapsulated solid sphere nano-assemblies (Figure 32). Due to the negatively charged nature of DSPS liposomes and the PEG brushes present on the surfaces of both DSPS and DOPC liposomes, only minor interaction with the GPMV membrane was observed with an average of 1 – 2 liposomes per individual GPMV.

Polymersome-based sub-compartments

In comparison to liposomes, polymersomes are known to have a higher mechanical stability due to their thicker membranes, which makes them a superior and more sustainable option for sub-compartments within GPMVs.[55,56] Transfer of SRB-loaded polymersomes from the cytoplasm of HepG2 cells into GPMV cavities was observed (Figure 32, Figure S30-32), and free diffusion of polymersomes within GPMV cavities was possible even after storage at 20°C for 7 days. Polymersome-like structures were observed in ruptured GPMV structures in TEM (Figure S30-31). As with liposomes, no loss or spreading of the fluorescent signal as a free dye within the GPMV was observed by CLSM (Figure S34). This integrity of the sub-compartments was confirmed by using FCS and comparing the molecular brightness (CPM) and diffusion times of sub-compartmentalized SRB-loaded polymersomes in GPMVs (CPM = 57.2 kHz) to free SRB-loaded polymersomes in solution (CPM = 140.6 kHz) (Figure S33-34). Both molecular brightness's of SRB-loaded polymersomes in GPMV and free polymersomes presented similar Gaussian distribution profiles in contrast to free SRB molecules in solution, which had an order of magnitude lower molecular brightness with a narrow distribution profile typical for a free dye (CPM = 13.0 kHz). Further FCS analysis of SRB-loaded polymersomes within GPMVs revealed that the diffusion of polymersomes shifts to longer diffusion (τ_d = 8459 µs) times when polymersomes are within the cytoplasm-like environment of GPMVs (τ_d = 11757 µs) in agreement with the results demonstrating that the cytoplasm is transferred into the GPMVs during the GPMV formation (Figure 30). To further prove the high degree in which the inner composition of GPMVs can be controlled, we transferred free water-soluble e-GFP together with SRB-loaded

$PMOXA_{44}$-$PDMS_6$-$PMOXA_{44}$ polymersomes into GPMVs strengthening the findings of sub-compartmentalization.

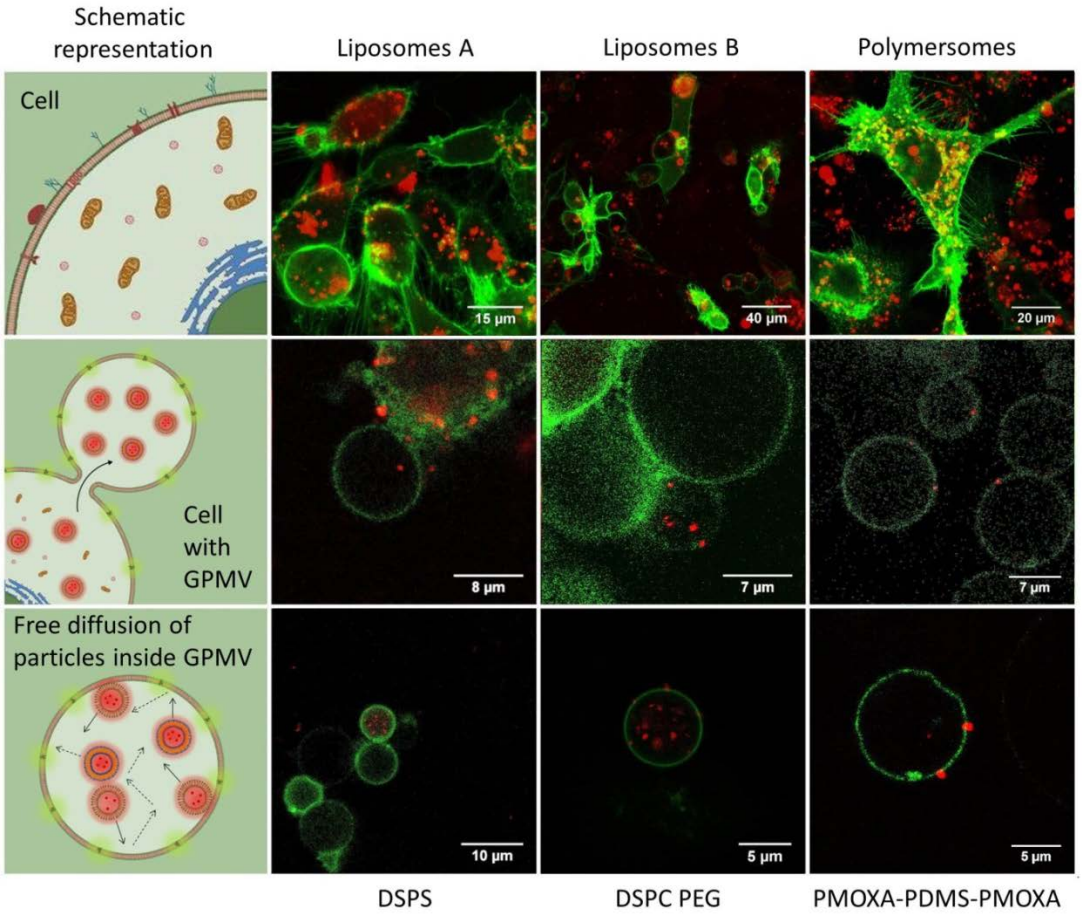

Figure 32. Transfer of artificial nano-sized hollow sphere objects from the HepG2 cytoplasm into GPMV. Top: *HepG2 cells after uptake.* ***Middle:*** *HepG2 cells after vesiculation.* ***Bottom:*** *Isolated GPMVs.* ***Panel a)*** *SRB-loaded DSPS liposomes.* ***Panel b)*** *SRB-loaded DSPC-PEG liposomes.* ***Panel c)*** *PMOXA-PDMS-PMOXA polymersomes. SRB:Red and GFP:Green.*

MOLECULAR FACTORIES BASED ON GPMVS, MF-GMPVS (MULTICOMPARTMENTALIZATION WITHIN GPMVS)

Due to their biomolecule compatibility $PMOXA_{44}$-$PDMS_6$-$PMOXA_{44}$ polymersomes were previously reported[115] as biomimetic nano-compartment spaces, here referred to as catalytic compartments (CatCs), which allowed enzymes to function while confined to the aqueous cavities of polymersomes equipped with bacterial membrane proteins (OmpF). The confinement of enzymes inside CatCs mirrors the natural enzymatic compartmentalization in organelles, since the enzyme confinement within a limited space of a few nanoliters lowers

the enzymatic K_m, and thereby increases the enzyme-substrate affinity in addition to protecting the enzyme from degradation.[167] Due to their robust polymeric nature CatCs preserve their structure after cellular integration and have recently been applied as artificial-organelles.[119]

Here CatCs were prepared by loading the oxidative model enzyme, horseradish peroxidase (HRP) into $PMOXA_{44}$-$PDMS_6$-$PMOXA_{44}$ polymersome cavities. In order to allow the encapsulated enzyme access to substrates through the robust polymer membrane, the bacterial outer membrane protein F (OmpF) was functionally reconstituted in the polymer membrane to form functional nano-compartment spaces.[202] This type of CatCs has been applied recently as an artificial cell organelle with good biocompatibility and preservation of function and architecture upon cellular uptake and has been shown to function in an *in vivo environment*.[119] The prepared CatCs were characterized by DLS and TEM in terms of structure, and by the fluorescent enzymatic Amplex UltraRed assay in terms of functionality (Figure S35-38) with HRP-loaded polymersomes with unpermeabilized membranes serving as a control.

Multi-compartmentalization of CatCs within the GPMV cavities represents a design for the first functional hybrid cell-like molecular factory where a predominantly synthetic artificial organelle functions in a cell-derived artificial cell. The separate localization of the fluorescent signals of SRB and e-GFP indicates that sub-compartments within individual GPMV can exist within a distinct nano-environment that is different from the rest of the GPMVs, (Figure 33). GPMVs loaded with CatCs were derived from HepG2 cells, as described above for SRB-loaded polymersomes, and Amplex UltraRed was chosen as an enzymatic substrate to evaluate the CatCs functionality once within cavities of GPMVs, as the small molecular weight molecule has previously been shown to diffuse through lipid membranes and the plasma membrane of cells, but not through polymersome membranes (Figure 34).[115,203] Along with H_2O_2, HRP encapsulated within CatCs catalyzes the reaction of AR to a fluorescent resorufin-like product in a stoichiometric manner, with a rate limiting step determined by the diffusion of H_2O_2 through the lipid membrane. However, the oxidation of Amplex UltraRed by HRP and H_2O_2 is difficult to follow using CLSM, as the fluorescent resorufin-like product also diffuses out of the GPMVs as it is. In order to demonstrate that the reaction takes place within the GPMV cavities, we made use of local production of H_2O_2. The enzymatic substrates H_2O_2 and AR were added to the GPMV solution and allowed to diffuse into the cavities for 2 hours. At first, no significant change in fluorescence was observed within the GPMV cavities, due to product diffusion out of the cavities. However,

since the diffusion of AR into the aqueous cavities of GPMVs is faster than that of H_2O_2, the 2-hour delay allowed AR to accumulate within the GPMVs.[204] To visualize the reaction of AR to resorufin-like product, we illuminated the GPMVs with a focused 545 nm and thereby speeding up the reaction of AR, in presence of HRP, to the fluorescent resorufin-like product.[204] Compared to GPMVs equipped with control CatCs, an increase in fluorescence was observed limited to the illumination time. The fluorescence within GPMVs subsequently decreased after ceasing illumination, due to product diffusion out of the GPMV cavities. GPMVs loaded with control nanoreactors (HRP polymersomes without OmpF) and GPMVs filled by only cytoplasm demonstrated only a minor or no increase in fluorescence, as the AR substrate cannot effectively diffuse through the polymersome membranes unless they are permeabilized with OmpF nor can the reaction take place efficiently without the HRP catalyst (Figure S38).[170,204] In this way we demonstrate that by fulfilling the requisites of having a substrate permeable outer compartment membrane and an inner molecular machinery that supports multi-compartmentalization, GPMVs can be used to provide enzymatic reactions on demand in a cell-like manner.

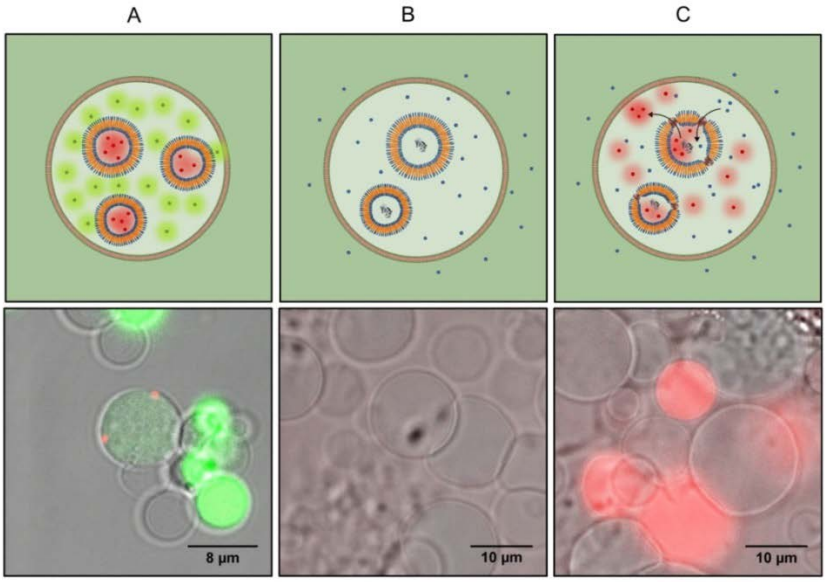

Figure 33. Functional MF-GMPVs: Schematic representation of multi-compartmentalized GPMVs. A) *GPMVs loaded with water soluble e-GFP and SRB-loaded PMOXA-PDMS-PMOXA polymersomes.* ***B)*** *GPMVs loaded with PMOXA-PDMS-PMOXA polymersomes with encapsulated HRP after addition of substrates H_2O_2 and Amplex UltraRed. C) GPMVs loaded with OmpF-equipped PMOXA-PDMS-PMOXA polymersomes with encapsulated HRP after addition of substrates H_2O_2 and Amplex UltraRed.*

TOWARDS IN VIVO SYSTEMS

Size, composition, sub-compartmentalization and the unique possibility of customization make e-GPMVs the closest cell mimic available up till now. However, a crucial aspect necessary to be considered is their stability, toxicity and applicability in a relevant *in vivo* environment. In previous artificial-cell studies this has been neglected - micro compartment spaces acting as cell mimics were only shown to function *in vitro* where they interacted with their environment, among themselves[21] or with other eukaryotic / prokaryotic cells[79] in culture. In order to demonstrate that our e-GPMVs sustain their structure in an *in vivo environment,* we decided to test the artificial cell system in zebrafish embryos as an animal model, which has previously been used to bridge the gap between *in vitro* studies and studies in mammalian organisms (i.e. mice). Due to their optical transparency, relative straightforward genetic modification (i.e. eGFP tagging of immune cells or vasculature) zebrafish embryos have proven themselves on several occasions as great models for pharmacokinetic behaviors of drugs and nanoparticles[205,206] and disease models.[207] In order to promote e-GPMV stability *in vivo* and decrease unspecific protein absorption we choose for injection eGPMV, which had membranes enhanced with Cholesterol-polyethylene glycol-5000 as described above (Figure 34). In addition, we loaded the eGPMV inner cavity with water soluble RFP (Figure 34) serving as a marker for the hollow sphere nature of eGPMVs. Once injected intravenously via the duct of cuvier of the zebrafish embryos eGPMVs in the size of 10 μm were observed circulating in the vasculature of zebrafish for up to 4 hours (Image 34). No acute toxicity, such as change in behavior i.e. mobility, seizures, heart failure or other toxic effects such as malformations, denaturation of tissue fluids or yolk mass was observed in 16 out of 18 ZFE injected with eGPMVs. 2 of the 18 ZFE died due to apparent heart failure or thrombus formation at the injection site. The process of GPMV integration in the organism set in directly after the eGPMV injection, however only smaller eGPMVs (2-5 μm) were seen integrated in the zebrafish tissue most likely due to their size (Figure 34). Surprisingly eGPMVs that transferred from circulation to tissue retained their hollow sphere architecture even after 24h. Their hollow sphere architecture and preservation of the vesicular cargo was verified by photo bleaching experiments within the GPMV cavities, where RFP exhibited a typical exponential photo bleaching behavior (Figure 34).[208,209]

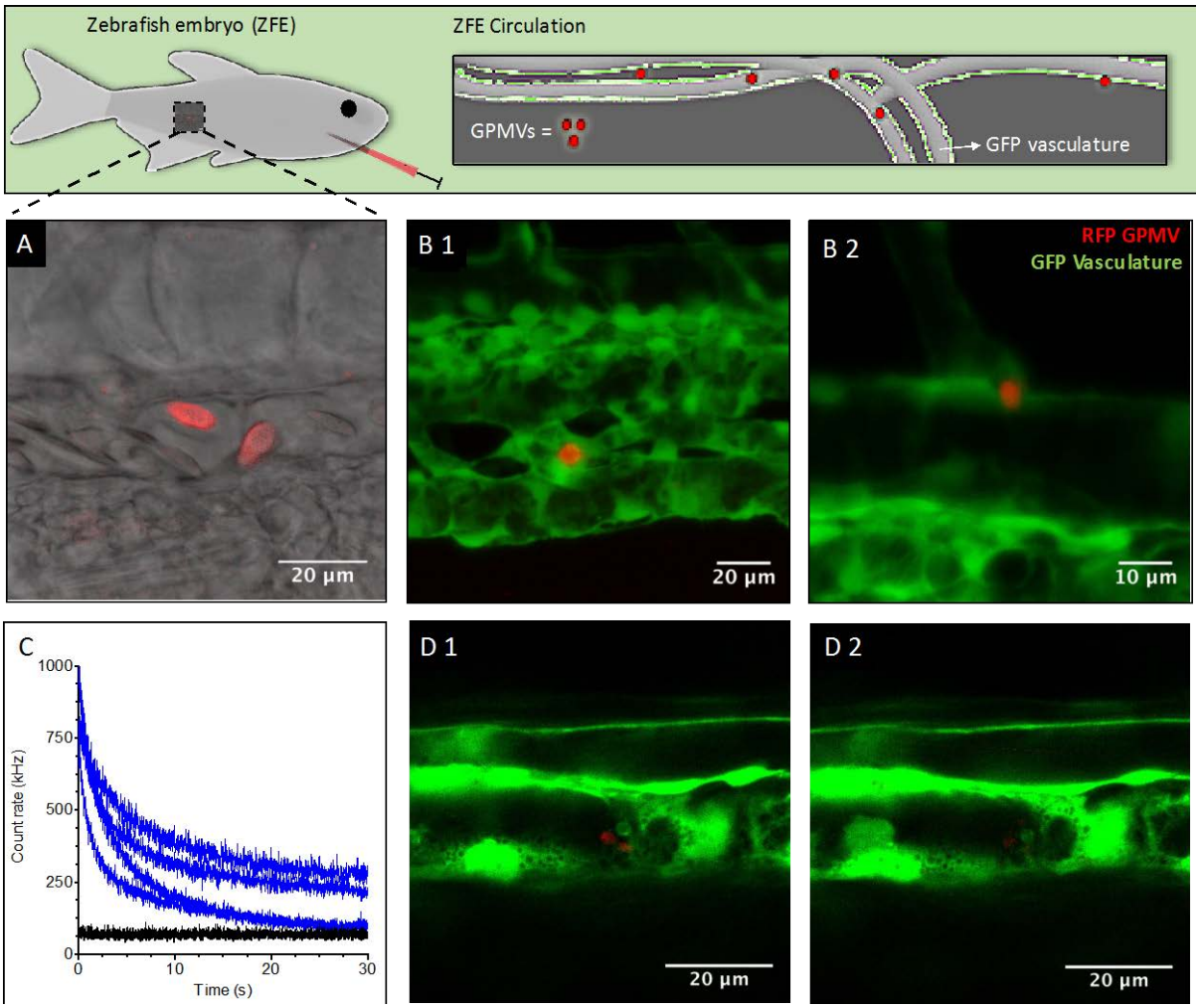

Figure 34. Towards in vivo systems. A) *RFP-loaded GPMVs in ZFE circulation.* ***B 1-2)*** *Maxiumum projection image of RFP-loaded GPMVs in ZFE.* ***C)*** *Photobleaching of RFP-loaded in GPMVs in ZFE after 24h.* ***D1)*** *RFP-loaded GPMV in ZFE before photobleaching.* ***D2)*** *RFP-loaded GPMVs after Photobleaching.*

CONCLUSION

Life is chemistry that takes place in very defined circumstances. This work represents the first report of a cell-like molecular factory, MF-GMPV based on giant plasma membrane vesicles combined with synthetic functional compartments that allow chemical reactions to happen in life-like conditions. Such a hierarchical approach in compartmentalization allows the lower-level synthetic functional compartments within the GPMV to act as independent anatomically discreet units that specialize in their own function, making them nanoscale versions of nature own organelles. The possibility of designing molecular factories by manipulating cellular material (cytoplasm and plasma membrane) by genetic modification together with the

encapsulation of solid sphere structures nanoparticles / vesicular structures (liposomes, polymersomes) in the cytoplasm-like cavities of the GPMVs represents the basis of these molecular factories.

When encapsulated in GPMVs, solid sphere structures can further be used as sensors when there are active objects on their surfaces (i.e. fluoropores), and enzyme-equipped polymersomes with a reconstituted membrane protein (OmpF) can be encapsulated inside the GPMVs as enzymatic nanoreactors where they retain their functionality. When substrates were added to the outer solution of the GPMVs, it was shown that they could penetrate both the membrane of the GPMVs and the inner compartment membranes of the synthetic nanoreactors equipped with OmpF pores. This allowed the enzymatic reaction to take place in the inner cavities of the nanoreactors. Successful substrate conversion was visualized by the fluorescent product (resorufin-like product), which could leave the polymersome and diffuse inside the GPMV cavity, which thus allowed the substrates to be transported to the inside and the product to diffuse out of these polymersomes. Finally, we demonstrate that equipped GPMVs can act as artificial cell mimics – retaining their membrane and inner composition if they are injected into multicellular organisms. To the best of our knowledge, this is the first time that a molecular factory functioning as a cell-like mimic has been be constructed and has been tested *in* vivo by taking advantage of the fundamental nature of GPMVs.

Chapter 6

CONCLUSION AND OUTLOOK

Towards the development of cell mimics, the creation of giant unilamellar vesicles (GUVs and GPMVs) with inserted functional biomolecules or membrane proteins could be realized in this work. Due to their size in the micrometer range, which corresponds to the size of eucaryotic cells, GUVs and GPMVs have the unique advantage that they can be visualized and analysed by microscopy techniques in real-time. This allows getting a deeper insight into biological processes.

We demonstrated that synthetic GUVs are suitable platforms to study the permeating properties of biopores. It was possible to insert the small pore-forming peptide gramicidin with preserved functionality into the membranes of polymer GUVs. The functional insertion was successful in a small library of PMOXAx-PDMSy-PMOXAx copolymers, which self-assemble in giant unilamellar vesicles (GUVs) with membrane thickness ranging from 9.2 to 16.2 nm. Due to the mismatch between the pore length and the polymer membrane thickness the functional insertion in thicker membranes was not possible. The functionality of this biopore which is known to allow transport of protons could be visualized by the encapsulation of a fluorescent pH-sensitive dye inside the GUV cavities. Proton gradients between the environment of GUVs and their inner cavity served to assess the exchange of protons across the membrane upon gA insertion. With this approach pH self-regulating GUVs, which maintain their integrity in different pH gradient conditions could be created.

Further it was possible to use synthetic GUVs in order to visualize an enzymatic reaction inside their cavities by the functional reconstitution of the membrane protein OmpF, a next step towards mimicking cell architecture. This was the first time a membrane protein could be reconstituted into the membrane of polymer GUVs with preserved functionality which is shown by initiating an *in situ* enzymatic reaction with a fluorescent product produced inside GUV cavities where the enzyme was encapsulated. The pore OmpF allowed the diffusion of substrates and products through the membrane of GUVs. Due to the fluorescent product the model enzyme reaction inside the GUV cavities was monitored in real-time and gave insight into both the substrate conversion rate by the encapsulated enzyme and the reconstitution of the functional membrane protein (OmpF) in synthetic GUV membranes. The encapsulated enzyme could diffuse freely inside the large GUV cavities. Further there seems to be a size-

dependent trend in enzyme conversion rate in respect of GUV diameters. Due to their micro-sizes, GUVs provide the unique opportunity for observing the behavior of biomolecules within their defined confined spaces via microscopic techniques. The approach of equipping the synthetic membranes together with the cavities of GUVs with biomolecules opens the way towards cell-like compartments as novel materials. These bio-equipped GUVs not only offer increased stability and lower membrane permeability compared to lipid GUVs, they further facilitate the control of specific catalytic reaction inside confined spaces mimicking the size and architecture of native cells. This straightforward approach serves to obtain deeper insights of biological processes or interactions of biomolecules with membranes in real-time or as biosensors. Therefore they allow the relevant study of bio-processes *in vitro* in a simple manner. Thinking even further ahead, molecular factories and advanced cell mimics could be developed by encapsulating in cell-sized GUVs various polymersomes loaded with different types of enzyme inside their cavities.

Finally the first bioinspired molecular factory with functionality as a real cell mimic could be realized based on micrometer-sized giant plasma membrane vesicles (GPMVs).

GPMVs are cell-derived giant vesicles consisting of an outer compartment architecture (membrane) and an inner composition, which both directly mirror the composition of cells from which they originate except the larger organelles like for example nuclei and Golgi apparatus making measurements easier and are the closest cell-mimic available on the market up to now.

In a step towards the development of bioinspired molecular factories with functionality as cell mimics, we created sophisticated hybrid molecular factories based on GPMVs, which are equipped with a synthetic molecular machinery inside their cavities that provides functionality. Such a hierarchical approach in compartmentalization allows the lower-level synthetic functional compartments encapsulated within the cavities of the GPMVs to act as independent anatomically discreet units that specialize in their own function, making them nanoscale versions of nature own organelles.

The realization of the bioinspired molecular factory was achieved via the encapsulation of nanoreactors inside the GPMV cavities where they retained their functionality. These nanoreactors represented enzyme-equipped polymersomes with a reconstituted membrane protein (OmpF), which was essential to allow substrates and the product to pass the polymer membrane. Therefore, the substrates which were added to outer solution could pass the GPMV membranes and further the inner compartment membranes of the synthetic nanoreactors to reach the enzyme. The functionality of the nanoreactors when encapsulated

inside GPMVs could be visualized due to the generated fluorescent product of the enzymatic reaction which could leave the nanoreactors and diffused into the cavities of the GPMVs. As a result the cavity of the GPMVs showed fluorescence.

Finally equipped GPMVs retained their architectures (membrane and inner composition) when injected into multicellular organisms – Zebrafish embryos. This was the first time that a molecular factory functioning as cell mimic has been tested in vivo by taking advantage of the fundamental nature of GPMVs.

The successful creation of synthetic GUVs equipped with functional biomolecules like the small pore forming peptide gA and the bacterial membrane protein OmpF shows great promise towards the reconstitution of more sensitive membrane proteins, or further the reconstitution of different kinds of membrane proteins at the same time into the polymer membranes of GUVs. Further the realization of the first artificial molecular factory by using GPMVs opens the way towards the production of man-made artificial cells. The option to design both, their membranes by gene modification and their inner cavities by equipping them with any kind of biomolecules, compartments and nanoreactors could enable the creation towards closer cell mimics for example different functional reconstituted membrane proteins/receptors etc. combined with different kinds of functional compartments inside their cavities would give us a deeper insight into the cell metabolism of native cells.

The creation of artificial cell-sized compartments used as biomimetic microscale platforms to visualize and imitate biological processes in real-time can increase our knowledge about understanding native cells, the smallest unit of life. A micrometer-sized artificial cell makes it possible to get a deeper insight into the otherwise hidden world in the nanometer range.

Chapter 7

MATERIALS AND METHODS

CHAPTER 3

Materials

Gramicidin from Bacillus aneurinolyctus (Bacillus brevis), linear polypeptide antibiotic complex A mixture of gramicidins A, B, C, and D, 8-hydroxypyrene-1,3,6-trisulfonic acid trisodium salt (pyranine), 5(6)-carboxyfluorescein, monosodium phosphate (NaH_2PO_4), potassium phosphate dibasic (K_2HPO_4), potassium phosphate monobasic (KH_2PO_4), sodium chloride (NaCl), sodium hydroxide (NaOH), hydrochloric acid (HCl), ethanol (EtOH), and dimethyl sulfoxide (DMSO), C_2H_6OS, were obtained from Sigma Aldrich (Buchs, Switzerland) and were used as received. 6-(((4,4-difluoro-5-(2-thienyl)-4-bora-3a,4a-diaza-s-indacene-3-yl)styryloxy)acetyl) aminohexanoic acid, succinimidyl ester (BODIPY) 630/650 fluorophore was purchased from Molecular Probes (Eugene, United States). Asante Natrium Green-2 (ANG-2) and Asante Potassium Green-2 (APG-2) were purchased from TEFLabs Inc.

Preparation of giant unilamellar vesicles (GUVs) and insertion of gA

GUVs were formed by the electroformation technique[210] using a Nanion Vesicle Prep Pro setup (Nanion Technologies, Munich, Germany). Briefly, 50 μL of a 4 mg/mL polymer stock solution in EtOH was spread on an indium tin oxide (ITO) coated glass slide to form a smooth polymer film on the glass surface, followed by drying for 45 min in high vacuum. By using an O-ring, a closed chamber was formed filled with a solution containing 100 mm sucrose, 10 mm K_2HPO_4/KH_2PO_4, pH 5.5 and 0.05 mM 5(6)-carboxyfluorescein (Sigma). Electroformation was performed overnight, in dark at RT (2.0 V, 3.0 Hz).

For imaging, GUVs containing gA were formed by addition of 0.7 μL 0.32 mg/mL gA (567 nM final concentration) to GUVs solution. gA insertion was tested by changing the pH with 1 μL of 0.4 M NaOH. The intrinsic permeability of GUVs to proton outflux was verified by incubating solutions of GUVs with 0.7 μL DMSO:EtOH (1:1) ratio solvent, and 1 μL 0.4 M of NaOH.

Confocal laser scanning microscopy (CLSM)

CLSM experiments were performed on a confocal laser-scanning microscope (Zeiss LSM 510-META/Confocor2, Carl Zeiss, Jena, Germany). An Argon/2 laser (λ = 488 nm, 30 mW, 25% power output, 0.5% transmission) as the excitation source. A main dichromatic beam splitter (HFT 488/543), a secondary dichroic beam splitter (NFT 515) and a band pass filter (BP 505-530) were used in all experiments. In case of BODIPY, a He–Ne laser (λ = 633 nm) was used as the excitation source with a transmission of 15%, and main dichromatic beam splitter (HFT UV/488/543/633), a secondary dichroic beam splitter (NFT 545) and a band pass filter (LP 650). The images were recorded with a water immersion objective (C-Apochromat 40x/1.2W). Each sample was scanned unidirectionally using an automatically controlled time series with a cycle delay of 5s.

GUV solutions were diluted in 60 mM K_2HPO_4/KH_2PO_4 buffer and transferred to plasma-cleaned 8-well borosilicate microscopy chambers (ThermoFischer Scientific). For visualization purposes, GUV membranes were stained with Bodipy 630/650. Gramicidin insertion in GUV membranes was observed by using a fluorescently labeled amphiphilic peptide (OG488-K8-gA), containing the complete gA sequence labeled with OregonGreen488. As both OG488 and Bodipy have different excitation and emission wavelengths (OG488: λex = 501/λem = 526, and Bodipy 630/650: λex = 625/λem = 640 respectively), CLSM is suitable for their concurrent visualization.

CHAPTER 4

Materials

Reagents and materials were of the highest commercially available grade and used without further purification, unless indicated. Reagents were purchased from Sigma-Aldrich unless otherwise specified. n-octyl-β-D-glucopyranoside (OG) (Anatrace), Amplex UltraRed, 30% H_2O_2 (Sigma Aldrich), Horseradish Peroxidase Type IV (Sigma Aldrich), Atto 488 maleimide (ATTO-TEC GmbH), Atto 488 succinimide ester, (ATTO-TEC GmbH), sucrose (Sigma Aldrich) and polystyrene beads (2-10 µm) (Spherotech). A 4-15% Mini-PROTEAN® TGX™ Precast Gels SDS (Biorad).

Polymer synthesis

PMOXA-*b*-PDMS-*b*-PMOXA (poly(2-methyl-2-oxazoline) - *block* - poly(dimethylsiloxane) – *block* – poly(2-methyl-2-oxazoline)) triblock copolymer ($A_7B_{49}A_7$) was synthesized according to the protocol described previously.[83]

GUV preparation

GUVs were prepared by the film rehydration method. Briefly 0.2 mg of the polymer PMOXA-*b*-PDMS-*b*-PMOXA ($A_7B_{49}A_7$), dissolved in 50 µL ETOH was dried for 1h under vacuum. Afterwards the film was rehydrated with 680 µL 300 mM sucrose in ddH_2O. The sample was then held at RT overnight without stirring.

OmpF expression and extraction

The OmpF K89 R270 cysteine mutant (OmpF-M) expression and extraction was done as previously reported in [115,170]. First under aseptic conditions, a loop full of cells from an ampicillin resistant *Escherichia Coli* strain BL21 stock culture that overexpressed the OmpF K89 R270 mutant was smeared onto the surface of a lysogeny broth (LB), ampicillin (100 mg mL^{-1} ampicillin) agar plate. After 16 hours of incubation at 37 °C, a single colony was selected and transferred from the plate to 10 mL of terrific broth (TB) liquid medium with 100 mg mL^{-1} ampicillin (4 flasks in total). 5 L TB medium with 100 mg mL^{-1} ampicillin was inoculated with 15 mL of the overnight culture (OD = 0.1-0.5), and the optical density of the growing culture was followed by measuring the absorbance at 600 nm. When the absorbance reached an OD of 0.6, IPTG was added to a final concentration of 1 mM in order to start the

over-expression of the OmpF-M gene. The bacteria were grown for 16 more hours at 25 ºC, with vigorous stirring, then the *E. Coli* cells were pelleted at 7.000 *g* for 8 min at 4 ºC. Pellets were stored at -25 ºC, and on the following day were re-suspended in 50 mL of 25 mM Tris-HCl pH 7.4. 10 mg DNase and 10 mg RNase were added, and the cell suspension French pressed five times at 1,000 bar. 1 mL of 20% SDS was added per 10 mL of cell suspension and incubated for 1 h at 60 ºC. The suspension was centrifuged at 50.000 *g* at 23 ºC for 1 hour. The supernatant was removed and the cell pellet incubated in 0.125% OG for 1 h at 37 ºC. The suspension was then centrifuged at 50.000 *g* for 1 hour at 23 ºC. Finally, the cell pellet was re-suspended in 3% OG in 10 mM phosphate buffer and homogenized. The suspension was centrifuged at 50.000 *g* and the protein concentration in the supernatant was determined by UV-Vis absorption at 280 nm. Before the reconstitution experiments were carried out, the protein was dialysed against 1L of 0.05 % OG in PBS for 16 hours and twice against PBS pH 7.4 for 2 hours. After the dialysis the protein concentration was adjusted to 1.2 mg mL^{-1}.

Labeling of OmpF-M

The OmpF K89 R270 double cysteine mutant in 3% OG was modified by attaching Atto 488 maleimide (MW 1067 kDa, Atto 488 maleimide, BioReagent, suitable for fluorescence, ≥90% from Sigma) to free thiol groups of cysteine residues. The same reaction was also performed in presence of either OmpF wild type (OmpF-WT) in 3% OG) or 3% octyl glucopyranoside. This served as a control of unspecific interactions of the fluorophore with other amino acid residues or OG micelles. 10 µL of 10mM Atto 488 dissolved in 5% DMSO in PBS buffer pH 7.4 was added to 400 µL of 0.9 mg mL^{-1} OmpF, and mixed. The protein was purified by washing 20 times with 1% OG in PBS pH 7.2 in Vivaspin-0.5 mL centrifugal filters for protein purification and concentration, molecular cut off: 10 kDA (10 min at 13 000 RPM). The volume was adjusted to 475 µL PBS pH 7.2 and the protein concentration was determined by UV-Vis spectroscopy. 40 µL of the purified protein fraction was taken for FCS analysis and SDS gel electrophoresis. Before the reconstitution experiments were carried out, the protein was dialysed against 1L of 0.05 % OG in PBS for 16 hours and twice against PBS pH 7.4 for 2 hours. No residual fluorescence was observed in the OG and OmpF-WT controls, as determined by FCS. The protein concentration was determined by UV-Vis spectroscopy (Nanodrop) and adjusted to 0.4 mg mL^{-1} with 0.05% OG, PBS.

Reconstitution of OmpF-M

Before the reconstitution the media of OmpF-M (PBS) was exchanged to ddH_2O by filtering using 10 kDa Amicons (4 x 400 µL ddH_2O). For control experiments the first flowthrough when exchanging the OmpF-M media from PBS to ddH_2O was taken and washed with 4 x 400 µL ddH_2O. The reconstitution was carried out by adding 10 µL of a solution of OmpF-M in water (≈1.2 mg mL^{-1}) calculated/measured by UV-Vis spectroscopy (Nanodrop, Thermofischer Scientific) or 10 µL of the control solution directly to the film formation solution (0.2 mg polymer PMOXA-*b*-PDMS-*b*-PMOXA ($A_7B_{49}A_7$) in 40 µL ETOH.

Flow cytometry

For flow cytometry measurements, the GUVs solution (containing GUVs in 300 mM sucrose solution in ddH_2O with encapsulated enzyme HRP) was diluted 1:1 with PBS and 600 µL of this solution was used for dialysis using 300 kDa cut-off Spectrapore dialysis tubes. The dialysis was carried out for 24 h and 3 x buffer (PBS) was exchanged during that time period approximately every 24h. Afterwards the volume was adjusted again to 600 µL. A sample volume of 400 µL was chosen in which 50 µL of the dialysed sample solution (polymer only-control, filtrate-control and OmpF-M sample) was added to 350 µL PBS and measured first without adding the reactants. Then 50 µL of the dialysed sample solution (polymer only-control, filtrate-control and OmpF-M sample) was added into 300 µL PBS. Afterwards 70 µL of a solution in PBS containing the reagents Amplex UltraRed and H_2O_2 was added to the GUV solution, carefully mixed by pipetting and immediately measured by flow cytometry.
Flow cytometry analysis was performed using a BD FACSCanto II flow cytometer (BD Bioscience, USA). Doublets were excluded using FSC and SSC detectors. For assessing the OmpF-Atto 488 reconstitution – single GUVs were excited at 488 and the emission was detected using FL-1 (533/30; Atto 488 channel). For assessing the Amplex UltraRed conversion, single giants were excited at 561 nm and the emission was detected in FL15 (586/15; resorufin channel). A total of 4000 events for each sample were analyzed, and data processed using Flow Jo VX software (TreeStar, Ashland, OR). The samples were measured in “slow flowthrough” mode and the cytometer nozzle was kept at an appropriate distance from the sampling tube in order to prevent shear forces, which could influence the GUV integrity.

Labeling of the enzyme HRP

1 mL of HRP (0.2 mg mL^{-1} 44 kDa, 4.5 µM) in sodium bicarbonate buffer (pH=8.2) was mixed with 10 µL of Atto 488 succinimide ester in DMSO (final dye concentration in this mixture 100 µM). The solution was placed on a shaker overnight (24 hours) at 20 ºC. Afterwards 500 µL of this solution was dialysed against PBS for 2 days using dialysing tubes with a 14 kDa cut-off Membra-Cel™ (Carl Roth, Germany) and the buffer was exchanged twice per day approximately every 8 hours. Afterwards the volume was adjusted again to 500 µL using PBS. By using spin-columns (Vivaspin500) with a 10 kDa cut-off the sample was washed 10 x with 500 µL PBS in each case. The next step was the FCS measurements to determine the success of the enzyme labeling. For enzyme encapsulation experiments in GUVs, the PBS was exchanged by 300 mM sucrose in ddH_2O by using spin-columns (Vivaspin500) with a 10 kDa cut-off. Therefore, the solution of HRP in PBS was washed 3 x using 400 µL 300 mM sucrose in ddH_2O. Afterwards FCS measurements were performed, and a SDS-PAGE gel prepared to verify the successful labeling of the enzyme. For control experiments the unlabeled HRP was used without further purification. To visualize the enzyme encapsulation by using the labeled enzyme, the same amount of enzyme was used as that of the unlabeled enzyme used for the reaction inside the GUVs.

Enzyme encapsulation

The enzyme HRP (0.05 µM for LSM experiments and 0.025 µM for flow cytometry experiments) in 680 µL sucrose solution was added to the dried polymer film with or without OmpF-M. The formed GUV solution was diluted 1:1 with PBS. Because of the higher molecular weight of the sucrose compared to the buffer components, the GUVs immediately drop down to the bottom/surface of the chamber, interact with the hydrophilic glass and form hemispheres. After 15 min, the sample (200 µL) was washed with PBS by 10 addition and removal steps of 50 µL PBS to remove any free enzyme.

Confocal laser Scanning microscopy (CLSM)

For LSM measurements, the solution of HRP-loaded GUVs or HRP-loaded GUVs equipped with OmpF-M in 300 mM sucrose solution in ddH_2O was diluted 1:1 with PBS (150 mM) for each sample to allow the GUVs to settle on the chamber surface due to a difference in density between the GUV inner cavity and outer environment.

GUVs were adsorbed (immobilized) on the borosilicate glass surface of a plasma-treated microscopy chamber (Nunc™ Lab-Tek™ Chamber Slide System, Thermo Fisher Scientific) filled with isosmotic buffer (PBS).

Briefly, the microscopy chamber slide was first oxygen-plasma cleaned for 5 minutes in order to generate hydroxyl groups on the glass surface. The microscopy chamber was then filled with the sample solutions (200 µL). After 15 min, the sample was washed with PBS by 10 addition and removal steps of 50 µL PBS to remove any free enzyme.

Suitable GUVs were selected in the LSM (laser scanning microscopy) mode.

Confocal laser Scanning microscopy (CLSM) measurements were performed at 20 °C using a confocal laser scanning microscope (ZEISS LSM 510 META-ConfoCor, inverted microscope ZEISS Axio Observer, Carl Zeiss, Germany) with a water immersion objective lens (C-Apochromate 40x/1.2W korr). For CLSM measurements, a He-Ne laser was used (λ = 543 nm, 5 % laser intensity) as the excitation source. A main dichromatic beam splitter (HFT 488/543) was used in all the experiments. The detector range was set to 560-615 nm. The pinhole was adjusted to 1 airy units and the gain was set to 700. Each sample was scanned unidirectionally using a scan time of 16.73 seconds per image and 512 x 512 pixels with a Bit Depth of 8 Bit. Videos were taken with an image recording time of 15.7 s/image and 1 s delay. Afterwards the mean fluorescence intensity of every raw image was calculated using the program ImageJ to calculate the fluorescence intensity.

For CLSM measurements, only GUVs $\geq$ 5 µm were selected. The substrates Amplex UltraRed (5 µL of 0.1 mmol mL^{-1} in DMSO) and H_2O_2 (5 µL of 0.1 mmol mL^{-1} in ddH_2O) were mixed and these 10 µL were added during the measurements.

FCS measurements

All FCS measurements were carried out using a ConfoCor2 instrument (Carl Zeiss, Germany) with a 40x, 1.2. water immersion C-Apochromat objective lens. Measurements were carried out at room temperature. An Argon 488 laser was used for excitation of the Atto 488 fluorophore at 488 nm (Laser power output 20%, 2.8 mW) with the appropriate filter sets (HFT 488, BP 505-550). The fluorescence signal was measured in real-time and the autocorrelation function was calculated by a software correlator (LSM 510 META-ConfoCor 2 System). Measurements were recorded over 3s and each measurement was repeated 30 times for measurements done with Atto 488 labeled HRP and repeated 60 times for

experiments done with Atto 488 labeled OmpF-M. Correlation curves that could not be fitted were excluded (<10%).

For determining the specific binding of Atto 488 succinimide ester to HRP and and Atto 488 malemide to OmpF-M, experimental auto correlation curves were fitted using a two-component model including the triplet state (Eq. 1).

Eq. 1:

$$G(\tau)_{fit} = 1 + \left(1 + \frac{T}{1-T} e^{-\frac{\tau}{\tau_{trip}}}\right) \frac{1}{N} \left[\frac{f_1}{1 + \frac{\tau}{\tau_{D1}}} \frac{1}{\sqrt{1 + R^2 \frac{\tau}{\tau_{D1}}}}\right] + \left(1 + \frac{T}{1-T} e^{-\frac{\tau}{\tau_{trip}}}\right) \frac{1}{N} \left[\frac{f_2}{1 + \frac{\tau}{\tau_{D2}}} \frac{1}{\sqrt{1 + R^2 \frac{\tau}{\tau_{D2}}}}\right]$$

τ_D represents the diffusion time, T the fraction of fluorophores in triplet state with triplet time τ_{trip}, N is the number of particles and R the structural parameter.
R and τ_D of free dye (Atto 488) were determined independently, experimental auto correlation curves were fitted using a one component model including triplet state (Eq. 2).

Eq. 2:

$$G(\tau)_{fit} = 1 + (1 + \frac{T}{1-T} e^{-\frac{\tau}{\tau_{trip}}}) \frac{1}{N} \left[\frac{1}{1 + \frac{\tau}{\tau_D}} \frac{1}{\sqrt{1 + R^2 \frac{\tau}{\tau_D}}}\right]$$

τ_D represents the diffusion time, T the fraction of fluorophores in triplet state with triplet time τ_{trip}, N is the number of particles and R the structural parameter. R and τ_D of free dye (Atto 488) were determined independently.
R and τ_D of Atto 488 were subsequently fixed in the fitting procedure in order to determine the % of free dye fraction, which represented the unreacted fluorophore still present in the solution after purification of HRP or OmpF-M conjugated with Atto 488.

The Amplex UltraRed (AR) conversion kinetics of free HRP in solution measured via Spectra max (Molecular devices)

(1) 10 µL of a mixture of AR (0.4 µmol mL^{-1}) and H_2O_2 (0.4 µmol mL^{-1}) in PBS was added to 200 µL of a solution of HRP (0.321 ng mL^{-1}) in 300mM sucrose in ddH_2O. (in sucrose)
(2) For comparison 10 µL of a mixture of AR (0.4 µmol mL^{-1}) and H_2O_2 (0.4µmol mL^{-1}) in PBS was added to 200 µL of a solution of HRP (20.0 ng mL^{-1}) in PBS. (in PBS)
(3) 10 µL of a mixture of AR (0.4 µmol mL^{-1}) and H_2O_2 (0.4 µmol mL^{-1}) in PBS was added to 200 µL of 300mM sucrose in ddH_2O. (without HRP)
(4) 10 µL of AR (0.4 µmol mL^{-1}) in PBS was added to 200 µL of a solution of HRP (20.0 ng mL^{-1}) in 300mM sucrose in ddH_2O. (without H_2O_2)
(5) 10 µL of H_2O_2 (0.4 µmol/mL) in PBS was added to 200 µL of a solution of HRP (20.0 ng mL^{-1}) in 300mM sucrose in ddH_2O. (without AR)

Preparation of OmpF nanoreactors with encapsulated enzyme

Polymersome nanoreactors were prepared at 20 ºC from the ABA triblock copolymer, PMOXA-*b*-PDMS-*b*-PMOXA ($A_7B_{49}A_7$) and OmpF K89 R270 as previously reported in [115,170]. The synthetic procedure and the polymer characterization are presented in [83]. Nanoreactors were generated using the film rehydration technique in the presence of OmpF-M, and HRP in either PBS buffer pH=7.4 or 300 mM sucrose in ddH_20 at 20ºC. Thin polymer films were rehydrated to a final polymer concentration of 2.5 mg mL^{-1}, HRP concentration of 0.2 mg mL^{-1}, and OmpF-M concentration of 80 µg mL^{-1}, respectively. Polymersomes without OmpF-M were also prepared in the absence of OmpF-M. Rehydrated films were stirred overnight at 20 ºC. On the following day all samples were extruded through an Avanti mini-extruder (Avanti Polar Lipids, Alabama, USA) using a 100 nm diameter pore-size polycarbonate membrane (11 times) in order to obtain size homogeneity. Non-encapsulated HRP was removed from the nanoreactors by dialysis against PBS at pH 7.4 at 20 ºC for 5 days, exchanging the buffer every 8 hours, using Spectrapore dialysis tubes with a molecular weight cut-off of 300 kDa (from Spectrum Laboratories Inc.) All activity measurements were performed on the following day.

Functionality of the enzyme reaction in OmpF nanoreactors under the same conditions

In order to verify if the sucrose buffer used in the rehydration solution of the polymer film affects OmpF-M insertion and the self-assembly of the PMOXA-*b*-PDMS-*b*-PMOXA ($A_7B_{49}A_7$) polymer, the insertion of the porin was tested on smaller polymersomes as previously reported[115,167] with the modification of using the sucrose buffer. Sucrose did not appear to influence the membrane permeability or architecture (Figure S5, S6) of the upermeabelized HRP-loaded polymersomes, nor did it influence the OmpF-M insertion into the polymersomes.

TEM

0.5 mg mL^{-1} HRP-loaded polymersomes or HRP-loaded polymersomes equipped with OmpF-M solution were used for for TEM imaging studies were negatively stained with 1.5% uranyl acetate solution and deposited on carbon-coated copper grids. A transmission electron microscope (Philips Morgagni 268D) at 293 K was used (Figure S3a).

Dynamic lightscattering

The measurements of D_H of polymersomes were performed on a Zetasizer Nano ZSP at 25 °C. The measure angle is 173° and the data were analyzed by intensity distribution. 450 µL of 0.5 mg mL^{-1} HRP-loaded polymersomes or HRP-loaded polymersomes equipped with OmpF-M solution were used for the measurements.

CHAPTER 5

Isolation of GMPVs

The supernatant from the 6-well plates was transferred to an Eppendorf tube and centrifuged at 100 g for 10 min to remove cells. 200 µL of the supernatant was transferred to poly-D-lysine- or plasma-activated 8-well microscopy chamber (Nunc™ Lab-Tek™ Chamber Slide System, Thermo Fisher Scientific).

Confocal laser Scanning microscopy (CLSM)

CLSM measurements were performed using a confocal laser scanning microscope (ZEISS LSM 880, inverted microscope ZEISS Axio Observer, Carl Zeiss, Germany) equipped with a water immersion objective (C-Apochromate 40x/1.2W korr FCS M27). Samples containing GFP and Q-dots were excited with an argon laser at 488 nm by setting the detector range to 499-521 nm for GFP and 640-714 for Q-dots. To measure the fluorescence of RFP-actin, SRB, resorufin, and RFP, a diode-pumped solid-state 561-10 laser (DPSS) at 561 nm was used as excitation source and the detector range set to 572-704 nm. A helium-neon laser (HeNe) at 633 nm was used to measure samples containing CellTracker™ Deep Red, and the fluorescent signal was collected with a detector range of 651-740 nm. Respectively, nano compartment beam splitters (MBS) of 488, 561 and 633 were used. Each sample was scanned unidirectional using 1024 x 1024 pixels with a Bit Depth of 16 Bit. Afterwards, every raw image was adjusted with ImageJ software.

Cells were imaged either 24h after treatment with transfection agents or nano-formulations. Cells stained with CellTracker™ Deep Red were imaged directly after the final washing step. To minimize spectral crosstalk the samples were scanned using sequential mode. The laser settings between cells that weren't treated and cells treated by transfection or addition of dye/nanoformulation, the photomultiplier tube gain, and the pinhole settings were kept constant during the analyses.

CellTracker™ Deep Red staining and GPMV packaging

HepG2 cells were either cultured at a density of $4x10^4$ cells per well in a µ-Slide 8 Well, Collagen IV: coverslip or at a density of $30x10^4$ in a 6 Well , in 200 µL or 500 µL DMEM growth medium (High Glucose DMEM, supplemented with 10% fetal calf serum, penicillin (100 units mL^{-1}) and streptomycin (100 µg mL^{-1})). 1 minute after culturing the cells 10 µL of

CellLight® Plasma Membrane-GFP BacMam 2.0 was added for cells cultured in 8 wells and 25 µL for cells cultured in 6 wells. Cells were incubated for 24 h at 37 ºC, 5% CO_2 to allow attachment on surface. After 24 h the medium was removed and CellTracker™ Deep Red was added according to the manufacturer's instructions. Cells were incubated for 30 min, then washed five times with DMEM growth medium.

GPMV membrane modifications PEG-5000, DiI, DOPE-Rhodamine, DOPE-FITC

HepG2 cells were either cultured at a density of $4x10^4$ cells per well in a µ-Slide 8 Well, Collagen IV: coverslip or at a density of $30x10^4$ in a 6 Well, in 200 µL or 500 µL DMEM growth medium (High Glucose DMEM, supplemented with 10% fetal calf serum, penicillin (100 units mL^{-1}), and streptomycin (100 µg mL^{-1})). Cells were incubated for 24 h at 37 ºC, 5% CO_2 to allow attachment to the surface.

For Cholesterol-PEG-5000 membrane modifications, Cholesterol-PEG-5000-FITC and Cholesterol-PEG-5000-CLS were purchased from Nanocs Inc and a 20 µg mL^{-1} solution was prepared in DMEM growth medium. Cells were treated with Cholesterol-PEG-5000-FITC for 10 minutes before removing the medium and adding GPMV formation buffer. For *in vivo* experiments cells were treated with a Cholesterol-PEG-5000-FITC and Cholesterol-PEG-CLS solution in a 20 µg mL^{-1} solution in DMEM for 1 h before removing the medium, washing the cells with PBS and adding the GPMV formation buffer.

For DOPE-FITC and DOPE-Rhodamine membrane modifications, DOPE-FITC and DOPE-Rhodamine were purchased from Avanti Polar lipids. 20 µg mL^{-1} solutions of either DOPE-FITC and DOPE-Rhodamine were prepared in DMEM growth medium. For GPMVs equipped with both DOPE-FITC and DOPE-Rhodamine, the 20 µg mL^{-1} solutions of either membrane marker were mixed in a 1:1 ratio (10 µg mL^{-1} final concentration). Cells were treated with DOPE-Rhodamine, DOPE-FITC or DOPE-FITC/DOPE-Rhodamine solutions for 10 minutes before removing the medium, washing the cells with PBS and adding GPMV formation buffer.

For DiD 633 Labelling a 10 µg mL^{-1} DiD solution was prepared in DMEM growth medium. Cells were treated with the 10 µg mL^{-1} DiD solution in DMEM growth medium for 10 min before removing the medium, washing the cells with PBS and adding GPMV formation buffer.

GFP and RFP transfection and GPMV packaging

HepG2 cells were either cultured at a density of $4x10^4$ cells per well in a µ-Slide 8 Well, Collagen IV: coverslip or at a density of $30x10^4$ in a 6 Well, in 200 µL or 500 µL DMEM growth medium (High Glucose DMEM, supplemented with 10% fetal calf serum, penicillin (100 units mL^{-1}), and streptomycin (100 µg mL^{-1})). Cells were incubated for 24 h at 37 ºC, 5% CO_2 to allow attachment to the surface. After 24 h GFP or GFP and RFP transfection agent were added. After 24 h, the medium was removed and GPMV formation buffer was added. Cells were imaged after incubation with GPMV buffer for 1 h at 37 ºC, 5% CO_2.

RFP actin transfection and GPMV packaging

HepG2 cells were either cultured at a density of $4x10^4$ cells per well in a µ-Slide 8 Well, Collagen IV: coverslip or at a density of $30x10^4$ in a 6 Well , in 200µL or 500µL DMEM growth medium (High Glucose DMEM, supplemented with 10% fetal calf serum, penicillin (100 units mL^{-1}), and streptomycin (100 µg mL^{-1})). 1 minute after culturing the cells, 10 µL of CellLight® Plasma Membrane-GFP BacMam 2.0 and CellLight® Actin-RFP, BacMam 2.0 were added for cells cultured in 8 wells and 25 µL for cells cultured in 6 wells, respectively. After 24 h the medium was removed and GPMV formation buffer was added. Cells were imaged after incubation with GPMV buffer for 1 hour at 37 ºC, 5% CO_2.

Quantum dot uptake and GPMV packaging

HepG2 cells were either cultured at a density of $4x10^4$ cells per well in a µ-Slide 8 Well, Collagen IV: coverslip or at a density of $30x10^4$ in a 6 Well, in 200 µL or 500 µL DMEM growth medium (High Glucose DMEM, supplemented with 10% fetal calf serum, penicillin (100 units mL^{-1}), and streptomycin (100 µg mL^{-1})). 1 minute after culturing the cells 10 µL of CellLight® Plasma Membrane-GFP BacMam 2.0 was added for cells cultured in 8 wells and 25µL for cells cultured in 6 wells. Cells were incubated for 24 h at 37 ºC, 5% CO_2 to allow attachment on surface. After 24 h the medium was removed and of Qdot® 655 ITK™ Carboxyl Quantum Dots were added diluted 1:100 in DMEM growth medium as provided by the manufacturer. After 24 h, cells were washed five times with DMEM growth medium. After the final wash step, DMEM growth medium was removed and GPMV buffer was added. Cells were imaged after incubation with GPMV buffer for 1 h at 37 ºC, 5% CO_2.

Polymersome uptake and GPMV packaging

HepG2 cells were either cultured at a density of $4x10^4$ cells per well in a µ-Slide 8 Well, Collagen IV: coverslip or at a density of $30x10^4$ in a 6 Well, in 200µL or 500 µL DMEM growth medium (High Glucose DMEM, supplemented with 10% fetal calf serum, penicillin (100 units mL^{-1}) and streptomycin (100 µg mL^{-1})). 1 min after culturing the cells, 10 µL of CellLight® Plasma Membrane-GFP BacMam 2.0 was added for cells cultured in 8 wells and 25 µL for cells cultured in 6 Wells. Cells were incubated for 24 h at 37 ºC, 5% CO_2 to allow attachment on surface. After 24h the medium was removed and PMOXA-PDMS-PMOXA polymersomes or negatively charged PMOXA-PDMS-PMOXA was added to a final concentration of 1mg mL^{-1}. After 24 h, cells were washed five times with DMEM growth medium. After the final wash step, DMEM growth medium was removed and GPMV buffer was added. Cells were imaged after incubation with GPMV buffer for 1 h at 37 ºC, 5% CO_2.

Liposome uptake and packaging

HepG2 cells were either cultured at a density of $4x10^4$ cells per well in a µ-Slide 8 Well, Collagen IV: coverslip or at a density of $30x10^4$ in a 6 Well, in 200 µL or 500 µL DMEM growth medium (High Glucose DMEM, supplemented with 10% fetal calf serum, penicillin (100 units mL^{-1}), and streptomycin (100 µg mL^{-1})). 1 min after culturing the cells 10 µL of CellLight® Plasma Membrane-GFP BacMam 2.0 was added for cells cultured in 8 wells and 25 µL for cells cultured in 6 wells. Cells were incubated for 24 h at 37 ºC, 5% CO_2 to allow attachment on surface. After 24 h the medium was removed and DSPS liposomes or PEGilated DOPC liposomes were added to a final concentration of 1 mg mL^{-1}. Cells were incubated for an additional 24 h DMEM growth medium. After 24 h cells were washed five times with DMEM growth medium. After the final wash step, DMEM growth medium was removed and GPMV buffer was added. Cells were imaged after incubation with GPMV buffer for 1 h at 37 ºC, 5% CO_2.

Solid sphere particle uptake and packaging

HepG2 cells were either cultured at a density of $4x10^4$ cells per well in a µ-Slide 8 Well, Collagen IV: coverslip or at a density of $30x10^4$ in a 6 Well, in 200 µL or 500 µL DMEM growth medium (High Glucose DMEM, supplemented with 10% fetal calf serum, penicillin (100 units mL^{-1}), and streptomycin (100 µg mL^{-1})), respectively. 1 minute after culturing the cells 10 µL of CellLight® Plasma Membrane-GFP BacMam 2.0 was added for cells cultured

in 8 wells and 25 µL for cells cultured in 6 wells. Cells were incubated for 24 h at 37 ºC, 5% CO_2 to allow attachment to the surface. After 24 h the medium was removed and 200 µL or 500 µL of 40 nm latex beads 5% solids in DI water diluted 1:1000 into DMEM growth medium, or 500 nm latex beads 2% solids in 2 mM sodium azide solution diluted 1: 10 000 into DMEM growth medium or 1 µm latex beads diluted 1: 10 000 into DMEM growth medium or 2 µm latex beads 2.5% solids in DI water were added to cells. Cells were incubated for an additional 24 h DMEM growth medium. After 24 h cells were washed five times with DMEM growth medium. After the final wash step, DMEM growth medium was removed and GPMV buffer was added. Cells were imaged after incubation with GPMV buffer for 1 h at 37 ºC, 5% CO_2.

PMOXA-PDMS-PMOXA catalytic nanocompartment uptake and GPMV packaging

HepG2 cells were either cultured at a density of $4x10^4$ cells per well in a µ-Slide 8 Well, Collagen IV: coverslip or at a density of $30x10^4$ in a 6 Well, in 200 µL or 500 µL DMEM growth medium (High Glucose DMEM, supplemented with 10% fetal calf serum, penicillin (100 units mL^{-1}), and streptomycin (100 µg mL^{-1})). 1 min after culturing the cells, 10 µL of CellLight® Plasma Membrane-GFP BacMam 2.0 was added for cells cultured in 8 wells and 25 µL for cells cultured in 6 wells. Cells were incubated for 24 h at 37 ºC, 5% CO_2 to allow attachment on surface. After 24 h the medium was removed and HRP-loaded PMOXA-PDMS-PMOXA polymersomes equipped with OmpF were added to a final concentration of 1 mg mL^{-1}. After 24 h cells were washed five times with DMEM growth medium. After the final wash step, DMEM growth medium was removed and GPMV buffer was added. Cells were imaged after incubation with GPMV buffer for 1 h at 37 ºC, 5% CO_2.

Preparation of OmpF equipped polymersomes

OmpF-equipped polymersomes ($A_6B_{44}A_6$) OmpF were prepared at RT from the ABA triblock copolymer, $PMOXA_6$-$PDMS_{44}$-$PMOXA_6$. The synthetic procedure and the polymer characterization are presented in Itel et al. 2014[82]. Polymersomes were generated using the film rehydration technique where the polymer was dried in the presence of OmpF K89 R270 cysteine mutant. Horseradish peroxidase (HRP) in PBS buffer pH=7.4 at RT was used as rehydration solution. Films were rehydrated to a final polymer concentration of 2.5 mg mL^{-1}, HRP concentration of 0.2 mg mL^{-1}, and OmpF concentration of 50 µg mL^{-1}, respectively. Control polymersomes were also prepared in the absence of OmpF. Rehydrated films were

stirred overnight at RT, protected from light. All samples were extruded through an Avanti mini-extruder (Avanti Polar Lipids, USA) using a 100 nm diameter pore-size polycarbonate membrane (7 times) at RT in order to obtain size homogeneity. The non-encapsulated enzyme was removed from the polymersomes by dialysis against PBS at pH 7.4 at RT for 5 days, exchanging the buffer every 3 hours during the day and leaving the buffer unchanged overnight, using Spectrapore dialysis tubes with a molecular weight cut-off of 300 kDa (Spectrum Laboratories Inc., USA).

Preparation of SRB-loaded polymersomes

SRB-loaded polymersomes were prepared at RT from the ABA triblock copolymer, $PMOXA_6$-$PDMS_{44}$-PMOXA6. The synthetic procedure and the polymer characterization are presented in Itel et al. 2014[82]. Polymersomes were generated using the film rehydration technique where the polymer was dried, and 1 mM sulforhodamine B in PBS buffer pH=7.4 at RT was used as rehydration solution. Rehydrated films were stirred overnight at RT, while being protected from light. All samples were extruded through an Avanti mini-extruder (Avanti Polar Lipids, USA) using a 100 nm diameter pore-size polycarbonate membrane (7 times) at RT in order to obtain size homogeneity. Non-encapsulated dye was removed from the polymersomes by using a HiTrap Desalting ready-to-use 5 mL column, prepacked with Sephadex G-25 Superfine, and equilibrated with PBS.

Liposome Preparation

Liposomes were prepared using the film-rehydration-extrusion method. In brief, dry lipid films were rehydrated at Tm+10°C using a 1 mM sulforhodamine B solution resulting in a total lipid concentration of 40 mM. Finally, samples were extruded 21 times through a 100 nm diameter pore-size polycarbonate membrane (11 times) at Tm+10°C using an Avanti mini-extruder (Avanti Polar Lipids, Alabama, USA).

Non-encapsulated dye was removed from the polymersomes by using a HiTrap Desalting ready-to-use 5 mL column, prepacked with Sephadex G-25 Superfine, equilibrated with PBS.

The following lipid formulations were prepared: DSPC:cholesterol:DSPE-PEG (48:42:10 %mol) and DSPS:cholesterol:DSPE-PEG (53:42:5 %mol).

Transfection of HepG2 cells

Cells were transfected using the mammalian expression plasmids pTagGFP-N and pTagRFP-N (Evrogen) encoding for the water-enhanced GFP or RFP under control of the cytomegalovirus promotor. Cells were seeded at a density of 2.5 x 10^4 cells/cm^2 on poly-D-lysine-coated or plasma-treated tissue culture slides and allowed to adhere for 24 h. For the transfection, plasmid DNA (pDNA) was complexed using Lipofectamine 3000 at a pDNA-to-Lipofectamine reagents ratio (w/V) of 2. Cells were transfected using 2.5 µg pDNA per 1000 mm^2 surface area. GUV formation was induced 24 h post transfection.

Dynamic lightscattering

The measurements of D_H of liposomes, polymersomes and catalytic nanocompartments were performed on a Zetasizer Nano ZSP at 25 °C. The measure angle is 173° and the data were analyzed by intensity distribution.

Transmission electron microscopy (TEM)

1:10 dilutions of the prepared polymersome, liposome and catalytic compartments were negatively stained with 1.5% uranyl acetate solution and deposited on carbon-coated copper grids. For GPMV TEM imaging, polymersome-loaded GPMVs were deposited on carbon-coated copper grids and deflated vesicles imaged. Transmission electron microscope (Philips Morgagni 268D) at 293 K was used.

Amplex UltraRed reaction in GPMVs

After isolating GPMVs loaded with CatCs from cells, 200 µL of the GPMV solution was deposited in a plasma activated 8-well microscopy chamber. The substrates Amplex UltraRed (5 µL of 0.1 mmol mL^{-1} in DMSO) and H_2O_2 (5 µL of 0.1 mmol mL^{-1} in ddH2O) were mixed and these 10 µL were added during the measurements. The reaction was then visualized 2 hours after mixing the GPMV solution with the reaction substrates in order to allow sufficient AR to diffuse into the GPMVs.

GPMVs preparation for ZFE injection.

HepG2 cells were cultured at a density of 30x10^4 in a 6 Well in 500 µL DMEM growth medium (High Glucose DMEM, supplemented with 10% fetal calf serum, penicillin (100

units mL^{-1}), and streptomycin (100 µg mL^{-1})). Cells were incubated for 24 h at 37 ºC, 5% CO_2 to allow attachment to the surface. After 24 h RFP transfection agent were added. Subsequently after 24 h cells were treated with 20 µM Cholesterol-PEG5000 (micelles) solution in PBS for 1 hour, the cells were washed with GPMV formation buffer, the medium was removed and GPMV formation buffer was added. GPMVs were collected from the cells, sedimented overnight and injected into ZFE. ZFE CLSM measurements were performed using a confocal laser scanning microscope (ZEISS LSM 880, inverted microscope ZEISS Axio Observer, Carl Zeiss, Germany) equipped with a water immersion objective (C-Apochromate 40x/1.2W korr FCS M27).

Zebrafish injections

Standard zebrafish embryo (ZFE) culture medium at pH 7.4 was prepared at final concentrations of 5 mM sodium chloride, 0.25 mM potassium chloride, 0.5 mM magnesium sulfate, 0.15 mM potassium dihydrogen phosphate, 0.05 mM sodium phosphate dibasic, 0.5 mM calcium chloride, 0.71 mM sodium bicarbonate, and 0.001 % (w/v) methylene blue.
Collected eggs from adult ABC/TU ZFE (Wildtype) and kdrl:GFP (GFP vasculature line) were kept in ZFE culture medium at 28°C. 1-Phenyl-2-thiourea (PTU) (0.03 mg mL^{-1}) was added 1-day post fertilization (dpf) in order to avoid pigment cell formation. Equipped GPMVs were injected into 2-dpf ZFE according to an adapted protocol originally designed for microangiography. ZFE were anesthetized using 0.01% tricaine (w/v) and cast into 0.3% (w/v) agarose containing the same amount of tricaine. Immobilized ZFE were injected with 3 nL of GPMV solution.

GPMVs preparation for ZFE injection

HepG2 cells were cultured at a density of $30x10^4$ in a 6 Well in 500 µL DMEM growth medium (High Glucose DMEM, supplemented with 10% fetal calf serum, penicillin (100 units mL^{-1}), and streptomycin (100 µg mL^{-1})). Cells were incubated for 24 h at 37 ºC, 5% CO_2 to allow attachment to the surface. After 24 h RFP transfection agent were added. Subsequently after 24 h cells were treated with 20 µM Cholesterol-PEG5000 solution in PBS for 1 hour, the cells were washed with GPMV formation buffer, the medium was removed and GPMV formation buffer was added. GPMVs were collected from the cells, sedimented overnight and injected into ZFE. ZFE CLSM measurements were performed using a confocal laser scanning microscope (ZEISS LSM 880, inverted microscope ZEISS Axio Observer,

Carl Zeiss, Germany) equipped with a water immersion objective (C-Apochromate 40x/1.2W korr FCS M27).

FCS Measurements

FCS Fluorescence correlation spectroscopy (FCS) measurements were carried out using a confocal laser scanning microscope (ZEISS LSM 880, inverted microscope ZEISS Axio Observer, Carl Zeiss, Germany) with a water immersion objective lens (C-Apochromate 40x/1.2W korr FCS M27). Measurements were taken at room temperature using a sample volume of 20 µL on a glass cover slide or within individual GUVs using the position mode. A diode-pumped solid-state 561-10 laser (DPSS) at 561 nm was used for excitation of the SRB fluorophore (λ = 561 nm) with the appropriate filter sets. The laser intensity was kept constant between individual measurements. The fluorescence signal was measured in real time and the autocorrelation function was calculated by a software correlator provided by the manufacturer (ZEN 2 Blue edition). Measurements were recorded over 2 s and each measurement was repeated 60 times. Correlation curves that presented a lower CPM than the calibration fluorophore (SRB) or could not be fitted were excluded.
For determining purification of free SRB from the formed liposomes and polymersomes, experimental auto correlation curves were fitted using a two-component model including the triplet state (Eq. 1).

Eq. 1:

$$G(\tau)_{fit} = 1 + \left(1 + \frac{T}{1-T} e^{-\frac{\tau}{\tau_{trip}}}\right) \frac{1}{N} \left[\frac{f_1}{1 + \frac{\tau}{\tau_{D1}}} \frac{1}{\sqrt{1 + R^2 \frac{\tau}{\tau_{D1}}}}\right] + \left(1 + \frac{T}{1-T} e^{-\frac{\tau}{\tau_{trip}}}\right) \frac{1}{N} \left[\frac{f_2}{1 + \frac{\tau}{\tau_{D2}}} \frac{1}{\sqrt{1 + R^2 \frac{\tau}{\tau_{D2}}}}\right]$$

τ_D represents the diffusion time, T the fraction of fluorophores in triplet state with triplet time τ_{trip}, N is the number of particles and R the structural parameter.

R and τ_D of free dye (SRB) were determined independently, experimental auto correlation curves were fitted using a one component model including triplet state (Eq. 2).

Eq. 2:

$$G(\tau)_{fit} = 1 + (1 + \frac{T}{1-T} e^{-\frac{\tau}{\tau_{trip}}}) \frac{1}{N} \left[\frac{1}{1 + \frac{\tau}{\tau_D}} \frac{1}{\sqrt{1 + R^2 \frac{\tau}{\tau_D}}} \right]$$

τ_D represents the diffusion time, T the fraction of fluorophores in triplet state with triplet time τ_{trip}, N is the number of particles and R the structural parameter. R and τ_D of free dye (SRB) were determined independently. R and τ_D of SRB were subsequently fixed in the fitting procedure in order to determine the % of free dye fraction, which represented the unencapsulated fluorophore still present in the solution after purification of SRB-loaded polymersomes / liposomes.

OmpF expression and purification

The OmpF K89 R270 cysteine mutant (OmpF-M) expression and extraction was done as previously reported in [112,128]. First under aseptic conditions, a loop full of cells from an ampicillin resistant *Escherichia Coli* strain BL21 stock culture that overexpressed the OmpF K89 R270 mutant was smeared onto the surface of a lysogeny broth (LB), ampicillin (100 mg mL^{-1} ampicillin) agar plate. After 16 hours of incubation at 37 °C, a single colony was selected and transferred from the plate to 10 mL of terrific broth (TB) liquid medium with 100 mg mL^{-1} ampicillin (4 flasks in total). 5 L TB medium with 100 mg mL^{-1} ampicillin was inoculated with 15 mL of the overnight culture (OD = 0.1-0.5), and the optical density of the growing culture was followed by measuring the absorbance at 600 nm. When the absorbance reached an OD of 0.6, IPTG was added to a final concentration of 1 mM in order to start the over-expression of the OmpF-M gene. The bacteria were grown for 16 more hours at 25 ºC, with vigorous stirring, then the *E. Coli* cells were pelleted at 7.000 *g* for 8 min at 4 ºC. Pellets were stored at -25 ºC, and on the following day were re-suspended in 50 mL of 25 mM Tris-HCl pH 7.4. 10 mg DNase and 10 mg RNase were added, and the cell suspension French pressed five times at 1,000 bar. 1 mL of 20% SDS was added per 10 mL of cell suspension and incubated for 1 h at 60 ºC. The suspension was centrifuged at 50.000 *g* at 23 ºC for 1 hour. The supernatant was removed and the cell pellet incubated in 0.125% OG for 1 h at 37 ºC. The suspension was then centrifuged at 50.000 *g* for 1 hour at 23 ºC. Finally, the cell pellet was re-suspended in 3% OG in 10 mM phosphate buffer and homogenized. The suspension was centrifuged at 50.000 *g* and the protein concentration in the supernatant was determined by UV-Vis absorption at 280 nm. Before the reconstitution experiments were

carried out, the protein was dialysed against 1L of 0.05 % OG in PBS for 16 hours and twice against PBS pH 7.4 for 2 hours. After the dialysis the protein concentration was adjusted to 1.2 mg mL^{-1}.

Preparation of OmpF equipped polymersomes

OmpF equipped polymersomes were prepared as described in Einfalt et al. at RT from the ABA triblock copolymer, $PMOXA_6$-$PDMS_{44}$-$PMOXA_6$, (A6B44A6) and OmpF K89 R270 cysteine mutant. The synthetic procedure and the polymer characterization are presented in Itel et al. Polymersomes were generated using the film rehydration technique where the polymer was dried in the presence of unmodified OmpF K89 R270 cysteine. Horseradish peroxidase (HRP) in PBS buffer pH=7.4 at RT were used as rehydration solutions. Films were rehydrated to a final polymer concentration of 2.5 mg mL^{-1}, HRP concentration of 0.2 mg mL^{-1}, and OmpF concentration of 80 µg mL^{-1}, respectively. Control catalytic nanocompartments were also prepared in the absence of OmpF. Rehydrated films were stirred at RT for 24 h. All samples were extruded through an Avanti mini-extruder (Avanti Polar Lipids, USA) using a 100 nm diameter pore-size polycarbonate membrane (6 times) at RT in order to obtain size homogeneity. Non-encapsulated enzyme was removed from the polymersomes by dialysis against PBS at pH 7.4 at RT for 4 consequitve days using Spectrapore dialysis tubes, MWCO 300 kDa (Spectrum Laboratories Inc., USA); the buffer was exchanged every 3 hours during the day, but was left unchanged overnight.

Amplex UltraRed enzymatic assay

The increase in emission fluorescence intensity was analyzed using a LS 55 Fluorescence Spectrometer (Perkin Elmer). For the measurement, 10 µL of the catalytic nanocompartments equipped with OmpF or without OmpF were transferred to 220 µL of the reaction mixture (4.5 µM H_20_2 and 3.4 µM Amplex Ultra Red) in PBS at pH 7.4. Subsequently the reaction mixture was excited at 530 nm and the emission intensity was monitored at 590 nm. Fluorescence was expressed as relative fluorescence units (RFU) and was measured at the same instrument setting in all experiments.

Chapter 8

APENDIX – SUPPLEMENTARY INFORMATION

CHAPTER 3

GUV membrane staining and visualization by LSM

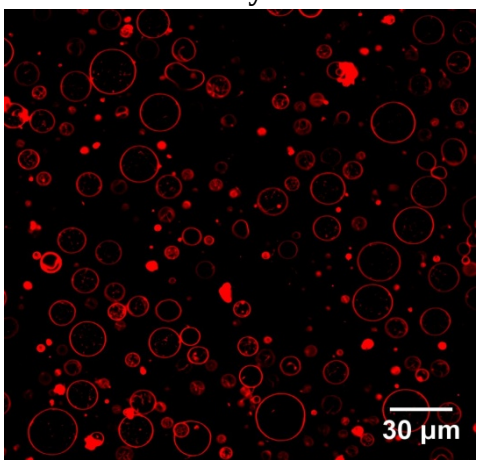

Figure S1. *GUVs formation identified by staining the membrane with Bodipy 633, measured with CLSM.*

Proton outflux through GUV membranes

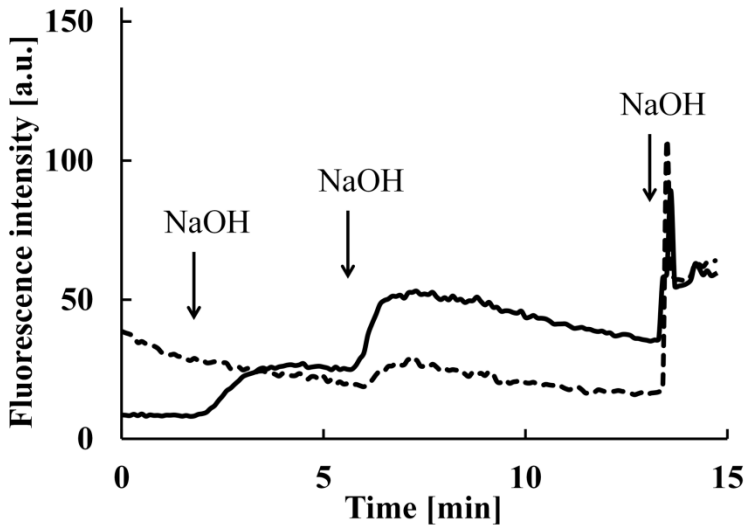

Figure S2. *Fluorescence intensity change over time of 5(6)-carboxyfluorescein (CF) inside and outside of polymer GUVs ($A_7B_{42}A_7$) in the presence of DMSO/EtOH. Fluorescence intensity inside GUVs (dotted line), and outside GUVs (solid line).*

Below, Figures S3-7, we provide the evidence for the successful insertion and functionality of gA in GUVs for $A_6B_{34}A_6$, $A_6B_{44}A_6$, $A_7B_{49}A_7$, $A_{12}B_{63}A_{12}$, and $A_{12}B_{87}A_{12}$. Left part consists in microscopy micrographs before and after addition of NaOH. Each image, specific for each polymer in part, consists of three subparts. The GUVs were monitored upon NaOH addition and without gA (upper part), DMSO/EtOH and NaOH without gA (middle part), and DMSO/EtOH with gA and NaOH (bottom part).

Right column contains the plots of the fluorescent intensity over time inside GUVs (dotted line) compared with the background - the outside part of the GUVs (solid line). The steadily decrease of the fluorescence intensity is attributed to the CF photobleaching in time. An increase in the intensity occurred immediately after pH increase in the outside environment of GUVs. Multiple peaks represent consecutive addition of NaOH, after the system was equilibrated. Where the fluorescence intensity was similar in both cases (inside and outside GUVs), we concluded that the membrane was permeabilized due to the gA addition. It has to be noted that on the micrographs some polymer chunks are also visible, which are typical byproducts obtained when transferring the GUV solution from electroformation chamber to storage tubes. This phenomenon is similar as observed in the case of lipid GUVs obtained by electroformation.[212] The polymer chunks did not have any influence on the experiments we performed with the polymer GUVs.

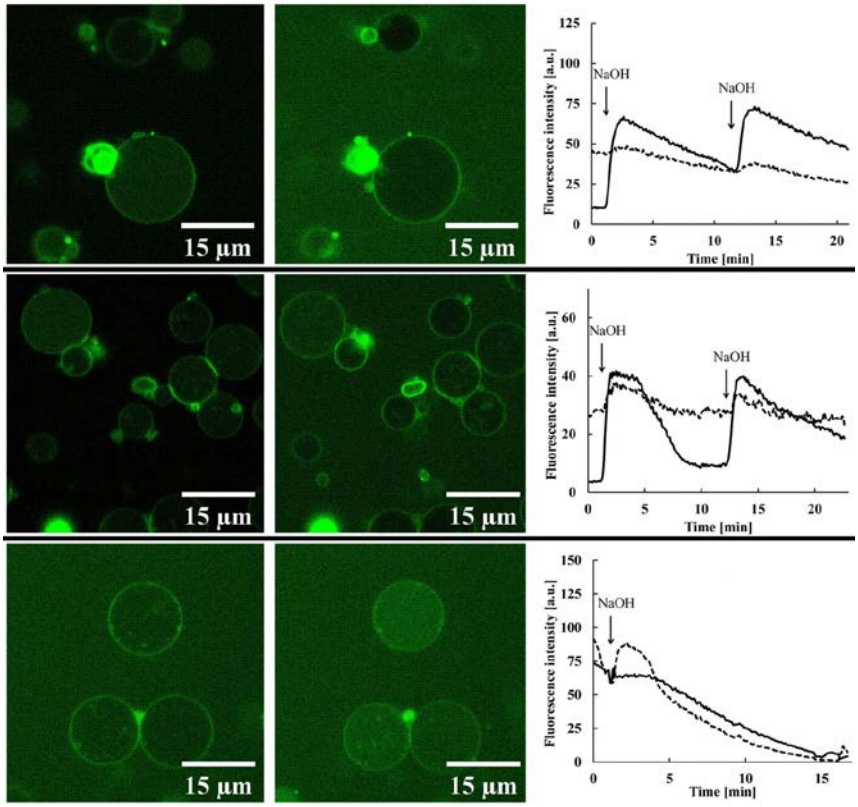

Figure S3. *Successful proton outflux through the $A_6B_{34}A_6$ membranes of GUVs.*

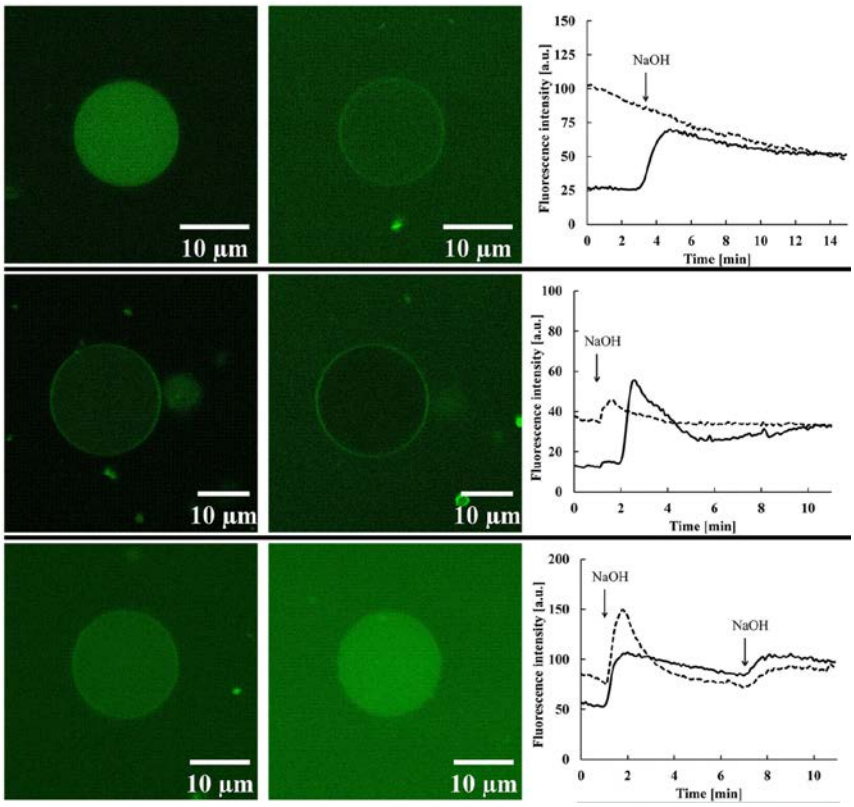

Figure S4. *Successful proton outflux through the $A_6B_{44}A_6$ membranes of GUVs.*

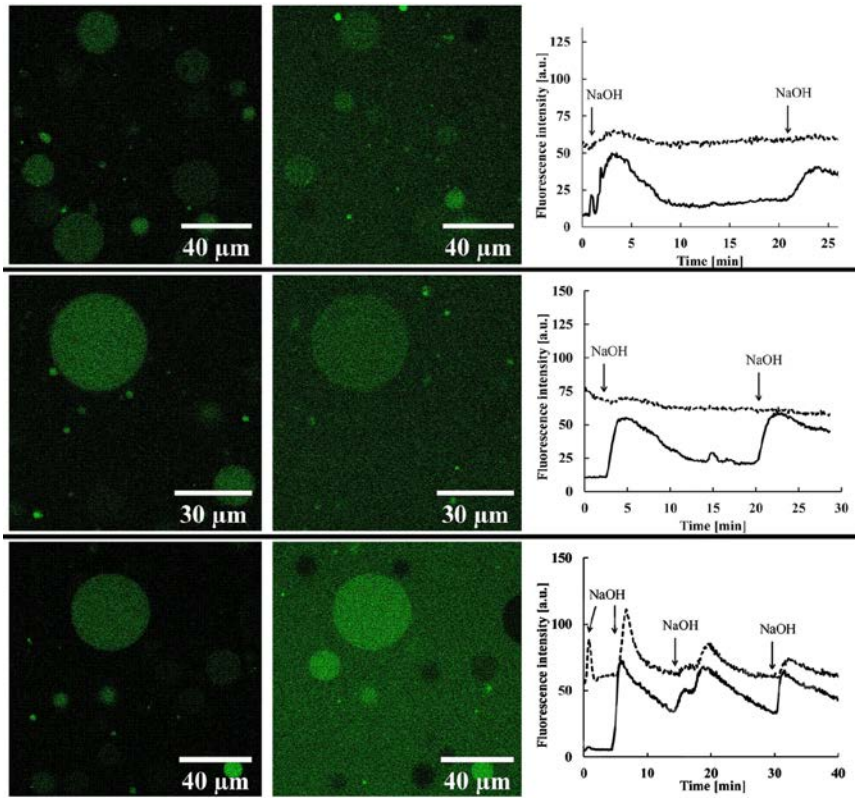

Figure S5. *Successful proton outflux through the $A_7B_{49}A_7$ membranes of GUVs.*

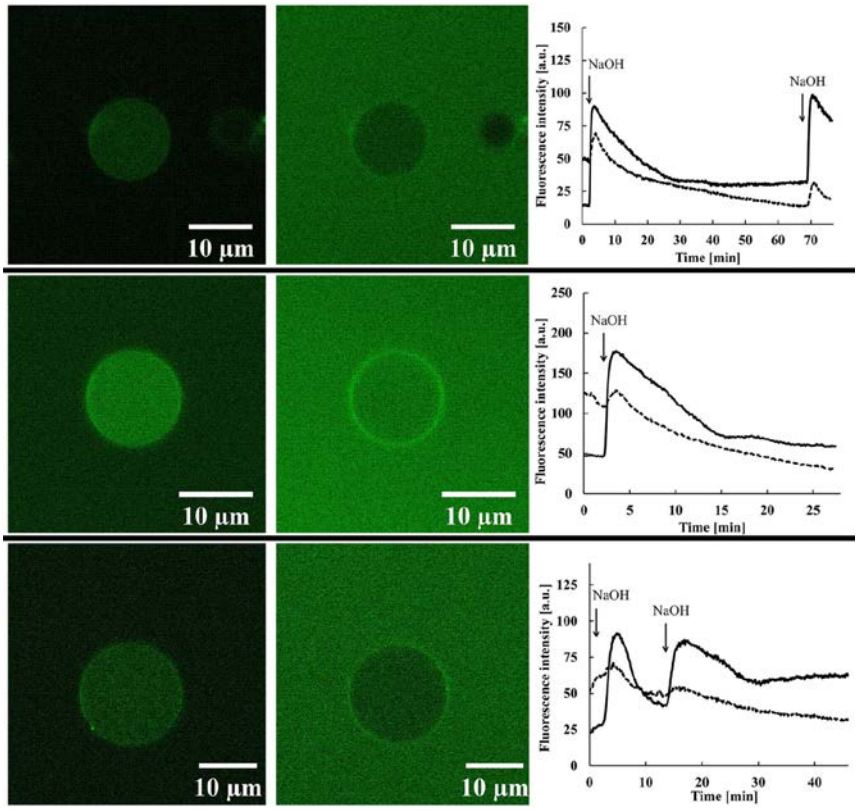

Figure S6. *No proton outflux through the $A_{12}B_{63}A_{12}$ membranes of GUVs.*

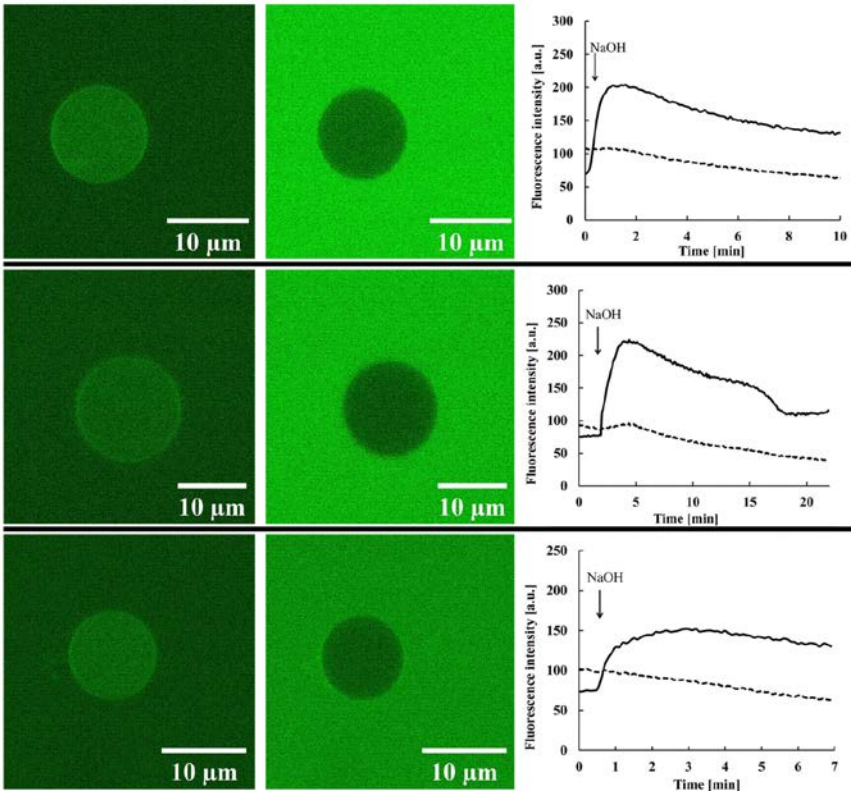

Figure S7. *No proton outflux through the $A_{12}B_{87}A_{12}$ membranes of GUVs.*

CHAPTER 4

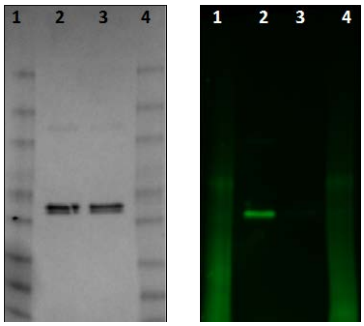

Figure S8. 4-15% SDS Gel chromatograpy. Left: *Coomasie Blue stain* ***Right:*** *488 Fluorescence.* ***1)*** *Benchmark protein ladder,* ***2)*** *Atto 488 conjugated OmpF-M,* ***3)*** *OmpF-M* ***4)*** *Benchmark protein ladder.*

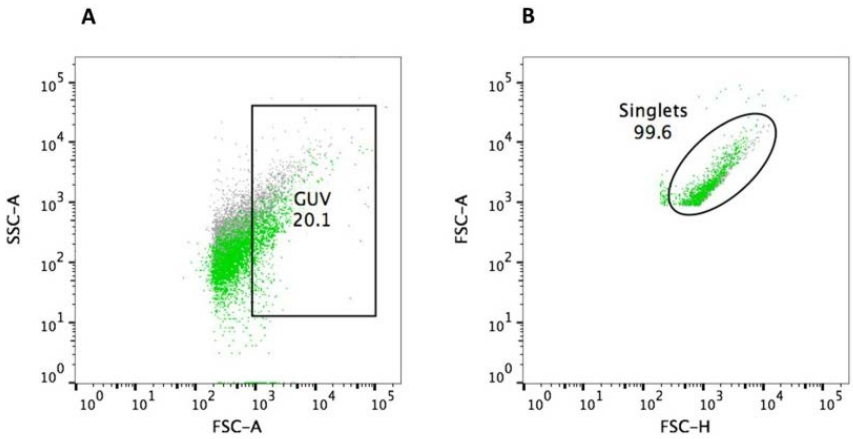

Figure S9. A) and B) *Flow cytometry gating of OmpF-Atto 488 equipped (green) or unequipped PMOXA-b-PDMS-b-PMOXA ($A_7B_{49}A_7$) GUVs(grey).*

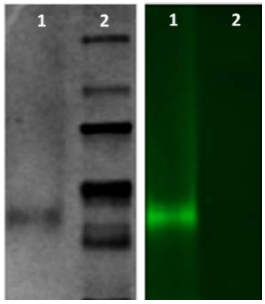

Figure S10. Left: *4-15% SDS-PAGE Gel with comassie stained labeled HRP-Atto 488.* ***Right:*** *Gel showing fluorescence of labeled HRP-Atto 488.* ***1)*** *HRP-Atto 488,* ***2)*** *Protein ladder.*

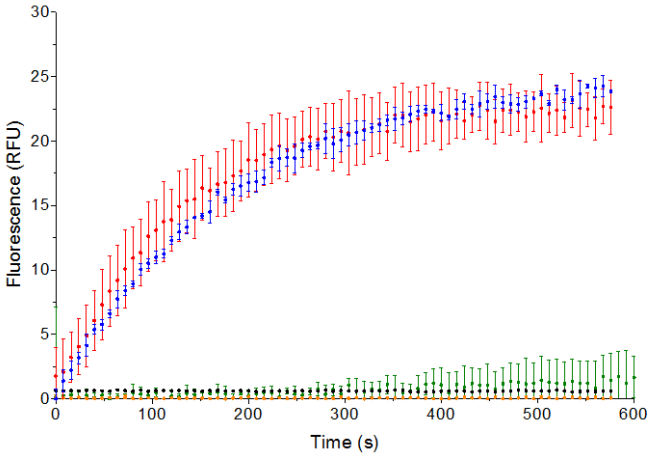

Figure S11. Amplex UltraRed conversion kinetics of free HRP in solution. ***Red:*** *Amplex UltraRed conversion in PBS pH 7.4,* ***Blue:*** *Amplex UltraRed conversion in 300 mM sucrose,* ***Green:*** *Amplex UltraRed conversion without the presence of* H_2O_2 *in PBS pH 7.4,* ***Black:*** *Amplex UltraRed conversion without the presence of HRP,* ***Orange:*** *Amplex UltraRed coversion without the presence of Amplex UltraRed.*

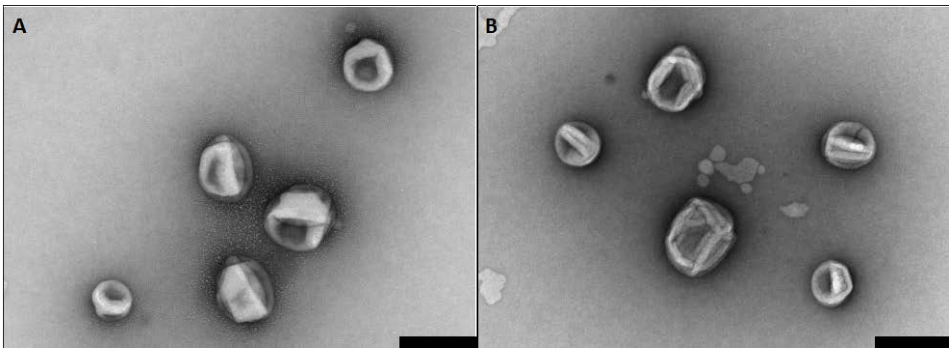

Figure S12. *TEM micrographs of HRP- loaded polymersomes where sucrose was used as the rehydration solution.* ***A)*** *OmpF equipped polymersomes and* ***B)*** *polymersomes without OmpF. Scale bar 200 nm.*

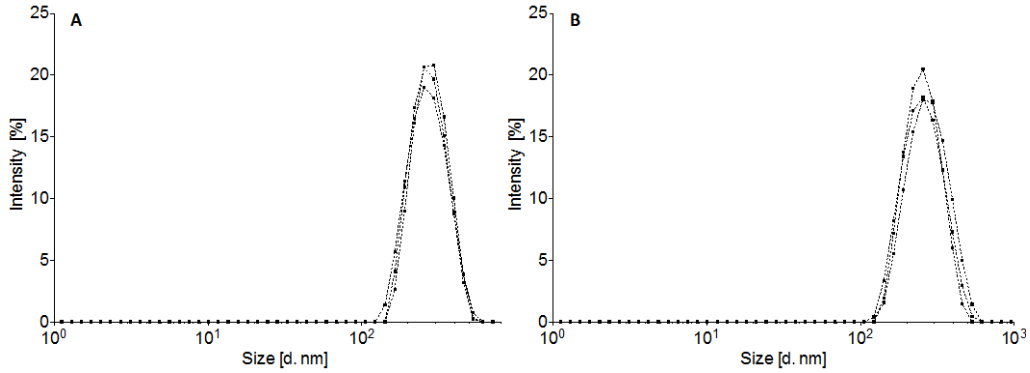

Figure S13. Dynamic light scattering analysis of A) *OmpF-M equipped HRP-loaded PMOXA-b-PDMS-b-PMOXA ($A_7B_{49}A_7$) polymersomes and* ***B)*** *HRP-loaded PMOXA-b-PDMS-b-PMOXA ($A_7B_{49}A_7$) polymersomes.*

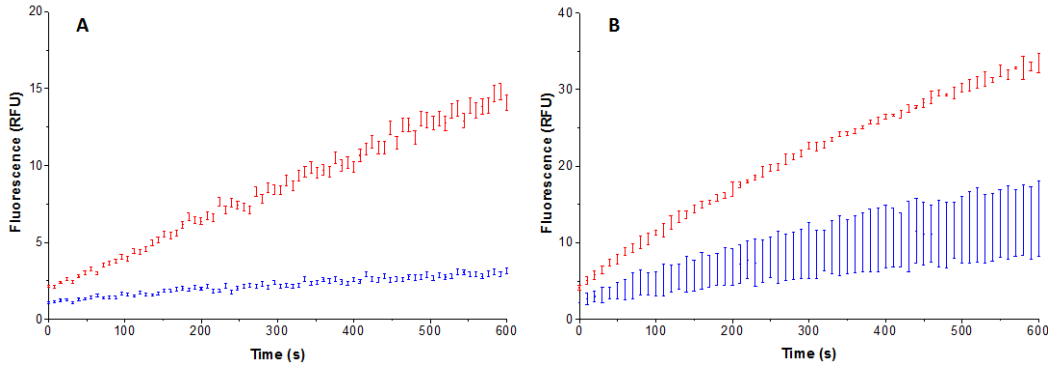

Figure S14. *Amplex red conversion kinetics of HRP-loaded polymersomes equipped with OmpF-M (red) or unequipped (blue), where PBS was used as the rehydration solution* ***A)*** *and where 300mM sucrose was used as the rehydration solution* ***B)****.*

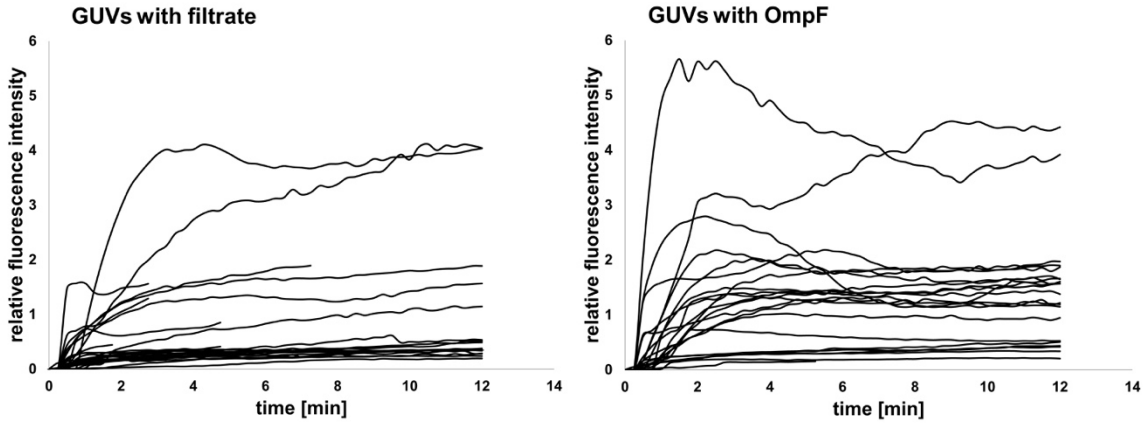

Figure S15 *Temporal variation of the relative fluorescence intensity of the resorufin-like product inside the cavities of single GUVs after addition of the reagents H_2O_2 and Amplex UltraRed. Each curve represents one GUV.* ***Left:*** *GUVs with filtrate control.* ***Right:*** *GUVs with reconstituted OmpF-M.*

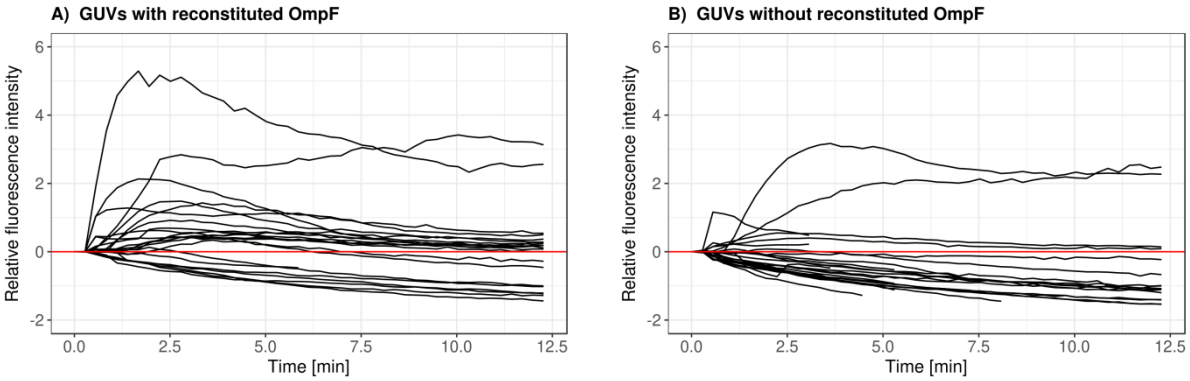

Figure S16. *Temporal variation of the relative fluorescence intensity of the resorufin-like product inside the cavities of single GUVs after background subtraction and after addition of the reagents H_2O_2 and Amplex UltraRed. Each curve represents one GUV.* ***Left:*** *GUVs with reconstituted OmpF.* ***Right:*** *GUVs without OmpF-M.*

GUVs without OmpF (26 vesicles):	GUVs with reconstituted OmpF (22 Vesicles):
27% showed fluorescence activity (7)	**68% showed fluorescence acticity (15)**
73% remained dark (19)	31% remained dark (7)

Table 2. *Fluorescence activity of GUVs after the enzyme reaction.* ***Left:*** *GUVs without OmpF.* ***Right:*** *GUVs with reconstituted OmpF.*

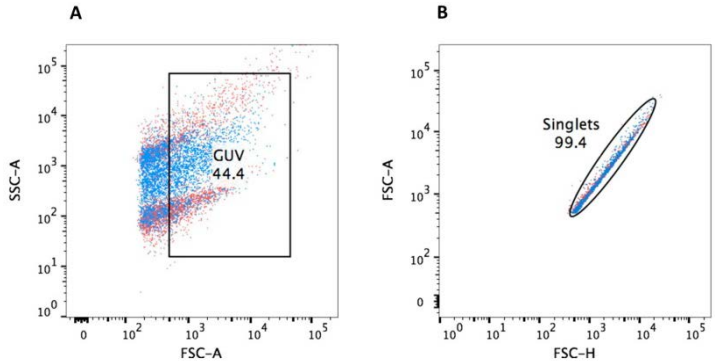

Figure S17. *Flow cytometry analysis - Amplex UltraRed enzymatic assay.* ***A)*** *Flow cytometry gating (FSC-A, SSC-A) and* ***B)*** *single giant selection by FSC-H / FSC –A of OmpF equipped (red) or unequipped PMOXA-b-PDMS-b-PMOXA ($A_7B_{49}A_7$) GUVs (blue).*

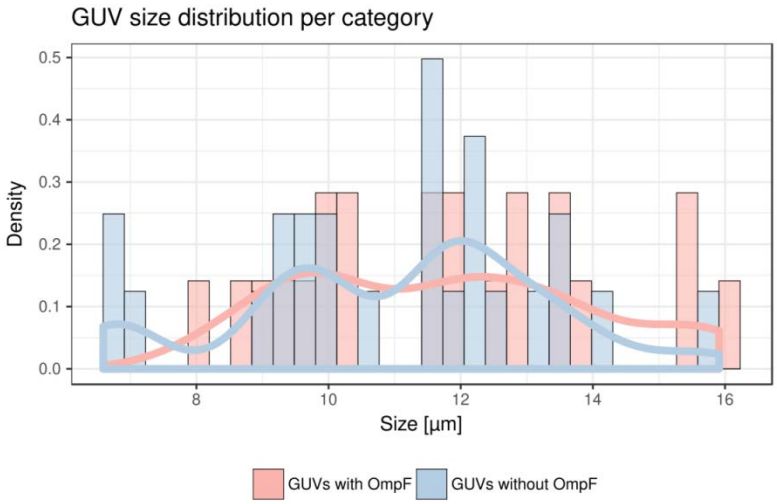

Figure S18. *Size distribution of GUVs, including density distribution and histogram.*

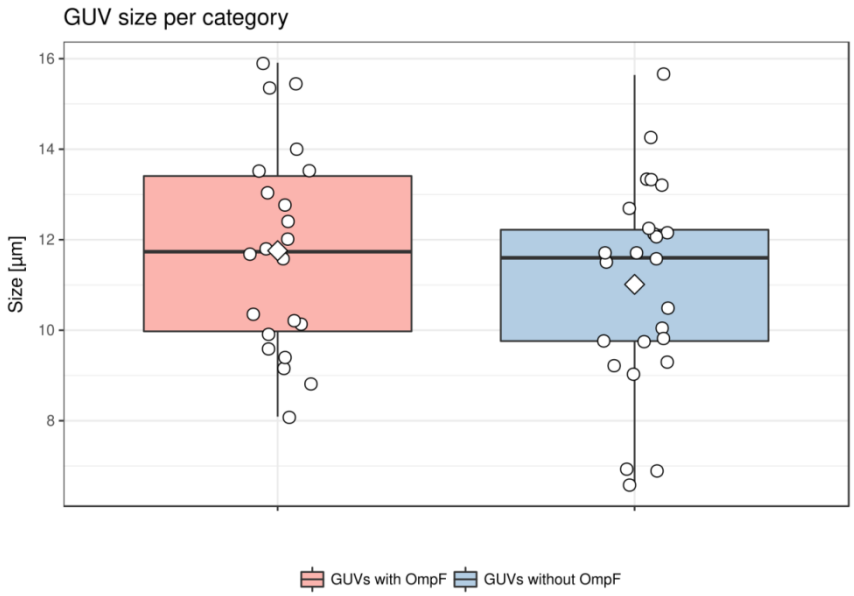

Figure S19. Boxplot of the size distribution of all GUVs measured. *The population of GUVs equipped with OmpF are shown in red and the population of GUVs without OmpF are shown in blue.*

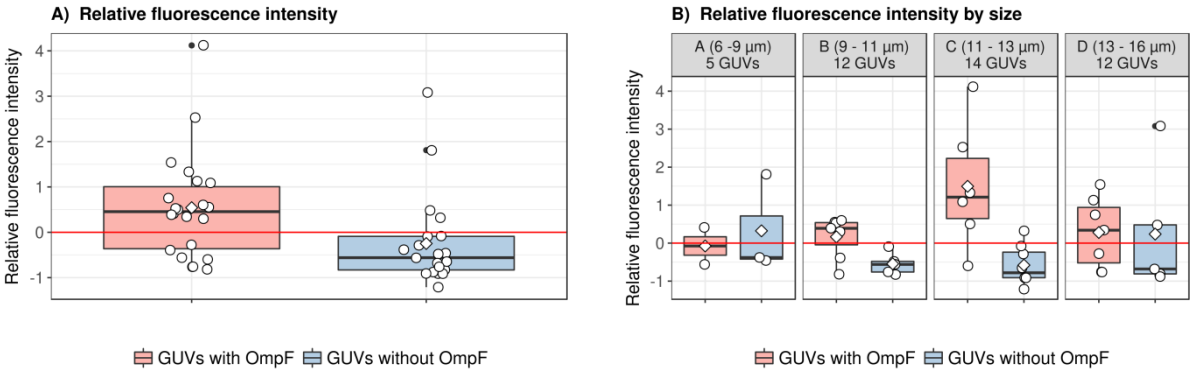

Figure S20. A) *Relative fluorescence intensity of the resorufin-like product inside the cavities of single GUVs after background subtraction over time and after addition of H_2O_2 and Amplex UltraRed.* ***B)*** *Relative fluorescence intensity by size of the resorufin-like product inside the cavities of single GUVs after background subtraction over time and after addition of H_2O_2 and Amplex UltraRed.*

CHAPTER 5

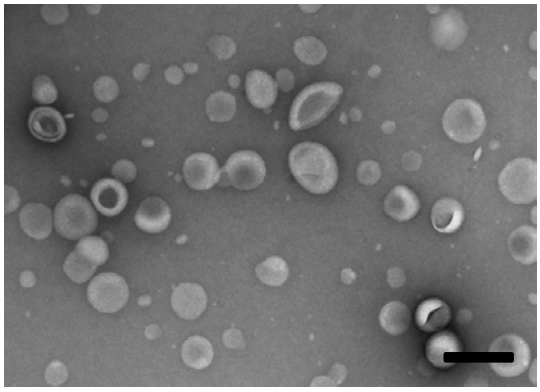

Figure S21. *Transmission electron microscopy micrograph of SRB-loaded DSPC:Cholesterol:DSPE-PEG (48:42:10 %mol) liposomes. Scale bar: 200 nm.*

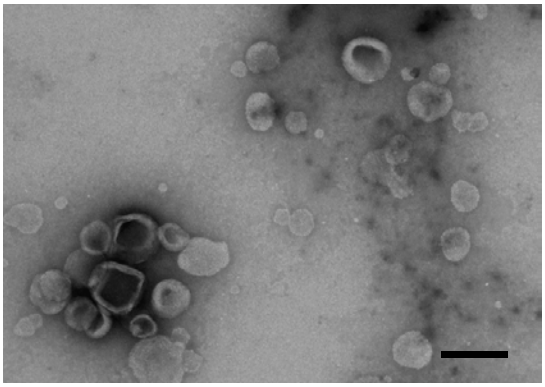

Figure S22. *Transmission electron microscopy micrograph of SRB-loaded DSPS:Cholesterol:DSPE-PEG (53:42:5 %mol). Scale bar: 200 nm.*

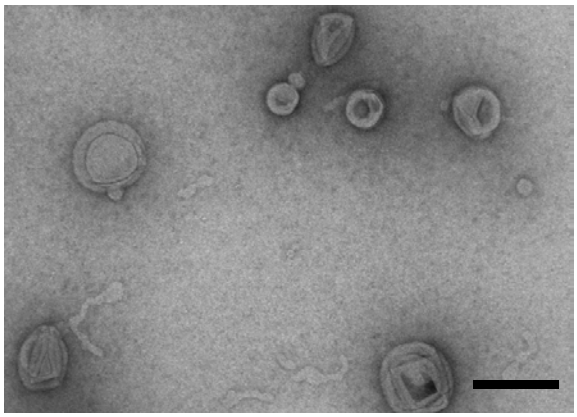

Figure S23. *Transmission electron microscopy of SRB-loaded $PMOXA_{44}$-$PDMS_{6}$-$PMOXA_{44}$ polymersomes. Scale bar: 200 nm.*

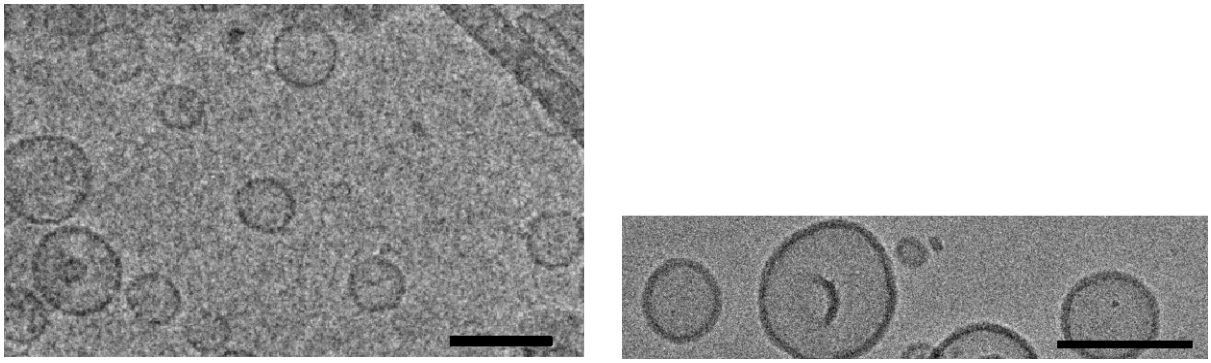

Figure S24. *Cryogenic transmission electron microscoy of $PMOXA_{44}$-$PDMS_{6}$-$PMOXA_{44}$ polymersomes. Scale bar left: 200nm. Scale bar right: 50 nm.*

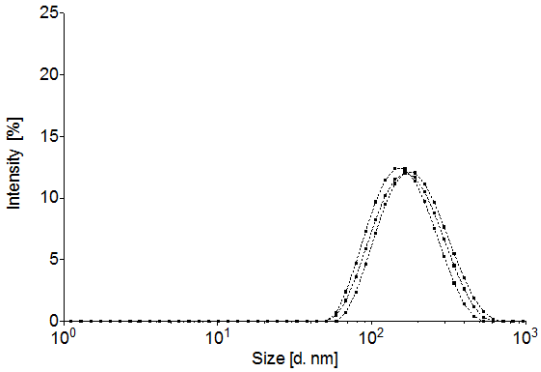

Figure S25. *Intensity distribution by DLS of SRB-loaded $PMOXA_{44}$-$PDMS_{6}$-$PMOXA_{44}$ polymersomes. (n=3).*

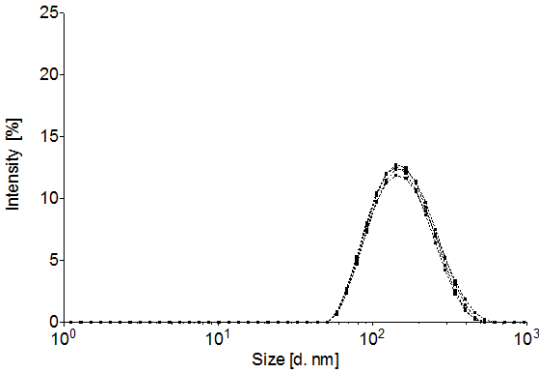

Figure S26. *Intensity distribution by DLS of SRB-loaded DSPS:Cholesterol:DSPE-PEG (53:42:5 %mol) liposomes (n=3).*

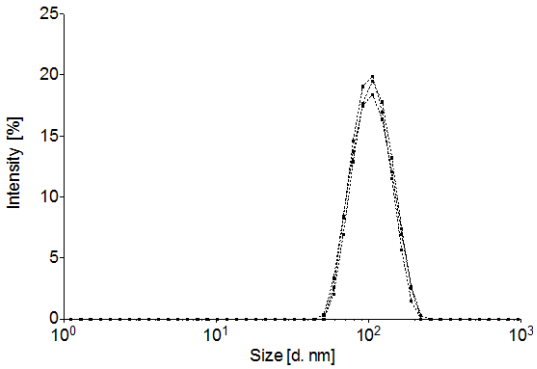

Figure S27. *Intensity distribution by DLS of SRB-loaded DSPC:Cholesterol:DSPE-PEG (48:42:10 %mol) liposomes (n=3).*

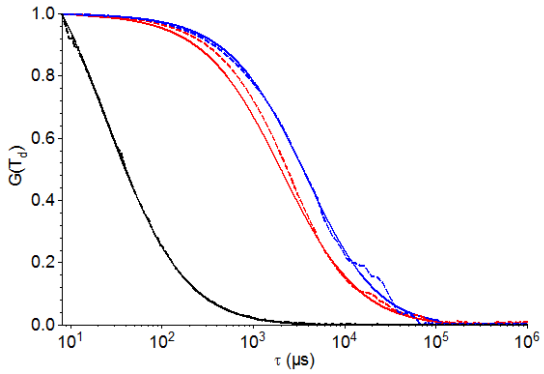

Figure S28: FCS analysis of SRB-loaded DSPS and DSPC liposomes in PBS pH 7.4. *FCS autocorrelation curves of free SRB in PBS pH 7.4 (Black), SRB-loaded DSPS liposomes in PBS pH 7.4 (Blue) SRB-loaded DSPC liposomes in PBS pH 7.4 (Red). Dotted line – experimental auto correlation curves, Full line – fit. Curves normalized to 1 to facilitate comparison.*

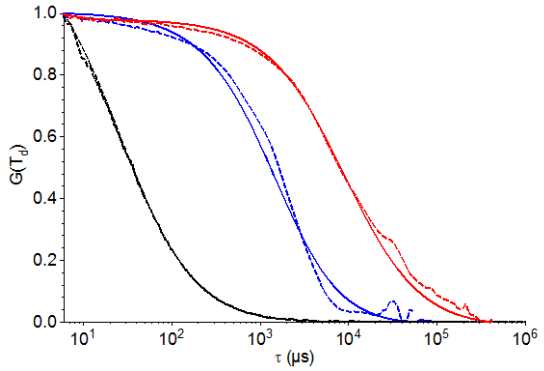

Figure S29: *FCS analysis of SRB-loaded PMOXA$_{44}$-PDMS$_6$-PMOXA$_{44}$ polymersomes in PBS pH 7.4 (Blue) and SRB-loaded PMOXA$_{44}$-PDMS$_6$-PMOXA$_{44}$ polymersomes within GPMVs (Red). Dotted line – experimental auto correlation curves, Full line – fit. Curves normalized to 1 to facilitate comparison.*

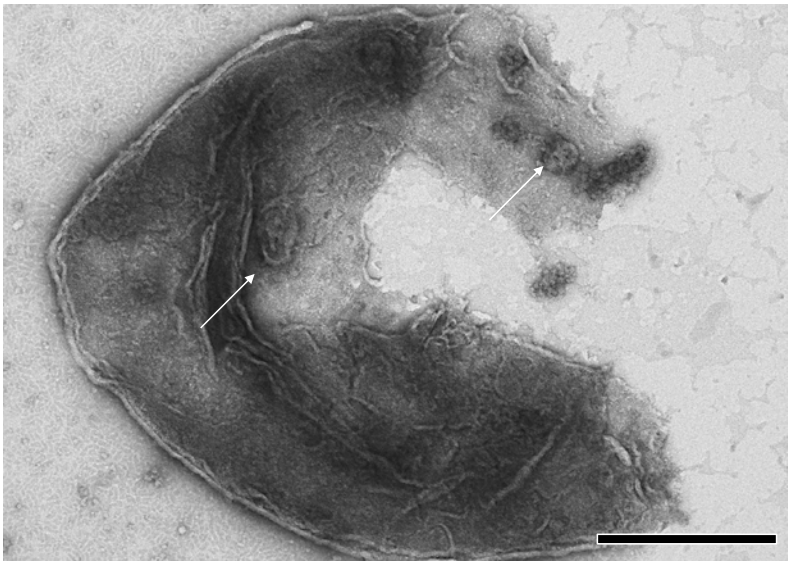

Figure S30. *TEM micrograph of a $PMOXA_{44}$-$PDMS_{6}$-$PMOXA_{44}$ polymersome-loaded HepG2-derived GPMV. Scale bar: 500 nm. Arrowheads: Subcompartmentalized GPMVs.*

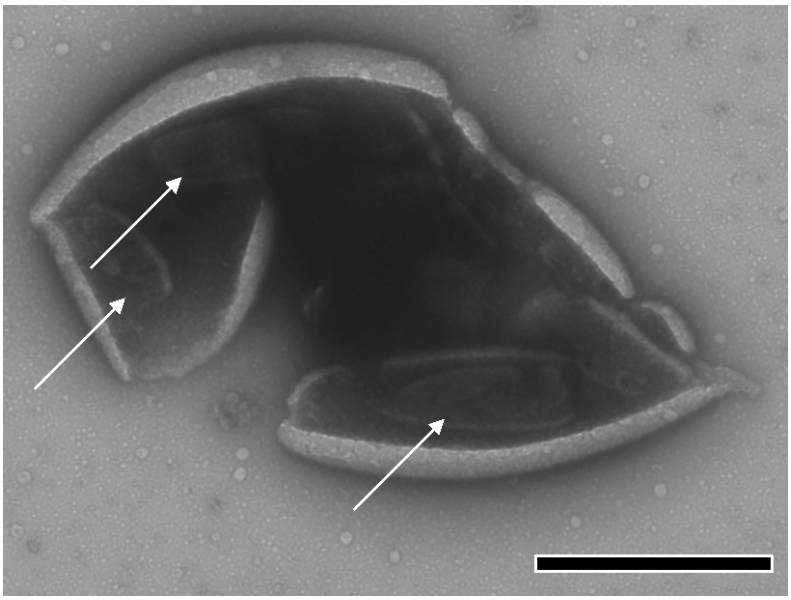

Figure S31. *TEM micrograph of a PMOXA-PDMS-PMOXA polymersome-loaded HepG2-derived GPMV. Scale bar: 500 nm. Arrowheads: Subcompartmentalized GPMVs.*

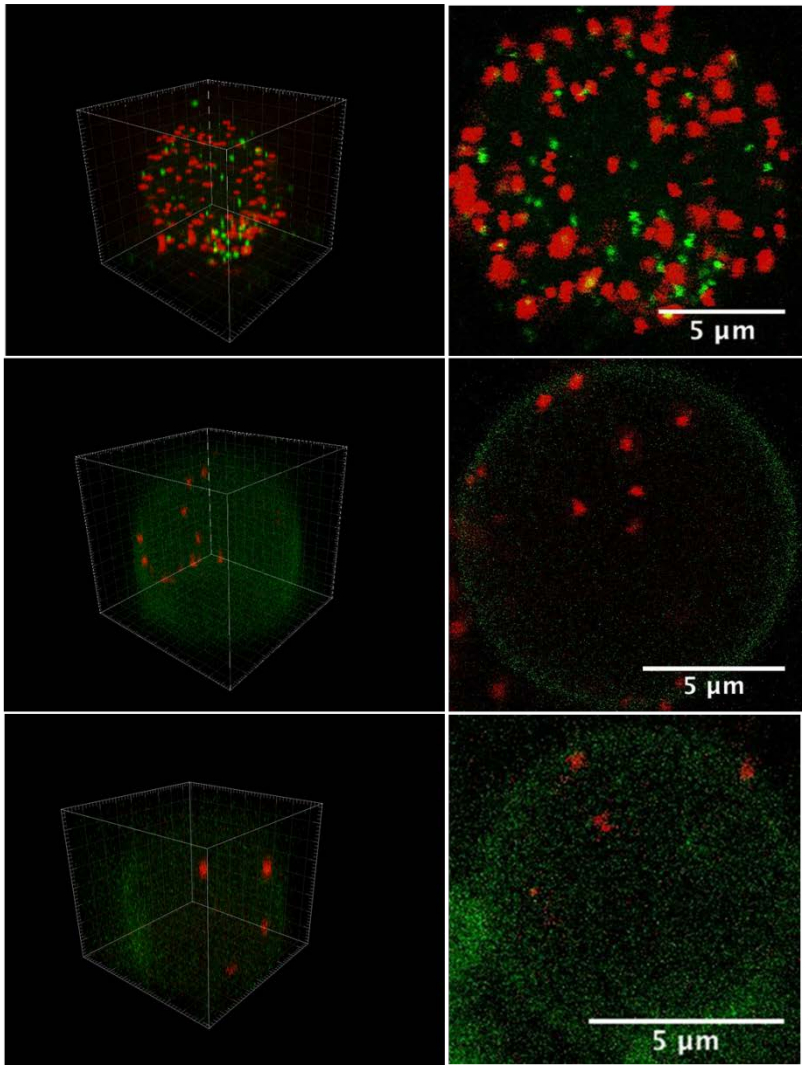

Figure S32. Left: *3D representation of GPMVs* ***Right:*** *Maximum projection image of 3D representation.* ***Top panel****: GPMVs equipped with SRB (red) and CF (green)-loaded* $PMOXA_{44}$-$PDMS_{6}$-$PMOXA_{44}$ *polymersomes.* ***Middle panel:*** *Plasma membrane equipped with e-GFP Lck Tyrosine kinase (green) filled with SRB-loaded PMOXA-PDMS-PMOXA polymersomes (red).* ***Bottom panel:*** *GPMVs equipped with e-GFP Lck Tyrosine kinase (green) filled with SRB-loaded DSPC-PEG liposomes (red).*

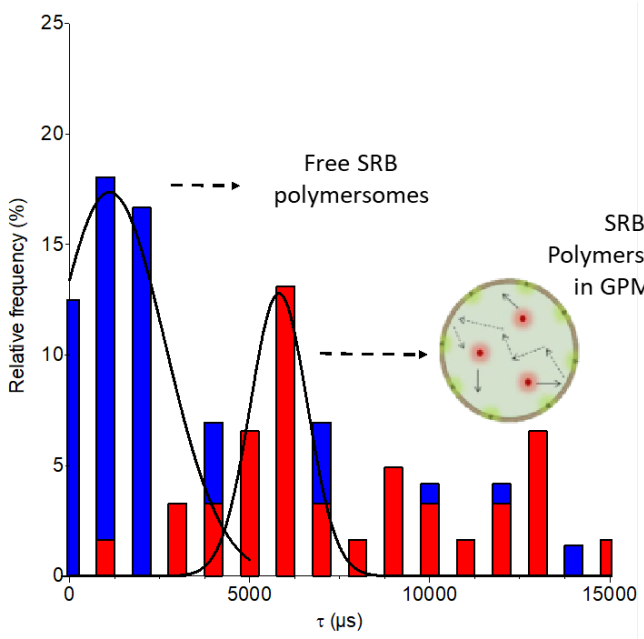

Figure S33: Frequency distribution of diffusion times taken from individual FCS measurements. *SRB-loaded PMOXA$_{44}$-PDMS$_6$-PMOXA$_{44}$ polymersomes in PBS pH 7.4 (Blue) and SRB-loaded PMOXA$_{44}$-PDMS$_6$-PMOXA$_{44}$ polymersomes within GPMVs (Red).*

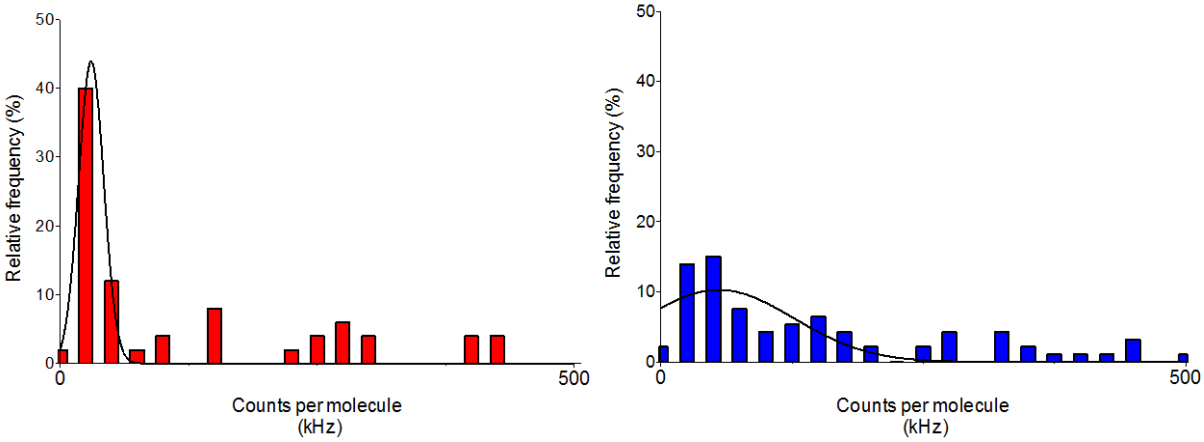

Figure S34: Frequency distribution of molecular brightness's taken from individual FCS measurements*. FCS analysis of SRB-loaded PMOXA-PDMS-PMOXA polymersomes in GPMVs (Red) and PBS pH 7.4 (Blue).*

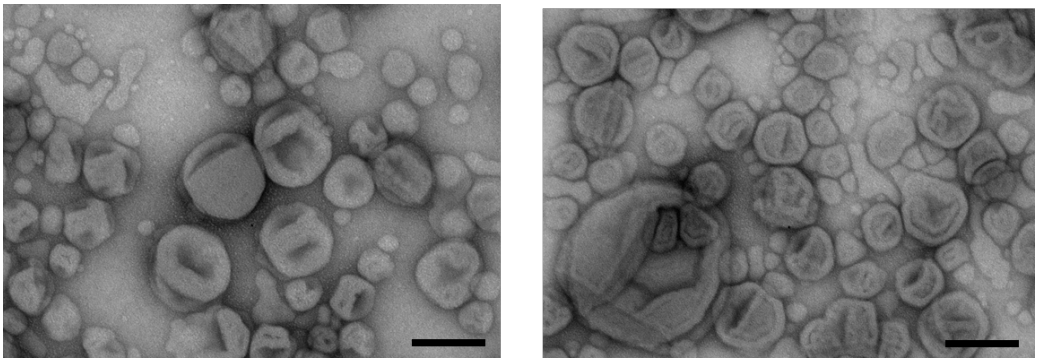

Figure S35. *TEM micrograph of a $PMOXA_{44}$-$PDMS_6$-$PMOXA_{44}$ polymersomes loaded with HRP.* ***Left:*** *OmpF equipped HRP-loaded polymersomes.* ***Right:*** *HRP-loaded polymersomes. GPMV. Scale bar 100 nm.*

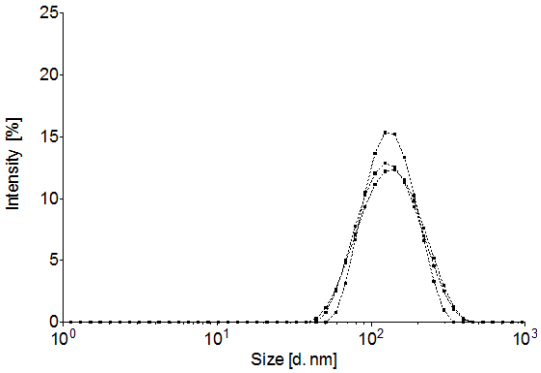

Figure S36. *Intensity distribution by DLS of OmpF equipped HRP-loaded $PMOXA_{44}$-$PDMS_6$-$PMOXA_{44}$ polymersomes.*

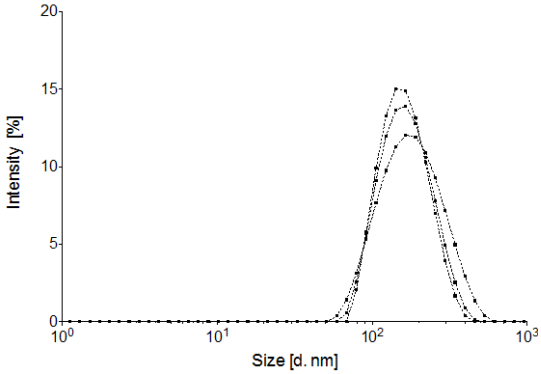

Figure S37. *Intensity distribution of DLS measurement of HRP-loaded $PMOXA_{44}$-$PDMS_6$-$PMOXA_{44}$ polymersomes (n=3).*

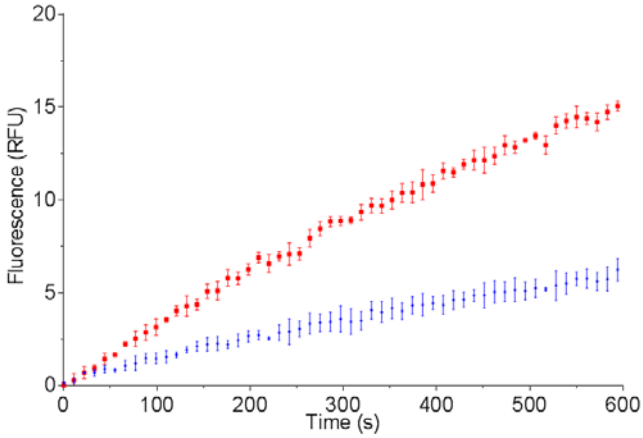

Figure S38. *Fluorescence intensity (Ex: 530 Em:590) resulting from the enzymatic conversion of Amplex UltraRed into the resorufin-like product by HRP encapsulated in catalytic nanocompartments, measured free in solution (PBS pH 7.4). (Red) Catalytic nanocompartments loaded with HRP and equipped with OmpF K89 R270, (Blue) Catalytic nanocompartments without OmpF.*

REFERENCES

1. Salehi-Reyhani, A., Ces, O. & Elani, Y. Artificial cell mimics as simplified models for the study of cell biology. *Exp. Biol. Med.* **242,** 1309–1317 (2017).
2. Xavier, J. C., Patil, K. R. & Rocha, I. Systems Biology Perspectives on Minimal and Simpler Cells. *Microbiol. Mol. Biol. Rev.* **78,** 487–509 (2014).
3. Steinberg-Yfrach, G. *et al.* Light-driven production of ATP catalysed by F0F1-ATP synthase in an artificial photosynthetic membrane. *Nature* **392,** 479–482 (1998).
4. Lentini, R. *et al.* Integrating artificial with natural cells to translate chemical messages that direct *E. coli* behaviour. *Nat. Commun.* **5,** 4012 (2014).
5. Adamala, K. P., Martin-Alarcon, D. A., Guthrie-Honea, K. R. & Boyden, E. S. Engineering genetic circuit interactions within and between synthetic minimal cells. *Nat. Chem.* **9,** 431–439 (2016).
6. Elani, Y., Law, R. V. & Ces, O. Protein synthesis in artificial cells: using compartmentalisation for spatial organisation in vesicle bioreactors. *Phys. Chem. Chem. Phys.* **17,** 15534–15537 (2015).
7. Elani, Y., Law, R. V. & Ces, O. Vesicle-based artificial cells as chemical microreactors with spatially segregated reaction pathways. *Nat. Commun.* **5,** 5305 (2014).
8. Rafelski, S. M. & Marshall, W. F. Building the cell: design principles of cellular architecture. *Nat. Rev. Mol. Cell Biol.* **9,** 593 (2008).
9. Buchner, E. & Rapp, R. Alkoholische Gährung ohne Hefezellen. *Berichte Dtsch. Chem. Ges.* **30,** 2668–2678 (1897).
10. Stano, P., Carrara, P., Kuruma, Y., Souza, T. P. de & Luisi, P. L. Compartmentalized reactions as a case of soft-matter biotechnology: synthesis of proteins and nucleic acids inside lipid vesicles. *J. Mater. Chem.* **21,** 18887–18902 (2011).
11. Oberholzer, T., Albrizio, M. & Luisi, P. L. Polymerase chain reaction in liposomes. *Chem. Biol.* **2,** 677–682 (1995).
12. Fischer, A., Franco, A. & Oberholzer, T. Giant vesicles as microreactors for enzymatic mRNA synthesis. *ChemBioChem* **3,** 409–417 (2002).
13. Nomura, S. M. *et al.* Gene Expression within Cell-Sized Lipid Vesicles. *ChemBioChem* **4,** 1172–1175 (2003).
14. Noireaux, V., Bar-Ziv, R., Godefroy, J., Salman, H. & Libchaber, A. Toward an artificial cell based on gene expression in vesicles. *Phys. Biol.* **2,** P1 (2005).
15. Godovac-Zimmermann, J. & Brown, L. R. Perspectives for mass spectrometry and functional proteomics. *Mass Spectrom. Rev.* **20,** 1–57 (2001).
16. Peters, R. J. R. W. *et al.* Cascade Reactions in Multicompartmentalized Polymersomes. *Angew. Chem. Int. Ed.* **53,** 146–150 (2014).
17. Kobori, S., Ichihashi, N., Kazuta, Y. & Yomo, T. A controllable gene expression system in liposomes that includes a positive feedback loop. *Mol. Biosyst.* **9,** 1282 (2013).
18. Xiao, Q. *et al.* Bioactive cell-like hybrids coassembled from (glyco)dendrimersomes with bacterial membranes. *Proc. Natl. Acad. Sci.* **113,** E1134–E1141 (2016).

19. Ashley, C. E. *et al.* The targeted delivery of multicomponent cargos to cancer cells by nanoporous particle-supported lipid bilayers. *Nat. Mater.* **10,** 389–397 (2011).
20. Kreft, O., Prevot, M., Möhwald, H. & Sukhorukov, G. B. Shell-in-Shell Microcapsules: A Novel Tool for Integrated, Spatially Confined Enzymatic Reactions. *Angew. Chem. Int. Ed.* **46,** 5605–5608 (2007).
21. Qiao, Y., Li, M., Booth, R. & Mann, S. Predatory behaviour in synthetic protocell communities. *Nat. Chem.* **9,** 110 (2017).
22. Stano, P. & Luisi, P. L. Semi-synthetic minimal cells: origin and recent developments. *Curr. Opin. Biotechnol.* **24,** 633–638 (2013).
23. Walde, P. Building artificial cells and protocell models: Experimental approaches with lipid vesicles. *BioEssays* **32,** 296–303 (2010).
24. Elani, Y. Construction of membrane-bound artificial cells using microfluidics: a new frontier in bottom-up synthetic biology. *Biochem. Soc. Trans.* **44,** 723–730 (2016).
25. Martino, C. *et al.* Protein Expression, Aggregation, and Triggered Release from Polymersomes as Artificial Cell-like Structures. *Angew. Chem. Int. Ed.* **51,** 6416–6420 (2012).
26. Martino, C. & deMello, A. J. Droplet-based microfluidics for artificial cell generation: a brief review. *Interface Focus* **6,** (2016).
27. Khopade, A. J. & Caruso, F. Stepwise self-assembled poly(amidoamine) dendrimer and poly(styrenesulfonate) microcapsules as sustained delivery vehicles. *Biomacromolecules* **3,** 1154–1162 (2002).
28. Matosevic, S. & Paegel, B. M. Layer-by-layer cell membrane assembly. *Nat. Chem.* **5,** 958 (2013).
29. Elani, Y., Solvas, X. C. I., Edel, J. B., Law, R. V. & Ces, O. Microfluidic generation of encapsulated droplet interface bilayer networks (multisomes) and their use as cell-like reactors. *Chem. Commun.* **52,** 5961–5964 (2016).
30. Spector, A. A. & Yorek, M. A. Membrane lipid composition and cellular function. *J. Lipid Res.* **26,** 1015–1035 (1985).
31. Phillips, R., Ursell, T., Wiggins, P. & Sens, P. Emerging roles for lipids in shaping membrane-protein function. *Nature* (2009). doi:10.1038/nature08147
32. Booth, P. J. Sane in the membrane: designing systems to modulate membrane proteins. *Curr. Opin. Struct. Biol.* **15,** 435–440 (2005).
33. Perozo, E., Kloda, A., Cortes, D. M. & Martinac, B. Physical principles underlying the transduction of bilayer deformation forces during mechanosensitive channel gating. *Nat. Struct. Mol. Biol.* **9,** 696 (2002).
34. Pinot, M. *et al.* Effects of Confinement on the Self-Organization of Microtubules and Motors. *Curr. Biol.* **19,** 954–960 (2009).
35. Booth, P. J. *et al.* Evidence That Bilayer Bending Rigidity Affects Membrane Protein Folding. *Biochemistry (Mosc.)* **36,** 197–203 (1997).
36. Attard, G. S., Templer, R. H., Smith, W. S., Hunt, A. N. & Jackowski, S. Modulation of CTP:phosphocholine cytidylyltransferase by membrane curvature elastic stress. *Proc. Natl. Acad. Sci.* **97,** 9032–9036 (2000).
37. Working, E. B., Andrews, A. C. The Structure of the Phospholipids. *Chem. Rev.* **29**, 245-256 (1941).

38. Alberts, B. *et al. Molecular Biology of the Cell*, 2002.
39. Tan, S., Tan, H. T. & Chung, M. C. M. Membrane proteins and membrane proteomics. *PROTEOMICS* **8,** 3924–3932 (2008).
40. van Spriel, A. B., van den Bogaart, G. & Cambi, A. Editorial: Membrane domains as new drug targets. *Front. Physiol.* **6,** (2015).
41. Cournia, Z. *et al.* Membrane Protein Structure, Function and Dynamics: A Perspective from Experiments and Theory. *J. Membr. Biol.* **248,** 611–640 (2015).
42. Nicolson, G. L. The Fluid—Mosaic Model of Membrane Structure: Still relevant to understanding the structure, function and dynamics of biological membranes after more than 40years. *Biochim. Biophys. Acta BBA - Biomembr.* **1838,** 1451–1466 (2014).
43. Dufourc, E. J. Sterols and membrane dynamics. *J. Chem. Biol.* **1,** 63–77 (2008).
44. Li, J. *et al.* A review on phospholipids and their main applications in drug delivery systems. *Asian J. Pharm. Sci.* **10,** 81–98 (2015).
45. Seddon, A. M., Curnow, P. & Booth, P. J. Membrane proteins, lipids and detergents: not just a soap opera. *Biochim. Biophys. Acta BBA - Biomembr.* **1666,** 105–117 (2004).
46. Hatzakis, N. S. *et al.* How curved membranes recruit amphipathic helices and protein anchoring motifs. *Nat. Chem. Biol.* **5,** 835 (2009).
47. Tonnesen, A., Christensen, S. M., Tkach, V. & Stamou, D. Geometrical Membrane Curvature as an Allosteric Regulator of Membrane Protein Structure and Function. *Biophys. J.* **106,** 201–209 (2014).
48. Sens, P., Johannes, L. & Bassereau, P. Biophysical approaches to protein-induced membrane deformations in trafficking. *Curr. Opin. Cell Biol.* **20,** 476–482 (2008).
49. Callan-Jones, A. & Bassereau, P. Curvature-driven membrane lipid and protein distribution. *Curr. Opin. Solid State Mater. Sci.* **17,** 143–150 (2013).
50. Mai, Y. & Eisenberg, A. Self-assembly of block copolymers. *Chem. Soc. Rev.* **41,** 5969 (2012).
51. G. Skirtach, A., M. Yashchenok, A. & Möhwald, H. Encapsulation, release and applications of LbL polyelectrolyte multilayer capsules. *Chem. Commun.* **47,** 12736–12746 (2011).
52. Vriezema, D. M. *et al.* Self-Assembled Nanoreactors. *Chem. Rev.* **105**, 1445-1490 (2005).
53. Rijn, P. van *et al.* Challenges and advances in the field of self-assembled membranes. *Chem. Soc. Rev.* **42,** 6578–6592 (2013).
54. Discher, D. E. & Ahmed, F. Polymersomes. *Annu. Rev. Biomed. Eng.* **8,** 323–341 (2006).
55. Discher, B. M. *et al.* Polymersomes: Tough Vesicles Made from Diblock Copolymers. *Science* **284,** 1143–1146 (1999).
56. Discher, D. E. & Eisenberg, A. Polymer Vesicles. *Science* **297,** 967–973 (2002).
57. Palivan, C. G., Fischer-Onaca, O., Delcea, M., Itel, F. & Meier, W. Protein–polymer nanoreactors for medical applications. *Chem. Soc. Rev.* **41,** 2800–2823 (2012).
58. Marguet, M., Bonduelle, C. & Lecommandoux, S. Multicompartmentalized polymeric systems: towards biomimetic cellular structure and function. *Chem. Soc. Rev.* **42,** 512–529 (2012).

59. Karayianni, M. & Pispas, S. Self-Assembly of Amphiphilic Block Copolymers in Selective Solvents. in *Fluorescence Studies of Polymer Containing Systems* 27–63 (Springer, Cham, 2016). doi:10.1007/978-3-319-26788-3_2
60. Walde, P., Cosentino, K., Engel, H. & Stano, P. Giant Vesicles: Preparations and Applications. *ChemBioChem* **11,** 848–865 (2010).
61. Dimova, R. *et al.* A practical guide to giant vesicles. Probing the membrane nanoregime via optical microscopy. *J. Phys. Condens. Matter* **18,** S1151 (2006).
62. Hammer, D. A. & Kamat, N. P. Towards an artificial cell. *FEBS Lett.* **586,** 2882–2890 (2012).
63. Shum, H. C., Kim, J.-W. & Weitz, D. A. Microfluidic Fabrication of Monodisperse Biocompatible and Biodegradable Polymersomes with Controlled Permeability. *J. Am. Chem. Soc.* **130,** 9543–9549 (2008).
64. Perro, A. *et al.* Mastering a Double Emulsion in a Simple Co-Flow Microfluidic to Generate Complex Polymersomes. *Langmuir* **27,** 9034–9042 (2011).
65. Yildiz, M. E., Prud'homme, R. K., Robb, I. & Adamson, D. H. Formation and characterization of polymersomes made by a solvent injection method. *Polym. Adv. Technol.* **18,** 427–432 (2007).
66. Lomora, M., Itel, F., Dinu, I. A. & Palivan, C. G. Selective ion-permeable membranes by insertion of biopores into polymersomes. *Phys. Chem. Chem. Phys.* **17,** 15538–15546 (2015).
67. Lim, S. K., de Hoog, H.-P., Parikh, A. N., Nallani, M. & Liedberg, B. Hybrid, Nanoscale Phospholipid/Block Copolymer Vesicles. *Polymers* **5,** 1102–1114 (2013).
68. Nam, J., Beales, P. A. & Vanderlick, T. K. Giant Phospholipid/Block Copolymer Hybrid Vesicles: Mixing Behavior and Domain Formation. *Langmuir* **27,** 1–6 (2011).
69. Le Meins, J.-F., Schatz, C., Lecommandoux, S. & Sandre, O. Hybrid polymer/lipid vesicles: state of the art and future perspectives. *Mater. Today* **16,** 397–402 (2013).
70. Fuhrmann, G., Herrmann, I. K. & Stevens, M. M. Cell-derived vesicles for drug therapy and diagnostics: opportunities and challenges. *Nano Today* **10,** 397–409 (2015).
71. Hoerl, B. J. & Scott, R. E. Plasma membrane vesiculation: A cellular response to injury. *Virchows Arch. B Cell Pathol. Zell-Pathol.* **27,** 335–345 (1978).
72. Del Piccolo, N., Placone, J., He, L., Agudelo, S. C. & Hristova, K. Production of Plasma Membrane Vesicles with Chloride Salts and Their Utility as a Cell Membrane Mimetic for Biophysical Characterization of Membrane Protein Interactions. *Anal. Chem.* **84,** 8650–8655 (2012).
73. Kelly, C. V. *et al.* Pulsed-laser creation and characterization of giant plasma membrane vesicles from cells. *J. Biol. Phys.* **35,** 279–295 (2009).
74. Sezgin, E. *et al.* Elucidating membrane structure and protein behavior using giant plasma membrane vesicles. *Nat. Protoc.* **7,** 1042–1051 (2012).
75. Levental, K. R. & Levental, I. Giant Plasma Membrane Vesicles: Models for Understanding Membrane Organization. *Curr. Top. Membr.* **75,** 25–57 (2015).
76. Säälik, P. *et al.* Penetration without cells: Membrane translocation of cell-penetrating peptides in the model giant plasma membrane vesicles. *J. Controlled Release* **153,** 117–125 (2011).

77. Dubavik, A. *et al.* Penetration of Amphiphilic Quantum Dots through Model and Cellular Plasma Membranes. *ACS Nano* **6,** 2150–2156 (2012).
78. Ge, M. *et al.* Ordered and Disordered Phases Coexist in Plasma Membrane Vesicles of RBL-2H3 Mast Cells. An ESR Study. *Biophys. J.* **85,** 1278–1288 (2003).
79. Gadok, A. K. *et al.* Connectosomes for Direct Molecular Delivery to the Cellular Cytoplasm. *J. Am. Chem. Soc.* **138,** 12833–12840 (2016).
80. Gadok, A. K. *et al.* The Display of Single-Domain Antibodies on the Surfaces of Connectosomes Enables Gap Junction-Mediated Drug Delivery to Specific Cell Populations. *Biochemistry (Mosc.)* (2017). doi:10.1021/acs.biochem.7b00688
81. Habel, J. *et al.* Selecting analytical tools for characterization of polymersomes in aqueous solution. *RSC Adv.* **5,** 79924–79946 (2015).
82. Bleul, R., Maskos, M., Polymersomes: Synthesis and Applications, *Encyclopedia of Polymer Science and Technology*, (Chapter 3), (2014).
83. Itel, F. *et al.* Molecular Organization and Dynamics in Polymersome Membranes: A Lateral Diffusion Study. *Macromolecules* **47,** 7588–7596 (2014).
84. Jaskiewicz, K., Makowski, M., Kappl, M., Landfester, K. & Kroeger, A. Mechanical Properties of Poly(dimethylsiloxane)-block-poly(2-methyloxazoline) Polymersomes Probed by Atomic Force Microscopy. *Langmuir* **28,** 12629–12636 (2012).
85. Dieu, L. H., Wu, D., Palivan, C. G., Balasubramanian, V. & Huwyler, J. Polymersomes conjugated to 83-14 monoclonal antibodies: Invitro targeting of brain capillary endothelial cells. *Eur J Pharm Biopharm* **88,** 316–324 (2014).
86. Jalmar, O. *et al.* Caspase-8 Binding to Cardiolipin in Giant Unilamellar Vesicles Provides a Functional Docking Platform for Bid. *PLOS ONE* **8,** e55250 (2013).
87. Garten, M. *et al.* Whole-GUV patch-clamping. *Proc. Natl. Acad. Sci.* **114,** 328–333 (2017).
88. Men, Y., Peng, F., Tu, Y., Hest, J. C. M. van & Wilson, D. A. Methods for production of uniform small-sized polymersome with rigid membrane. *Polym. Chem.* **7,** 3977–3982 (2016).
89. Rodríguez-García, R. *et al.* Polymersomes: smart vesicles of tunable rigidity and permeability. *Soft Matter* **7,** 1532–1542 (2011).
90. Sauer, M., Haefele, T., Graff, A., Nardin, C. & Meier, W. Ion-carrier controlled precipitation of calcium phosphate in giant ABA triblock copolymer vesicles. *Chem. Commun.* **0,** 2452–2453 (2001).
91. Carlsen, A., Glaser, N., Le Meins, J.-F. & Lecommandoux, S. Block Copolymer Vesicle Permeability Measured by Osmotic Swelling and Shrinking. *Langmuir* **27,** 4884–4890 (2011).
92. Yildiz, U. H. *et al.* Polymersomes: Third-Party ATP Sensing in Polymersomes: A Label-Free Assay of Enzyme Reactions in Vesicular Compartments (Small 3/2014). *Small* **10,** 441–441 (2014).
93. Onaca, O., Enea, R., Hughes, D. W. & Meier, W. Stimuli-Responsive Polymersomes as Nanocarriers for Drug and Gene Delivery. *Macromol. Biosci.* **9,** 129–139 (2009).
94. Meng, F., Zhong, Z. & Feijen, J. Stimuli-Responsive Polymersomes for Programmed Drug Delivery. *Biomacromolecules* **10,** 197–209 (2009).

95. Li, M.-H. & Keller, P. Stimuli-responsive polymer vesicles. *Soft Matter* **5,** 927–937 (2009).
96. Discher, B. M., Hammer, D. A., Bates, F. S. & Discher, D. E. Polymer vesicles in various media. *Curr. Opin. Colloid Interface Sci.* **5,** 125–131 (2000).
97. Kagawa Yasuo. 5477.full.pdf. Available at: http://www.jbc.org/content/246/17/5477.full.pdf. (Accessed: 21st January 2018)
98. Rigaud, J.-L. Membrane proteins: functional and structural studies using reconstituted proteoliposomes and 2-D crystals. *Braz. J. Med. Biol. Res.* **35,** 753–766 (2002).
99. Jørgensen, I. L., Kemmer, G. C. & Pomorski, T. G. Membrane protein reconstitution into giant unilamellar vesicles: a review on current techniques. *Eur. Biophys. J.* **46,** 103–119 (2017).
100. Dezi, M., Cicco, A. D., Bassereau, P. & Lévy, D. Detergent-mediated incorporation of transmembrane proteins in giant unilamellar vesicles with controlled physiological contents. *Proc. Natl. Acad. Sci.* **110,** 7276–7281 (2013).
101. Chernomordik, L. V. & Kozlov, M. M. Protein-Lipid Interplay in Fusion and Fission of Biological Membranes. *Annu. Rev. Biochem.* **72,** 175–207 (2003).
102. Lin, Q. & London, E. The Influence of Natural Lipid Asymmetry Upon the Conformation of a Membrane-Inserted Protein (Perfringolysin O). *J. Biol. Chem.* jbc.M113.533943 (2014). doi:10.1074/jbc.M113.533943
103. Almendro-Vedia, V. G. *et al.* Nonequilibrium fluctuations of lipid membranes by the rotating motor protein F1F0-ATP synthase. *Proc. Natl. Acad. Sci. U. S. A.* **114,** 11291–11296 (2017).
104. Nardin, C., Thoeni, S., Widmer, J., Winterhalter, M. & Meier, W. Nanoreactors based on (polymerized) ABA-triblock copolymer vesicles. *Chem. Commun.* **0,** 1433–1434 (2000).
105. Lee, A. G. How lipids affect the activities of integral membrane proteins. *Biochim. Biophys. Acta BBA - Biomembr.* **1666,** 62–87 (2004).
106. Rigaud, J.-L. & Lévy, D. Reconstitution of Membrane Proteins into Liposomes. in *Methods in Enzymology* **372,** 65–86 (Academic Press, 2003).
107. Habel, J. *et al.* Aquaporin-Based Biomimetic Polymeric Membranes: Approaches and Challenges. *Membranes* **5,** 307–351 (2015).
108. Kumar, M., Habel, J. E. O., Shen, Y., Meier, W. P. & Walz, T. High-Density Reconstitution of Functional Water Channels into Vesicular and Planar Block Copolymer Membranes. *J. Am. Chem. Soc.* **134,** 18631–18637 (2012).
109. Itel, F., Najer, A., Palivan, C. G. & Meier, W. Dynamics of Membrane Proteins within Synthetic Polymer Membranes with Large Hydrophobic Mismatch. *Nano Lett.* **15,** 3871–3878 (2015).
110. Pata, V. & Dan, N. The Effect of Chain Length on Protein Solubilization in Polymer-Based Vesicles (Polymersomes). *Biophys. J.* **85,** 2111–2118 (2003).
111. Picker, A., Nuss, H., Guenoun, P. & Chevallard, C. Polymer Vesicles as Microreactors for Bioinspired Calcium Carbonate Precipitation. *Langmuir* **27,** 3213–3218 (2011).
112. Choi, H.-J. & Montemagno, C. D. Artificial Organelle: ATP Synthesis from Cellular Mimetic Polymersomes. *Nano Lett.* **5,** 2538–2542 (2005).

113. Choi, H. J. & Montemagno, C. D. Light-Driven Hybrid Bioreactor Based on Protein-Incorporated Polymer Vesicles. *IEEE Trans. Nanotechnol.* **6,** 171–176 (2007).
114. Lanyi, J. K. & Pohorille, A. Proton pumps: mechanism of action and applications. *Trends Biotechnol.* **19,** 140–144 (2001).
115. Einfalt, T. *et al.* Stimuli-Triggered Activity of Nanoreactors by Biomimetic Engineering Polymer Membranes. *Nano Lett.* **15,** 7596–7603 (2015).
116. Pawar, P. V., Gohil, S. V., Jain, J. P. & Kumar, N. Functionalized polymersomes for biomedical applications. *Polym. Chem.* **4,** 3160–3176 (2013).
117. Dobrunz, D., Toma, A. C., Tanner, P., Pfohl, T. & Palivan, C. G. Polymer Nanoreactors with Dual Functionality: Simultaneous Detoxification of Peroxynitrite and Oxygen Transport. *Langmuir* **28,** 15889–15899 (2012).
118. M. Kuiper, S. *et al.* Enzymes containing porous polymersomes as nano reaction vessels for cascade reactions. *Org. Biomol. Chem.* **6,** 4315–4318 (2008).
119. Tanner, P., Balasubramanian, V. & Palivan, C. G. Aiding Nature's Organelles: Artificial Peroxisomes Play Their Role. *Nano Lett.* **13,** 2875–2883 (2013).
120. Zetterlund, P. B. Controlled/living radical polymerization in nanoreactors: compartmentalization effects. *Polym. Chem.* **2,** 534–549 (2011).
121. Cotanda, P. & O'Reilly, R. K. Molecular recognition driven catalysis using polymeric nanoreactors. *Chem. Commun.* **48,** 10280–10282 (2012).
122. Sanlés-Sobrido, M., Pérez-Lorenzo, M., Rodríguez-González, B., Salgueiriño, V. & Correa-Duarte, M. A. Highly Active Nanoreactors: Nanomaterial Encapsulation Based on Confined Catalysis. *Angew. Chem. Int. Ed.* **51,** 3877–3882 (2012).
123. Meng, F. & Zhong, Z. Polymersomes Spanning from Nano- to Microscales: Advanced Vehicles for Controlled Drug Delivery and Robust Vesicles for Virus and Cell Mimicking. *J. Phys. Chem. Lett.* **2,** 1533–1539 (2011).
124. Lundberg, P. *et al.* pH-triggered self-assembly of biocompatible histamine-functionalized triblock copolymers. *Soft Matter* **9,** 82–89 (2012).
125. Cabane, E., Malinova, V., Menon, S., Palivan, C. G. & Meier, W. Photoresponsive polymersomes as smart, triggerable nanocarriers. *Soft Matter* **7,** 9167–9176 (2011).
126. Hu, J., Zhang, G. & Liu, S. Enzyme-responsive polymeric assemblies, nanoparticles and hydrogels. *Chem. Soc. Rev.* **41,** 5933–5949 (2012).
127. Liao, L. *et al.* A Convergent Synthetic Platform for Single-Nanoparticle Combination Cancer Therapy: Ratiometric Loading and Controlled Release of Cisplatin, Doxorubicin, and Camptothecin. *J. Am. Chem. Soc.* **136,** 5896–5899 (2014).
128. Cheng, R., Meng, F., Deng, C., Klok, H.-A. & Zhong, Z. Dual and multi-stimuli responsive polymeric nanoparticles for programmed site-specific drug delivery. *Biomaterials* **34,** 3647–3657 (2013).
129. Car, A. *et al.* pH-Responsive PDMS-b-PDMAEMA Micelles for Intracellular Anticancer Drug Delivery. *Biomacromolecules* **15,** 3235–3245 (2014).
130. Wei, H., Zhuo, R.-X. & Zhang, X.-Z. Design and development of polymeric micelles with cleavable links for intracellular drug delivery. *Prog. Polym. Sci.* **38,** 503–535 (2013).
131. Wei, H. *et al.* Dual Responsive, Stabilized Nanoparticles for Efficient In Vivo Plasmid Delivery. *Angew. Chem. Int. Ed.* **52,** 5377–5381 (2013).

132. Engler, A. C. *et al.* Polycarbonate-Based Brush Polymers with Detachable Disulfide-Linked Side Chains. *ACS Macro Lett.* **2,** 332–336 (2013).
133. Chu, X.-P., Papasian, C. J., Wang, J. Q. & Xiong, Z.-G. Modulation of acid-sensing ion channels: Molecular mechanisms and therapeutic potential. *Int. J. Physiol. Pathophysiol. Pharmacol.* **3,** 288–309 (2011).
134. Hu, J., Miura, S., Na, K. & Bae, Y. H. PH-responsive and charge shielded cationic micelle of poly(l-histidine)- block-short branched PEI for acidic cancer treatment. *J. Controlled Release* **172,** 69–76 (2013).
135. Lomas, H. *et al.* Biomimetic pH Sensitive Polymersomes for Efficient DNA Encapsulation and Delivery. *Adv. Mater.* **19,** 4238–4243 (2007).
136. Wang, C., Yu, S., Chen, W. & Sun, C. Highly Efficient Light-Trapping Structure Design Inspired By Natural Evolution. *Sci. Rep.* **3,** 1025 (2013).
137. Matini, T. *et al.* Synthesis and characterization of variable conformation pH responsive block co-polymers for nucleic acid delivery and targeted cell entry. *Polym. Chem.* **5,** 1626–1636 (2014).
138. Montenegro, J., Braun, J., Fischer-Onaca, O., Meier, W. & Matile, S. Synthetic polyion-counterion transport systems in polymersomes and gels. *Org. Biomol. Chem.* **9,** 6623–6628 (2011).
139. Kumar, M., Grzelakowski, M., Zilles, J., Clark, M. & Meier, W. Highly permeable polymeric membranes based on the incorporation of the functional water channel protein Aquaporin Z. *Proc. Natl. Acad. Sci. U. S. A.* **104,** 20719–20724 (2007).
140. Roy, D. & Sumerlin, B. S. Glucose-sensitivity of boronic acid block copolymers at physiological pH. *ACS Macro Lett.* **1,** 529–532 (2012).
141. Spulber, M. *et al.* Photoreaction of a hydroxyalkyphenone with the membrane of polymersomes: A versatile method to generate semipermeable nanoreactors. *J. Am. Chem. Soc.* **135,** 9204–9212 (2013).
142. Gaitzsch, J., Appelhans, D., Wang, L., Battaglia, G. & Voit, B. Synthetic bio-nanoreactor: Mechanical and chemical control of polymersome membrane permeability. *Angew. Chem. - Int. Ed.* **51,** 4448–4451 (2012).
143. Gräfe, D., Gaitzsch, J., Appelhans, D. & Voit, B. Cross-linked polymersomes as nanoreactors for controlled and stabilized single and cascade enzymatic reactions. *Nanoscale* **6,** 10752–10761 (2014).
144. Wallace, B. A. Gramicidin channels and pores. *Annu. Rev. Biophys. Biophys. Chem.* **19,** 127–157 (1990).
145. Andersen, O. S. Ion movement through gramicidin A channels. Studies on the diffusion-controlled association step. *Biophys. J.* **41,** 147–165 (1983).
146. Helfrich, P. & Jakobsson, E. Calculation of deformation energies and conformations in lipid membranes containing gramicidin channels. *Biophys. J.* **57,** 1075–1084 (1990).
147. Harroun, T. A., Heller, W. T., Weiss, T. M., Yang, L. & Huang, H. W. Experimental evidence for hydrophobic matching and membrane-mediated interactions in lipid bilayers containing gramicidin. *Biophys. J.* **76,** 937–945 (1999).
148. Jing, W., Wu, Z. & Wang, E. Electrochemical study of gramicidin D forming ion-permeable channels in the bilayer lipid membranes. *Electrochimica Acta* **44,** 99–102 (1998).

149. Sychev, S. V., Barsukov, L. I. & Ivanov, V. T. Conformation of gramicidin A in Triton X-100 micelles from CD and FTIR data: A clean example of antiparallel double β5.6 helix formation. *J. Pept. Sci.* **19,** 452–458 (2013).
150. Oliynyk, V. *et al.* Selective and ATP-driven transport of ions across supported membranes into nanoporous carriers using gramicidin A and ATP synthase. *Phys. Chem. Chem. Phys.* **15,** 2733–2740 (2013).
151. Clement, N. R. & Gould, J. M. Pyranine (8-Hydroxy-1,3,6-pyrenetrisulfonate) as a Probe of Internal Aqueous Hydrogen Ion Concentration in Phospholipid Vesicles. *Biochemistry (Mosc.)* **20,** 1534–1538 (1981).
152. González-Pérez, A., Stibius, K. B., Vissing, T., Nielsen, C. H. & Mouritsen, O. G. Biomimetic triblock copolymer membrane arrays: A stable template for functional membrane proteins. *Langmuir* **25,** 10447–10450 (2009).
153. Balasubramanian, V. *et al.* A surprising system: polymeric nanoreactors containing a mimic with dual-enzyme activity. *Soft Matter* **7,** 5595–5603 (2011).
154. Kelkar, D. A. & Chattopadhyay, A. The gramicidin ion channel: A model membrane protein. *Biochim. Biophys. Acta - Biomembr.* **1768,** 2011–2025 (2007).
155. Goulian, M. *et al.* Gramicidin channel kinetics under tension. *Biophys. J.* **74,** 328–337 (1998).
156. Graff, A. *et al.* Amphiphilic copolymer membranes promote nadh: Ubiquinone oxidoreductase activity: Towards an electron-transfer nanodevice. *Macromol. Chem. Phys.* **211,** 229–238 (2010).
157. Meier, W., Nardin, C. & Winterhalter, M. Reconstitution of channel proteins in (Polymerized) ABA triblock copolymer membranes. *Angew. Chem. - Int. Ed.* **39,** 4599–4602 (2000).
158. Stoenescu, R., Graff, A. & Meier, W. Asymmetric ABC-triblock copolymer membranes induce a directed insertion of membrane proteins. *Macromol. Biosci.* **4,** 930–935 (2004).
159. Sueyoshi, D., Anraku, Y., Komatsu, T., Urano, Y. & Kataoka, K. Enzyme-Loaded Polyion Complex Vesicles as in Vivo Nanoreactors Working Sustainably under the Blood Circulation: Characterization and Functional Evaluation. *Biomacromolecules* **18,** 1189–1196 (2017).
160. Dinu, M. V. *et al.* Filling Polymersomes with Polymers by Peroxidase-Catalyzed Atom Transfer Radical Polymerization. *Macromol. Rapid Commun.* **36,** 507–514 (2015).
161. Zhang, X. *et al.* Active surfaces engineered by immobilizing protein-polymer nanoreactors for selectively detecting sugar alcohols. *Biomaterials* **89,** 79–88 (2016).
162. Kowal, J., Zhang, X., Dinu, I. A., Palivan, C. G. & Meier, W. Planar Biomimetic Membranes Based on Amphiphilic Block Copolymers. *ACS Macro Lett.* **3,** 59–63 (2014).
163. Letchford, K. & Burt, H. A review of the formation and classification of amphiphilic block copolymer nanoparticulate structures: micelles, nanospheres, nanocapsules and polymersomes. *Eur. J. Pharm. Biopharm. Off. J. Arbeitsgemeinschaft Pharm. Verfahrenstechnik EV* **65,** 259–269 (2007).
164. Lomora, M. *et al.* Polymersomes with engineered ion selective permeability as stimuli-responsive nanocompartments with preserved architecture. *Biomaterials* **53,** 406–414 (2015).

165. Küchler, A., Yoshimoto, M., Luginbühl, S., Mavelli, F. & Walde, P. Enzymatic reactions in confined environments. *Nat. Nanotechnol.* **11,** 409 (2016).
166. Garni, M. *et al.* Artificial Organelles: Reactions inside Protein–Polymer Supramolecular Assemblies. *Chim. Int. J. Chem.* **70,** 424–427 (2016).
167. Baumann, P., Spulber, M., Fischer, O., Car, A. & Meier, W. Investigation of Horseradish Peroxidase Kinetics in an "Organelle-Like" Environment. *Small* **13,** n/a-n/a (2017).
168. Peyret, A. *et al.* Polymersome Popping by Light-Induced Osmotic Shock under Temporal, Spatial, and Spectral Control. *Angew. Chem. Int. Ed.* **56,** 1566–1570 (2017).
169. Kim, A. J. *et al.* Proton Transport from Dendritic Helical-Pore-Incorporated Polymersomes. *Adv. Funct. Mater.* **19,** 2930–2936 (2009).
170. Edlinger, C. *et al.* Biomimetic Strategy To Reversibly Trigger Functionality of Catalytic Nanocompartments by the Insertion of pH-Responsive Biovalves. *Nano Lett.* **17,** 5790–5798 (2017).
171. Macháň, R. & Wohland, T. Recent applications of fluorescence correlation spectroscopy in live systems. *FEBS Lett.* **588,** 3571–3584 (2014).
172. Rigler, P. & Meier, W. Encapsulation of fluorescent molecules by functionalized polymeric nanocontainers: investigation by confocal fluorescence imaging and fluorescence correlation spectroscopy. *J. Am. Chem. Soc.* **128,** 367–373 (2006).
173. Chang, T. M. S. Therapeutic applications of polymeric artificial cells. *Nat. Rev. Drug Discov.* **4,** 221 (2005).
174. Lienert, F., Lohmueller, J. J., Garg, A. & Silver, P. A. Synthetic biology in mammalian cells: next generation research tools and therapeutics. *Nat. Rev. Mol. Cell Biol.* **15,** 95 (2014).
175. Snell-Rood, E. Interdisciplinarity: Bring biologists into biomimetics. *Nat. News* **529,** 277 (2016).
176. Lu, L., Hu, X. & Zhu, Z. Biomimetic sensors and biosensors for qualitative and quantitative analyses of five basic tastes. *TrAC Trends Anal. Chem.* **87,** 58–70 (2017).
177. Molinaro, R. *et al.* Biomimetic proteolipid vesicles for targeting inflamed tissues. *Nat. Mater.* **15,** 1037–1046 (2016).
178. Erlich, Y. & Zielinski, D. DNA Fountain enables a robust and efficient storage architecture. *Science* **355,** 950–954 (2017).
179. Loiseau, E. *et al.* Shape remodeling and blebbing of active cytoskeletal vesicles. *Sci. Adv.* **2,** e1500465 (2016).
180. Sun, S. *et al.* Chemical Signaling and Functional Activation in Colloidosome-Based Protocells. *Small* **12,** 1920–1927 (2016).
181. Tang, T.-Y. D., Swaay, D. van, deMello, A., Anderson, J. L. R. & Mann, S. In vitro gene expression within membrane-free coacervate protocells. *Chem. Commun.* **51,** 11429–11432 (2015).
182. Takinoue, M. & Takeuchi, S. Droplet microfluidics for the study of artificial cells. *Anal. Bioanal. Chem.* **400,** 1705–1716 (2011).
183. Wang, L. & Tonggu, L. Membrane protein reconstitution for functional and structural studies. *Sci. China Life Sci.* **58,** 66–74 (2015).

184. Kurihara, K. *et al.* Self-reproduction of supramolecular giant vesicles combined with the amplification of encapsulated DNA. *Nat. Chem.* **3,** 775 (2011).
185. Francastel, C., Schübeler, D., Martin, D. I. K. & Groudine, M. Nuclear compartmentalization and gene activity. *Nat. Rev. Mol. Cell Biol.* **1,** 137 (2000).
186. Diekmann, Y. & Pereira-Leal, J. B. Evolution of intracellular compartmentalization. *Biochem. J.* **449,** 319–331 (2013).
187. Scott, R. E. Plasma membrane vesiculation: a new technique for isolation of plasma membranes. *Science* **194,** 743–745 (1976).
188. Sezgin, E. *et al.* Elucidating membrane structure and protein behavior using giant plasma membrane vesicles. *Nat. Protoc.* **7,** 1042–1051 (2012).
189. Chen, J. *et al.* Influence of lipid composition on the phase transition temperature of liposomes composed of both DPPC and HSPC. *Drug Dev. Ind. Pharm.* **39,** 197–204 (2013).
190. du Plessis, J., Ramachandran, C., Weiner, N. & Müller, D. G. The influence of lipid composition and lamellarity of liposomes on the physical stability of liposomes upon storage. *Int. J. Pharm.* **127,** 273–278 (1996).
191. Allen, T. M. & Hansen, C. B. Pharmacokinetics of stealth versus conventional liposomes: effect of dose. *Biochim. Biophys. Acta* **1068,** 133–141 (1991).
192. Ott, C. & Lippincott-Schwartz, J. Visualization of live primary cilia dynamics using fluorescence microscopy. *Curr. Protoc. Cell Biol. Editor. Board Juan Bonifacino Al* **0 4,** Unit-4.26 (2012).
193. Chen, X., Zhang, X., Wang, H.-Y., Chen, Z. & Wu, F.-G. Subcellular Fate of a Fluorescent Cholesterol-Poly(ethylene glycol) Conjugate: An Excellent Plasma Membrane Imaging Reagent. *Langmuir* **32,** 10126–10135 (2016).
194. Schöps, R., Amado, E., S. Müller, S., Frey, H. & Kressler, J. Block copolymers in giant unilamellar vesicles with proteins or with phospholipids. *Faraday Discuss.* **166,** 303–315 (2013).
195. Celik, E. *et al.* Agonist Leukadherin-1 Increases CD11b/CD18-Dependent Adhesion Via Membrane Tethers. *Biophys. J.* **105,** 2517–2527 (2013).
196. Zhou, W. *et al.* CellTrace™ Far Red & CellTracker™ Deep Red—long term live cell tracking for flow cytometry and fluorescence microscopy. *J. Biol. Methods* **3,** e38 (2016).
197. Okada, T. & Ogura, T. High-resolution imaging of living mammalian cells bound by nanobeads-connected antibodies in a medium using scanning electron-assisted dielectric microscopy. *Sci. Rep.* **7,** 43025 (2017).
198. Boisselier, E. & Astruc, D. Gold nanoparticles in nanomedicine: preparations, imaging, diagnostics, therapies and toxicity. *Chem. Soc. Rev.* **38,** 1759–1782 (2009).
199. Yang, X. *et al.* In situ synthesis of porous silica nanoparticles for covalent immobilization of enzymes. *Nanoscale* **4,** 414–416 (2012).
200. Johnston, H. J. *et al.* Evaluating the uptake and intracellular fate of polystyrene nanoparticles by primary and hepatocyte cell lines in vitro. *Toxicol. Appl. Pharmacol.* **242,** 66–78 (2010).

201. Dan, N. Effect of liposome charge and PEG polymer layer thickness on cell–liposome electrostatic interactions. *Biochim. Biophys. Acta BBA - Biomembr.* **1564,** 343–348 (2002).
202. Graff, A., Winterhalter, M. & Meier, W. Nanoreactors from Polymer-Stabilized Liposomes. *Langmuir* **17,** 919–923 (2001).
203. Mishin, V., Gray, J. P., Heck, D. E., Laskin, D. L. & Laskin, J. D. Application of the Amplex Red/Horseradish Peroxidase Assay to Measure Hydrogen Peroxide Generation by Recombinant Microsomal Enzymes. *Free Radic. Biol. Med.* **48,** 1485–1491 (2010).
204. Zhao, B., Summers, F. A. & Mason, R. P. Photooxidation of Amplex red to resorufin: Implications of exposing the Amplex red assay to light. *Free Radic. Biol. Med.* **53,** 1080–1087 (2012).
205. Sieber, S. *et al.* Zebrafish as an early stage screening tool to study the systemic circulation of nanoparticulate drug delivery systems in vivo. *J. Controlled Release* **264,** 180–191 (2017).
206. Delvecchio, C., Tiefenbach, J. & Krause, H. M. The Zebrafish: A Powerful Platform for In Vivo, HTS Drug Discovery. *ASSAY Drug Dev. Technol.* **9,** 354–361 (2011).
207. Fenaroli, F. *et al.* Nanoparticles as Drug Delivery System against Tuberculosis in Zebrafish Embryos: Direct Visualization and Treatment. *ACS Nano* **8,** 7014–7026 (2014).
208. Shaner, N. C. *et al.* Improving the photostability of bright monomeric orange and red fluorescent proteins. *Nat. Methods* **5,** 545–551 (2008).
209. Dean, K. M. *et al.* Analysis of Red-Fluorescent Proteins Provides Insight into Dark-State Conversion and Photodegradation. *Biophys. J.* **101,** 961–969 (2011).
210. Angelova, M. I. & Dimitrov, D. S. Liposome electroformation. *Faraday Discuss. Chem. Soc.* **81,** 303–311 (1986).
211. Kita-Tokarczyk, K., Grumelard, J., Haefele, T. & Meier, W. Block copolymer vesicles—using concepts from polymer chemistry to mimic biomembranes. *Polymer* **46,** 3540–3563 (2005).
212. Morales-Penningston, N. F. *et al.* GUV preparation and imaging: Minimizing artifacts. *Biochim. Biophys. Acta BBA - Biomembr.* **1798,** 1324–1332 (2010).